

The *ALF* (Algorithms for Lattice Fermions) project release 2.0

Documentation for the auxiliary-field quantum Monte Carlo code.

Martin Bercx, Florian Goth, Johannes S. Hofmann, Jefferson S. E. Portela,
Jonas Schwab, Fakher F. Assaad

July 26, 2020

Copyright © 2016–2020 The *ALF* Project.

This is the ALF Project Documentation by the ALF contributors. It is licensed under a Creative Commons Attribution-ShareAlike 4.0 International License. You are free to share and benefit from this documentation as long as this license is preserved and proper attribution to the authors is given. For details see the ALF project homepage alf.physik.uni-wuerzburg.de.

Contents

1	Introduction	4
1.1	Motivation	4
1.2	Definition of the Hamiltonian	5
1.3	Outline and What is new (to be written)	6
2	Auxiliary Field Quantum Monte Carlo: finite temperature	6
2.1	Formulation of the method	6
2.1.1	The partition function	8
2.1.2	Observables	8
2.1.3	Rewighting and the sign problem	9
2.2	Updating schemes	10
2.2.1	Sampling of e^{-S_0}	10
2.2.2	Sequential single spin flips	11
2.2.3	Global updates in space	11
2.2.4	Global updates in time and space	12
2.2.5	Parallel tempering	12
2.2.6	Langevin dynamics	13
2.3	The Trotter error and checkerboard decomposition	16
2.3.1	Asymmetric Trotter decomposition	16
2.3.2	Symmetric Trotter decomposition	17
2.3.3	The <code>Symm</code> flag	18
2.4	Stabilization - a peculiarity of the BSS algorithm	19
3	Auxiliary Field Quantum Monte Carlo: projective algorithm	20
3.1	Specification of the trial wave function	21
3.2	Some technical aspects of the projective code.	22
3.3	Comparison of finite and projective codes.	22
4	Monte Carlo sampling	22
4.1	The Jackknife resampling method	24
4.2	An explicit example of error estimation	25
4.3	Pseudo code description	26

5	Data Structures and Input/Output	27
5.1	Implementation of the Hamiltonian and the lattice	27
5.1.1	The <code>Operator</code> type	28
5.1.2	Specification of the model	29
5.1.3	Handling of the fields: the <code>Fields</code> type	30
5.1.4	The <code>Lattice</code> and <code>Unit_cell</code> types	30
5.2	The observable types <code>Obser_Vec</code> and <code>Obser_Latt</code>	32
5.2.1	Scalar observables	33
5.2.2	Equal-time and time-displaced correlation functions	33
5.3	The trial wave function type	34
5.4	File structure	34
5.4.1	Input files	35
5.4.2	Output files – observables	36
6	Using the Code	37
6.1	Compiling and running	38
6.2	Error analysis	39
6.3	Performance & parameter optimization	41
7	The plain vanilla Hubbard model on the square and honeycomb lattices	42
7.1	The square lattice	42
7.1.1	Setting the Hamiltonian: <code>Ham_set</code>	42
7.1.1.1	The lattice: <code>Call Ham_latt</code>	42
7.1.1.2	The hopping term: <code>Call Ham_hop</code>	42
7.1.1.3	The interaction term: <code>Call Ham_V</code>	43
7.1.2	Observables	43
7.1.2.1	Allocating space for the observables: <code>Call Alloc_obs(Ltau)</code>	43
7.1.2.2	Measuring equal-time observables: <code>Obser(GR,Phase,Ntau)</code>	44
7.1.2.3	Measuring time displaced observables: <code>ObserT(NT, GTO,GOT,G00,GTT, PHASE)</code>	45
7.1.3	Numerical precision	45
7.2	The M_z -Hubbard model on a square lattice	45
7.2.1	The interaction term: <code>Call Ham_V</code>	45
7.2.2	The measurements: <code>Call Obser, Call ObserT</code>	46
7.2.3	Numerical precision	46
7.3	The $SU(2)$ -Hubbard model on the honeycomb lattice	46
7.3.1	Working with multi-orbital unit cells: <code>Call Ham_Latt</code>	46
7.3.2	The hopping term: <code>Call Ham_Hop</code>	46
7.3.3	Observables: <code>Call Obser, Call ObserT</code>	47
8	Predefined Structures	47
8.1	Predefined lattices	47
8.1.1	Square lattice, Fig. 5(a)	47
8.1.2	Bilayer Square lattice, Fig. 5(b)	48
8.1.3	N -leg Ladder lattice, Fig. 5(c)	48
8.1.4	Honeycomb lattice, Fig. 5(d)	49
8.1.5	Bilayer Honeycomb lattice, Fig. 5(e)	49
8.1.6	π -Flux lattice (deprecated)	50
8.2	Generic hopping matrices on bravais lattices	50
8.2.1	Setting up the hopping matrix: the <code>Hopping_Matrix_type</code>	50
8.2.2	An example: nearest neighbor hopping on the honeycomb lattice	53
8.2.3	Predefined hoppings	53
8.3	Predefined interaction vertices	55
8.3.1	$SU(N)$ Hubbard interaction	55
8.3.2	M_z -Hubbard interaction	56
8.3.3	$SU(N)$ V -interaction	56
8.3.4	Fermion-Ising coupling	56
8.3.5	Long-Range Coulomb repulsion	57
8.3.6	J_z - J_z interaction	57

8.4	Predefined observables	58
8.5	Predefined trial wave functions	58
8.5.1	Square	58
8.5.2	Honeycomb	58
8.5.3	N-leg ladder	59
8.5.4	Bilayer square	59
8.5.5	Bilayer honeycomb	59
9	Model Classes	59
9.1	SU(N) Hubbard models <code>Hamiltonian_Hubbard_mod.F90</code>	60
9.2	O(2N) t-V models <code>tV_mod.F90</code>	61
9.3	SU(N) Kondo lattice models <code>Kondo_mod.F90</code>	61
9.4	Models with long range Coulomb interactions <code>LRC_mod.F90</code>	61
9.5	Z_2 lattice gauge theories coupled to fermion and Z_2 matter <code>Z2_mod.F90</code>	61
10	Maximum Entropy	61
10.1	General setup	61
10.2	Single-particle quantities	62
10.3	Particle-hole quantities	63
10.4	Particle-Particle quantities	64
10.5	Zero-temperature, projective code	64
10.6	Performance, memory requirements and parallelization	64
11	Conclusions and Future Directions	66
12	Examples	66
12.1	The $SU(2)$ -Hubbard model on a square lattice coupled to a transverse Ising field	66
12.1.1	The Ising term.	67
12.1.2	The interaction term: <code>Call Ham_V</code>	67
12.1.3	The function <code>Real (Kind=8) function S0(n,nt)</code>	68
13	Miscellaneous	68
13.1	Other models	68
13.1.1	Kondo lattice model	68
13.1.2	$SU(N)$ Hubbard-Heisenberg models	69
13.1.3	Hubbard model in the canonical ensemble	69
13.1.4	Z_2 slave spin formulation of the Hubbard model	70
13.1.5	Z_2 gauge theory coupled to Z_2 matter.	72
13.1.6	Generalized t-V model	72
13.1.7	Long range Coulomb	72
	Acknowledgments	73
	References	73
	License	76

1 Introduction

To be summarized and slightly changed in order to reduce overlap with ALF 1.0 paper.//

1.1 Motivation

The auxiliary-field quantum Monte Carlo (QMC) approach is the algorithm of choice to simulate thermodynamic properties of a variety of correlated electron systems in the solid state and beyond [1, 2, 3, 4, 5, 6]. Apart from the physics of the canonical Hubbard model [7, 8], the topics one can investigate in detail include correlation effects in the bulk and on surfaces of topological insulators [9, 10], quantum phase transitions between Dirac fermions and insulators [11, 12, 13, 14, 15], deconfined quantum critical points [16, 17], topologically ordered phases [17], heavy fermion systems [18, 19], nematic [20] and magnetic [21] quantum phase transitions in metals, antiferromagnetism in metals [22], superconductivity in spin-orbit split bands [23], $SU(N)$ symmetric models [24, 25], long-ranged Coulomb interactions in graphene systems [26, 27], cold atomic gases [28], low energy nuclear physics [29], entanglement entropies and spectra [30, 31, 32, 33], etc. This ever-growing list of topics is based on algorithmic progress and on recent symmetry-related insights [34, 35, 36, 37] that lead to formulations free of the negative sign problem for a number of model systems with very rich phase diagrams.

Auxiliary-field methods can be formulated in very different ways. The fields define the configuration space \mathcal{C} . They can stem from the Hubbard-Stratonovich (HS) [38] transformation required to decouple the many-body interacting term into a sum of non-interacting problems, or they can correspond to bosonic modes with predefined dynamics such as phonons or gauge fields. In all cases, the result is that the grand-canonical partition function takes the form,

$$Z = \text{Tr} \left(e^{-\beta \hat{\mathcal{H}}} \right) = \sum_{\mathcal{C}} e^{-S(\mathcal{C})}, \quad (1)$$

where β corresponds to the inverse temperature and S is the action of non-interacting fermions subject to a space-time fluctuating auxiliary field. The high-dimensional integration over the fields is carried out stochastically. In this formulation of many body quantum systems, there is no reason for the action to be a real number. Thereby $e^{-S(\mathcal{C})}$ cannot be interpreted as a weight. To circumvent this problem one can adopt re-weighting schemes and sample $|e^{-S(\mathcal{C})}|$. This invariably leads to the so-called *negative sign problem*, with the associated exponential computational scaling in system size and inverse temperature [39]. The sign problem is formulation dependent and, as mentioned above, there has been tremendous progress at identifying an increasing number of models not affected by the negative sign problem which cover a rich domain of collective emergent phenomena. For continuous fields, the stochastic integrations can be carried out with Langevin dynamics or hybrid methods [40]. However, for many problems one can get away with discrete fields [41]. In this case, Monte Carlo importance sampling will often be put to use [42]. We note that due to the non-locality of the fermion determinant, see below, cluster updates, such as in the loop or stochastic series expansion algorithms for quantum spin systems [43, 44, 45], are hard to formulate for this class of problems. The search for efficient updating schemes that enable to move quickly within the configuration space, defines ongoing challenges.

Formulations do not differ only by the choice of the fields, continuous or discrete, and the sampling strategy, but also by the formulation of the action itself. For a given field configuration, integrating out fermionic degrees of freedom generically leads to a fermionic determinant of dimension βN where N is the volume of the system. Working with this determinant leads to the Hirsch-Fye approach [46] and the computational effort scales¹ as $\mathcal{O}(\beta N)^3$. The Hirsch-Fye algorithm is the method of choice for impurity problems, but has generically been outperformed by a class of so-called continuous-time quantum Monte Carlo approaches [47, 48, 49]. One key point of continuous-time methods is that they are action based and thereby allow one to handle the retarded interactions obtained when integrating out fermion or boson baths. In high dimensions and/or at low temperatures, the cubic scaling originating from the fermionic determinant is expensive. To circumvent this, the hybrid Monte-Carlo approach [50, 5] expresses the fermionic determinant in terms of a Gaussian integral thereby introducing a new variable in the Monte Carlo integration. The resulting algorithm is the method of choice for lattice gauge theories in 3+1 dimensions and has been used to provide *ab initio* estimates of light hadron masses starting from quantum chromodynamics [51]. The approach we consider here lies between the above two *extremes*. We keep the fermionic determinant, but formulate the problem so as to work only with $N \times N$ matrices. This Blankenbecler, Scalapino, Sugar (BSS) algorithm scales linearly in imaginary time β , but remains cubic

¹Here we implicitly assume the absence of negative sign problem

in the volume N . Furthermore, the algorithm can be formulated either in a projective manner [3, 4], adequate to obtain zero temperature properties in the canonical ensemble, or at finite temperatures in the grand-canonical ensemble [2].

The aim of the ALF project is to introduce a general formulation of the finite-temperature auxiliary-field QMC method with discrete fields so as enable one to promptly play with different model Hamiltonians at minimal programming cost. In this documentation, we summarize the essential aspects of the auxiliary-field QMC approach, and refer the reader to Refs. [52, 6] for complete reviews. In the following we show in all details how to implement a variety of models, run the code, and produce results for equal-time and time-displaced correlation functions. The program code is written in Fortran according to the 2003 standard and is able to natively utilize MPI for massively parallel runs on today's supercomputing systems.

1.2 Definition of the Hamiltonian

The first and most fundamental part of the project is to define a general Hamiltonian which can accommodate a large class of models. Our approach is to express the model as a sum of one-body terms, a sum of two-body terms each written as a perfect square of a one body term, as well as a one-body term coupled to an Ising field with dynamics to be specified by the user. Writing the interaction in terms of sums of perfect squares allows us to use generic forms of discrete approximations to the HS transformation [53, 54]. Symmetry considerations are imperative to increase the speed of the code. We therefore include a *color* index reflecting an underlying $SU(N)$ color symmetry as well as a *flavor* index reflecting the fact that after the HS transformation, the fermionic determinant is block diagonal in this index.

The class of solvable models includes Hamiltonians $\hat{\mathcal{H}}$ that have the following general form:

$$\hat{\mathcal{H}} = \hat{\mathcal{H}}_T + \hat{\mathcal{H}}_V + \hat{\mathcal{H}}_I + \hat{\mathcal{H}}_{0,I}, \text{ where} \quad (2)$$

$$\hat{\mathcal{H}}_T = \sum_{k=1}^{M_T} \sum_{\sigma=1}^{N_{\text{col}}} \sum_{s=1}^{N_{\text{fl}}} \sum_{x,y}^{N_{\text{dim}}} \hat{c}_{x\sigma s}^\dagger T_{xy}^{(ks)} \hat{c}_{y\sigma s} \equiv \sum_{k=1}^{M_T} \hat{T}^{(k)}, \quad (3)$$

$$\hat{\mathcal{H}}_V = \sum_{k=1}^{M_V} U_k \left\{ \sum_{\sigma=1}^{N_{\text{col}}} \sum_{s=1}^{N_{\text{fl}}} \left[\left(\sum_{x,y}^{N_{\text{dim}}} \hat{c}_{x\sigma s}^\dagger V_{xy}^{(ks)} \hat{c}_{y\sigma s} \right) + \alpha_{ks} \right] \right\}^2 \equiv \sum_{k=1}^{M_V} U_k \left(\hat{V}^{(k)} \right)^2, \quad (4)$$

$$\hat{\mathcal{H}}_I = \sum_{k=1}^{M_I} \hat{Z}_k \left(\sum_{\sigma=1}^{N_{\text{col}}} \sum_{s=1}^{N_{\text{fl}}} \sum_{x,y}^{N_{\text{dim}}} \hat{c}_{x\sigma s}^\dagger I_{xy}^{(ks)} \hat{c}_{y\sigma s} \right) \equiv \sum_{k=1}^{M_I} \hat{Z}_k \hat{I}^{(k)}. \quad (5)$$

The indices and symbols used above have the following meaning:

- The number of fermion *flavors* is set by N_{fl} . After the HS transformation, the action will be block diagonal in the flavor index.
- The number of fermion *colors* is set² by N_{col} . The Hamiltonian is invariant under $SU(N_{\text{col}})$ rotations.
- N_{dim} is the total number of spacial vertices: $N_{\text{dim}} = N_{\text{unit-cell}} N_{\text{orbital}}$, where $N_{\text{unit-cell}}$ is the number of unit cells of the underlying Bravais lattice and N_{orbital} is the number of (spacial) orbitals per unit cell.
- The indices x and y label lattice sites where $x, y = 1, \dots, N_{\text{dim}}$.
- Therefore, the matrices $\mathbf{T}^{(ks)}$, $\mathbf{V}^{(ks)}$ and $\mathbf{I}^{(ks)}$ are of dimension $N_{\text{dim}} \times N_{\text{dim}}$.
- The number of interaction terms is labeled by M_V and M_I . $M_T > 1$ would allow for a checkerboard decomposition.
- $\hat{c}_{y\sigma s}^\dagger$ is a second-quantized operator that creates an electron in a Wannier state centered around lattice site y , with color σ , and flavor index s . The operators satisfy the anti-commutation relations:

$$\left\{ \hat{c}_{y\sigma s}^\dagger, \hat{c}_{y'\sigma' s'} \right\} = \delta_{xx'} \delta_{ss'} \delta_{\sigma\sigma'}, \text{ and } \left\{ \hat{c}_{y\sigma s}, \hat{c}_{y'\sigma' s'} \right\} = 0. \quad (6)$$

²Note that in the code $N_{\text{col}} \equiv \mathbf{N_SUN}$.

The Ising part of the general Hamiltonian (2) is $\hat{\mathcal{H}}_{0,I} + \hat{\mathcal{H}}_I$ and has the following properties:

- \hat{Z}_k couples to a general one-body term. It is a general operator, such as the Ising spin operator corresponding to the Pauli matrix $\hat{\sigma}_z$ or the position operator.
- The dynamics of the Ising spins is given by $\hat{\mathcal{H}}_{0,I}$. This term is not specified here; it has to be specified by the user and becomes relevant when the Monte Carlo update probability is computed in the code (see Sec. 12.1 for an example).

Note that the matrices $\mathbf{T}^{(ks)}$, $\mathbf{V}^{(ks)}$ and $\mathbf{I}^{(ks)}$ explicitly depend on the flavor index s but not on the color index σ . The color index σ only appears in the second quantized operators such that the Hamiltonian is manifestly $SU(N_{\text{col}})$ symmetric. We also require the matrices $\mathbf{T}^{(ks)}$, $\mathbf{V}^{(ks)}$ and $\mathbf{I}^{(ks)}$ to be Hermitian, see Sec. ??.

1.3 Outline and What is new (to be written)

Later on update, and add a paragraph highlighting the changes/new features with respect to ALF 1.0

What's new: - Parallel tempering - Global updates / global tau - Projective approaches - Continuous fields - Langevin - Maxent - More models - Trotter symmetric - Predefined structures.

In order to use the code, a minimal understanding of the algorithm is necessary. In Sec. 2, we summarize the steps required to formulate the many-body, imaginary-time propagation in terms of a sum over HS and Ising fields of one-body, imaginary-time propagators. The user has to provide this one-body, imaginary-time propagator for a given configuration of HS and Ising fields. We also discuss the Monte Carlo updates, the strategies for numerical stabilization of the code, as well as the Monte Carlo sampling. In Sec. 3 we go very briefly through the projective method, used for obtaining ground-state properties. And, finally, we describe how the QMC data can be used to obtain spectral information using ALF's implementation of the stochastic maximum entropy method, in Sec. 10.

Section 5 is devoted to the data structures that are needed to implement the model, as well as to the input and output file structure. The data structure includes an `Operator` type to optimally work with sparse Hermitian matrices, a `Lattice` type to define one- and two-dimensional Bravais lattices, a generic `Fields` type, and two `Observable` types to handle scalar observables (e.g., total energy) and equal-time or time-displaced two-point correlation functions (e.g., spin-spin correlations).

Detailed instructions on how to compile and run the code are provided in Sec. 6. It is important to notice that the Monte Carlo simulation and the associated data analysis are separated processes: the QMC run dumps the results of *bins* sequentially into files which are then analyzed by analysis programs. In Sec. 6.2, we provide a brief description of the analysis programs for our observable types. The analysis programs allow for omitting a given number of initial bins in order to account for warm-up times. Also, a rebinning analysis is included to account for, *a posteriori*, long autocorrelation times.

In Sec. 12, we give explicit examples on how to use the code for the Hubbard model on square and honeycomb lattices, for different choices of the Hubbard-Stratonovich transformation (see Secs. 7.1, 7.2 and 7.3), as well as for the Hubbard model on a square lattice coupled to a transverse Ising field (see Sec. 12.1). Our implementation is rather general, allowing for a variety of other models to be simulated and, in Sec. 13, further examples are given, such as the Kondo lattice and the $SU(N)$ symmetric Hubbard-Heisenberg models.

Finally, in Sec. 11 we list a number of features being considered for future releases of the ALF program package.

2 Auxiliary Field Quantum Monte Carlo: finite temperature

Summarize and change slightly – or completely omit – in order to reduce overlap with ALF 1.0 paper (unless this paper is to be published as a 2nd version of the first).//

2.1 Formulation of the method

Our aim is to compute observables for the general Hamiltonian (2) in thermodynamic equilibrium as described by the grand-canonical ensemble. We show below how the grand-canonical partition function

can be rewritten as

$$Z = \text{Tr} \left(e^{-\beta \hat{\mathcal{H}}} \right) = \sum_C e^{-S(C)} + \mathcal{O}(\Delta\tau^2) \quad (7)$$

and define the space of configurations C . Note that the chemical potential term is already included in the definition of the one-body term $\hat{\mathcal{H}}_T$, see Eq. (3), of the general Hamiltonian.

The outline of this section is as follows. First, we derive the detailed form of the partition function and outline the computation of observables (Sec. 2.1.1 - 2.1.3). Next, we present a number of update strategies, namely local updates, global updates, and parallel tempering (Sec. 2.2). We also describe the measures we have implemented to make the code numerically stable (Sec. 2.4). Finally, we discuss the autocorrelations and associated time scales during the Monte Carlo sampling process (Sec. 4).

The essential ingredients of the auxiliary-field quantum Monte Carlo implementation in the ALF package are the following:

- We discretize the imaginary time propagation: $\beta = \Delta\tau L_{\text{Trotter}}$. Generically this introduces a systematic Trotter error of $\mathcal{O}(\Delta\tau)^2$ [55]. We note that there has been considerable effort at getting rid of the Trotter systematic error and to formulate a genuine continuous-time BSS algorithm [56]. To date, efforts in this direction are based on a CT-AUX type formulation [57, 58] and face two issues. The first issue is that they are restricted to a class of models with Hubbard-type interactions

$$(\hat{n}_i - 1)^2 = (\hat{n}_i - 1)^4, \quad (8)$$

such that the basic CT-AUX equation [59]

$$1 + \frac{U}{K} (\hat{n}_i - 1)^2 = \frac{1}{2} \sum_{s=\pm 1} e^{\alpha s (\hat{n}_i - 1)} \quad \text{with} \quad \frac{U}{K} = \cosh(\alpha) - 1 \quad \text{and} \quad K \in \mathbb{R} \quad (9)$$

holds. The second issue is that in the continuous-time approach it is hard to formulate a computationally efficient algorithm. Given this situation it turns out that the multi-grid method [60, 61, 62] is an efficient scheme to extrapolate to small imaginary-time steps so as to eliminate the Trotter systematic error if required.

- Having isolated the two-body term, we use the discrete HS transformation [53, 54]:

$$e^{\Delta\tau \lambda \hat{A}^2} = \sum_{l=\pm 1, \pm 2} \gamma(l) e^{\sqrt{\Delta\tau \lambda} \eta(l) \hat{A}} + \mathcal{O}(\Delta\tau^4), \quad (10)$$

where the fields η and γ take the values:

$$\begin{aligned} \gamma(\pm 1) &= 1 + \sqrt{6}/3, & \eta(\pm 1) &= \pm \sqrt{2(3 - \sqrt{6})}, \\ \gamma(\pm 2) &= 1 - \sqrt{6}/3, & \eta(\pm 2) &= \pm \sqrt{2(3 + \sqrt{6})}. \end{aligned} \quad (11)$$

Since the Trotter error is already of order $(\Delta\tau^2)$ per time slice, this transformation is next to exact.

- \hat{Z}_k can stand for a variety of operators, such as the Pauli matrix $\hat{\sigma}_z$, in which case the Ising spins take the values $s_k = \pm 1$, or the position operator – such that $\hat{Z}_k|\phi\rangle = \phi|\phi\rangle$, with ϕ a real number.
- From the above it follows that the Monte Carlo configuration space C is given by the combined spaces of Ising spin configurations and of HS discrete field configurations:

$$C = \{s_{i,\tau}, l_{j,\tau} \text{ with } i = 1 \cdots M_I, j = 1 \cdots M_V, \tau = 1 \cdots L_{\text{Trotter}}\}. \quad (12)$$

Here, the HS fields take the values $l_{j,\tau} = \pm 2, \pm 1$ and the Ising spins $s_{i,\tau}$ may, for instance, be a continuous real field or, if $\hat{Z}_k = \hat{\sigma}_z$, be restricted to ± 1 .

2.1.1 The partition function

With the above, the partition function of the model (2) can be written as follows.

$$\begin{aligned}
Z &= \text{Tr} \left(e^{-\beta \hat{\mathcal{H}}} \right) \\
&= \text{Tr} \left[e^{-\Delta \tau \hat{\mathcal{H}}_{0,I}} \prod_{k=1}^{M_V} e^{-\Delta \tau U_k (\hat{V}^{(k)})^2} \prod_{k=1}^{M_I} e^{-\Delta \tau \hat{\sigma}_k \hat{I}^{(k)}} \prod_{k=1}^{M_T} e^{-\Delta \tau \hat{T}^{(k)}} \right]^{L_{\text{Trotter}}} + \mathcal{O}(\Delta \tau^2) \\
&= \sum_C \left(\prod_{k=1}^{M_V} \prod_{\tau=1}^{L_{\text{Trotter}}} \gamma_{k,\tau} \right) e^{-S_{0,I}(\{s_{i,\tau}\})} \times \\
&\quad \text{Tr}_F \left\{ \prod_{\tau=1}^{L_{\text{Trotter}}} \left[\prod_{k=1}^{M_V} e^{\sqrt{-\Delta \tau U_k} \eta_{k,\tau} \hat{V}^{(k)}} \prod_{k=1}^{M_I} e^{-\Delta \tau s_{k,\tau} \hat{I}^{(k)}} \prod_{k=1}^{M_T} e^{-\Delta \tau \hat{T}^{(k)}} \right] \right\} + \mathcal{O}(\Delta \tau^2). \tag{13}
\end{aligned}$$

In the above, the trace Tr runs over the Ising spins as well as over the fermionic degrees of freedom, and Tr_F only over the fermionic Fock space. $S_{0,I}(\{s_{i,\tau}\})$ is the action corresponding to the Ising Hamiltonian, and is only dependent on the Ising spins so that it can be pulled out of the fermionic trace. We have adopted the short hand notation $\eta_{k,\tau} = \eta(l_{k,\tau})$ and $\gamma_{k,\tau} = \gamma(l_{k,\tau})$. At this point, and since for a given configuration C we are dealing with a free propagation, we can integrate out the fermions to obtain a determinant:

$$\begin{aligned}
&\text{Tr}_F \left\{ \prod_{\tau=1}^{L_{\text{Trotter}}} \left[\prod_{k=1}^{M_V} e^{\sqrt{-\Delta \tau U_k} \eta_{k,\tau} \hat{V}^{(k)}} \prod_{k=1}^{M_I} e^{-\Delta \tau s_{k,\tau} \hat{I}^{(k)}} \prod_{k=1}^{M_T} e^{-\Delta \tau \hat{T}^{(k)}} \right] \right\} = \\
&\prod_{s=1}^{N_{\text{fl}}} \left[\sum_{k=1}^{M_V} \sum_{\tau=1}^{L_{\text{Trotter}}} \sqrt{-\Delta \tau U_k} \alpha_{k,s} \eta_{k,\tau} \right]^{N_{\text{col}}} \times \\
&\prod_{s=1}^{N_{\text{fl}}} \left[\det \left(\mathbb{1} + \prod_{\tau=1}^{L_{\text{Trotter}}} \prod_{k=1}^{M_V} e^{\sqrt{-\Delta \tau U_k} \eta_{k,\tau} \mathbf{V}^{(ks)}} \prod_{k=1}^{M_I} e^{-\Delta \tau s_{k,\tau} \mathbf{I}^{(ks)}} \prod_{k=1}^{M_T} e^{-\Delta \tau \mathbf{T}^{(ks)}} \right) \right]^{N_{\text{col}}}, \tag{14}
\end{aligned}$$

where the matrices $\mathbf{T}^{(ks)}$, $\mathbf{V}^{(ks)}$, and $\mathbf{I}^{(ks)}$ define the Hamiltonian [Eq. (2) - (5)]. All in all, the partition function is given by:

$$\begin{aligned}
Z &= \sum_C e^{-S_{0,I}(\{s_{i,\tau}\})} \left(\prod_{k=1}^{M_V} \prod_{\tau=1}^{L_{\text{Trotter}}} \gamma_{k,\tau} \right) e^{N_{\text{col}} \sum_{s=1}^{N_{\text{fl}}} \sum_{k=1}^{M_V} \sum_{\tau=1}^{L_{\text{Trotter}}} \sqrt{-\Delta \tau U_k} \alpha_{k,s} \eta_{k,\tau}} \times \\
&\prod_{s=1}^{N_{\text{fl}}} \left[\det \left(\mathbb{1} + \prod_{\tau=1}^{L_{\text{Trotter}}} \prod_{k=1}^{M_V} e^{\sqrt{-\Delta \tau U_k} \eta_{k,\tau} \mathbf{V}^{(ks)}} \prod_{k=1}^{M_I} e^{-\Delta \tau s_{k,\tau} \mathbf{I}^{(ks)}} \prod_{k=1}^{M_T} e^{-\Delta \tau \mathbf{T}^{(ks)}} \right) \right]^{N_{\text{col}}} + \mathcal{O}(\Delta \tau^2) \\
&\equiv \sum_C e^{-S(C)} + \mathcal{O}(\Delta \tau^2). \tag{15}
\end{aligned}$$

In the above, one notices that the weight factorizes in the flavor index. The color index raises the determinant to the power N_{col} . This corresponds to an explicit $SU(N_{\text{col}})$ symmetry for each configuration. This symmetry is manifest in the fact that the single particle Green functions are color independent, again for each given configuration C .

2.1.2 Observables

In the auxiliary-field QMC approach, the single-particle Green function plays a crucial role. It determines the Monte Carlo dynamics and is used to compute observables:

$$\langle \hat{O} \rangle = \frac{\text{Tr} [e^{-\beta \hat{H}} \hat{O}]}{\text{Tr} [e^{-\beta \hat{H}}]} = \sum_C P(C) \langle \langle \hat{O} \rangle \rangle_C, \text{ with } P(C) = \frac{e^{-S(C)}}{\sum_C e^{-S(C)}}, \tag{16}$$

and $\langle \langle \hat{O} \rangle \rangle_C$ denotes the observed value of \hat{O} for a given configuration C . For a given configuration C one can use Wick's theorem to compute $O(C)$ from the knowledge of the single-particle Green function:

$$G(x, \sigma, s, \tau | x', \sigma', s', \tau') = \langle \langle \mathcal{T} \hat{c}_{x\sigma s}(\tau) \hat{c}_{x'\sigma' s'}^\dagger(\tau') \rangle \rangle_C \tag{17}$$

where \mathcal{T} corresponds to the imaginary-time ordering operator. The corresponding equal-time quantity reads,

$$G(x, \sigma, s, \tau | x', \sigma', s', \tau) = \langle \langle \hat{c}_{x\sigma s}(\tau) \hat{c}_{x'\sigma' s'}^\dagger(\tau) \rangle \rangle_C. \quad (18)$$

Since, for a given HS field, translation invariance in imaginary-time is broken, the Green function has an explicit τ and τ' dependence. On the other hand it is diagonal in the flavor index, and independent of the color index. The latter reflects the explicit $SU(N)$ color symmetry present at the level of individual HS configurations. As an example, one can show that the equal-time Green function at $\tau = 0$ reads [6]:

$$G(x, \sigma, s, 0 | x', \sigma, s, 0) = \left(\mathbb{1} + \prod_{\tau=1}^{L_{\text{Trotter}}} \mathbf{B}_\tau^{(s)} \right)_{x, x'}^{-1} \quad (19)$$

with

$$\mathbf{B}_\tau^{(s)} = \prod_{k=1}^{M_V} e^{\sqrt{-\Delta\tau} U_{k\eta_{k,\tau}} \mathbf{V}^{(ks)}} \prod_{k=1}^{M_I} e^{-\Delta\tau s_{k,\tau} \mathbf{I}^{(ks)}} \prod_{k=1}^{M_T} e^{-\Delta\tau \mathbf{T}^{(ks)}}. \quad (20)$$

To compute equal-time, as well as time-displaced observables, one can make use of Wick's theorem. A convenient formulation of this theorem for QMC simulations reads:

$$\langle \langle \mathcal{T} c_{\underline{x}_1}^\dagger(\tau_1) c_{\underline{x}'_1}(\tau'_1) \cdots c_{\underline{x}_n}^\dagger(\tau_n) c_{\underline{x}'_n}(\tau'_n) \rangle \rangle_C = \det \begin{bmatrix} \langle \langle \mathcal{T} c_{\underline{x}_1}^\dagger(\tau_1) c_{\underline{x}'_1}(\tau'_1) \rangle \rangle_C & \langle \langle \mathcal{T} c_{\underline{x}_1}^\dagger(\tau_1) c_{\underline{x}'_2}(\tau'_2) \rangle \rangle_C & \cdots & \langle \langle \mathcal{T} c_{\underline{x}_1}^\dagger(\tau_1) c_{\underline{x}'_n}(\tau'_n) \rangle \rangle_C \\ \langle \langle \mathcal{T} c_{\underline{x}_2}^\dagger(\tau_2) c_{\underline{x}'_1}(\tau'_1) \rangle \rangle_C & \langle \langle \mathcal{T} c_{\underline{x}_2}^\dagger(\tau_2) c_{\underline{x}'_2}(\tau'_2) \rangle \rangle_C & \cdots & \langle \langle \mathcal{T} c_{\underline{x}_2}^\dagger(\tau_2) c_{\underline{x}'_n}(\tau'_n) \rangle \rangle_C \\ \vdots & \vdots & \ddots & \vdots \\ \langle \langle \mathcal{T} c_{\underline{x}_n}^\dagger(\tau_n) c_{\underline{x}'_1}(\tau'_1) \rangle \rangle_C & \langle \langle \mathcal{T} c_{\underline{x}_n}^\dagger(\tau_n) c_{\underline{x}'_2}(\tau'_2) \rangle \rangle_C & \cdots & \langle \langle \mathcal{T} c_{\underline{x}_n}^\dagger(\tau_n) c_{\underline{x}'_n}(\tau'_n) \rangle \rangle_C \end{bmatrix}. \quad (21)$$

Here, we have defined the super-index $\underline{x} = \{x, \sigma, s\}$. In the subroutines `Obser` and `ObserT` of the module `Hamiltonian_Examples_mod.F90` (see Sec. 5.2) the user is provided with the equal-time and time-displaced correlation functions. Using the above formulation of Wick's theorem, arbitrary correlation functions can be computed. We note, however, that the program is limited to the calculation of observables that contain only two different imaginary times.

2.1.3 Reweighting and the sign problem

In general, the action $S(C)$ will be complex, thereby inhibiting a direct Monte Carlo sampling of $P(C)$. This leads to the infamous sign problem. The sign problem is formulation dependent and as noted above, much progress has been made at understanding the class of models that can be formulated without encountering this problem [34, 35, 36, 37]. When the average sign is not too small, we can nevertheless compute observables within a reweighting scheme. Here we adopt the following scheme. First note that the partition function is real such that:

$$Z = \sum_C e^{-S(C)} = \sum_C \overline{e^{-S(C)}} = \sum_C \text{Re} \left[e^{-S(C)} \right]. \quad (22)$$

Thereby³ and with the definition

$$\text{sign}(C) = \frac{\text{Re} \left[e^{-S(C)} \right]}{\left| \text{Re} \left[e^{-S(C)} \right] \right|}, \quad (23)$$

³The attentive reader will have noticed that for arbitrary Trotter decompositions, the imaginary time propagator is not necessarily Hermitian. Thereby, the above equation is correct only up to corrections stemming from the controlled Trotter systematic error.

the computation of the observable [Eq. (16)] is re-expressed as follows:

$$\begin{aligned}
\langle \hat{O} \rangle &= \frac{\sum_C e^{-S(C)} \langle \hat{O} \rangle_{(C)}}{\sum_C e^{-S(C)}} \\
&= \frac{\sum_C \text{Re} [e^{-S(C)}] \frac{e^{-S(C)}}{\text{Re} [e^{-S(C)}]} \langle \hat{O} \rangle_{(C)}}{\sum_C \text{Re} [e^{-S(C)}]} \\
&= \frac{\left\{ \sum_C |\text{Re} [e^{-S(C)}]| \text{sign} (C) \frac{e^{-S(C)}}{\text{Re} [e^{-S(C)}]} \langle \hat{O} \rangle_{(C)} \right\} / \sum_C |\text{Re} [e^{-S(C)}]|}{\left\{ \sum_C |\text{Re} [e^{-S(C)}]| \text{sign} (C) \right\} / \sum_C |\text{Re} [e^{-S(C)}]|} \\
&= \frac{\left\langle \text{sign} \frac{e^{-S}}{\text{Re} [e^{-S}]} \langle \hat{O} \rangle \right\rangle_{\bar{P}}}{\langle \text{sign} \rangle_{\bar{P}}} .
\end{aligned} \tag{24}$$

The average sign is

$$\langle \text{sign} \rangle_{\bar{P}} = \frac{\sum_C |\text{Re} [e^{-S(C)}]| \text{sign} (C)}{\sum_C |\text{Re} [e^{-S(C)}]|} , \tag{25}$$

and we have $\langle \text{sign} \rangle_{\bar{P}} \in \mathbb{R}$ per definition. The Monte Carlo simulation samples the probability distribution

$$\bar{P}(C) = \frac{|\text{Re} [e^{-S(C)}]|}{\sum_C |\text{Re} [e^{-S(C)}]|} . \tag{26}$$

such that the nominator and denominator of Eq. (24) can be computed.

The negative sign problem is still an issue because the average sign is a ratio of two partition functions and one can argue that

$$\langle \text{sign} \rangle_{\bar{P}} \propto e^{-\Delta N\beta} , \tag{27}$$

where Δ is intensive positive quantity and $N\beta$ denotes the Euclidean volume. In a Monte Carlo simulation the error scales as $1/\sqrt{T_{CPU}}$ where T_{CPU} corresponds to the computational time. Since the error on the average sign has to be much smaller than the average sign itself, one sees that:

$$T_{CPU} \gg e^{2\Delta N\beta} . \tag{28}$$

Two comments are in order. First, the presence of a sign problem invariably leads to an exponential increase of CPU time as a function of the Euclidean volume. And second, Δ is formulation dependent. For instance, at finite doping, the SU(2) invariant formulation of the Hubbard model presented in Sec. 7.1 has a much more severe sign problem than the formulation presented in Sec. 7.2 where the HS field couples to the z-component of the magnetization.

2.2 Updating schemes

The program allows for different types of updating schemes, which are described below and summarized in Tab. 1. In all of them, given a configuration C , we propose a new one, C' , with probability $T_0(C \rightarrow C')$ and accept it according to the Metropolis-Hastings acceptance-rejection probability,

$$P(C \rightarrow C') = \min \left(1, \frac{T_0(C' \rightarrow C)W(C')}{T_0(C \rightarrow C')W(C)} \right) , \tag{29}$$

so as to guarantee the stationarity condition. Here, $W(C) = |\text{Re} [e^{-S(C)}]|$.

2.2.1 Sampling of e^{-S_0}

This section refers to single spin-flip updates in the presence of a non-vanishing Ising action $S_0(C)$. This sampling scheme is used if the logical variable `Propose_S0` is set to `.true..`

Consider an Ising spin at space-time i, τ in the configuration C . Flipping this spin will generate the configuration C' and we will propose the move according to

$$T_0(C \rightarrow C') = \frac{e^{-S_0(C')}}{e^{-S_0(C')} + e^{-S_0(C)}} = 1 - \frac{1}{1 + e^{-S_0(C')}/e^{-S_0(C)}} \tag{30}$$

Updating schemes	Type	Description
<code>Propose_S0</code>	Logical	If true, proposes sequential local moves according to the probability e^{-S_0} .
<code>Global_tau_moves</code>	Logical	This option allows to carry out global moves on a single time slice. For a given time slice the user can define which part of the operator string is to be computed sequentially. This is specified by the variable <code>N_sequential_start</code> and <code>Nt_sequential_end</code> . A number of <code>N_tau_Global</code> user-defined global moves on the given time slice will then be carried out.
<code>Global_moves</code>	Logical	If true, allows for global moves in space and time. A user-defined number <code>N_Global</code> of global moves in space and time will be carried out at the end of each sweep.
<code>Tempering</code>	Compiling option	Requires MPI and runs the code in a parallel tempering mode, also see Sec. 2.2.5, 6.1.

Table 1: Variables required to control the updating scheme. Per default the program carries out sequential, single spin-flip sweeps, and logical variables are set to `false`.

Note that the function `S0` in the `Hamiltonian_example_mod.F90` module computes precisely the ratio $e^{-S_0(C')}/e^{-S_0(C)}$, therefore $T_0(C \rightarrow C')$ is obtained without any additional calculation. The proposed move is accepted with the probability:

$$P(C \rightarrow C') = \min \left(1, \frac{e^{-S_0(C)} W(C')}{e^{-S_0(C')} W(C)} \right). \quad (31)$$

Note that, as can be seen from Eq. (15), the bare action $S_0(C)$ determining the dynamics of the Ising spin in the absence of coupling to the fermions does not enter the Metropolis acceptance-rejection step.

2.2.2 Sequential single spin flips

The program adopts per default a sequential, single spin-flip strategy. It will visit sequentially each Hubbard-Stratonovich field in the space-time operator list and propose a spin flip. Consider the Ising spin $s_{i,\tau}$. We will flip it with probability 1, such that for this local move the proposal matrix is symmetric. If we are considering the Hubbard-Stratonovich field $l_{i,\tau}$ we will propose with probability 1/3 one of the other three possible fields. Again, for this local move, the proposal matrix is symmetric. Hence in both cases we will accept or reject the move according to

$$P(C \rightarrow C') = \min \left(1, \frac{W(C')}{W(C)} \right). \quad (32)$$

This default updating scheme can be overruled by, e.g., setting `Global_tau_moves` to `.true.` and not setting `Nt_sequential_start` and `Nt_sequential_end` (see Sec. 5.4.1). It is also worth noting that this type of sequential spin-flip updating does not satisfy detailed balance, but rather the more fundamental stationarity condition [42].

2.2.3 Global updates in space

This option allows one to carry out user-defined global moves on a single time slice. This option is enabled by setting the logical variable `Global_tau_moves` to `.true.`. To set the stage we recall that the propagation over a time step $\Delta\tau$ (see Eq. 20) can be written as:

$$e^{-V_{M_I+M_V}(s_{M_I+M_V,\tau})} \dots e^{-V_1(s_{1,\tau})} \prod_{k=1}^{M_T} e^{-\Delta\tau T^{(k)}} \quad (33)$$

where $e^{-V_n(s_n)}$ denotes one element of the operator list containing the HS fields. One can provide an interval of indices, `[Nt_sequential_start, Nt_sequential_end]`, in which the operators will be updated sequentially. Setting `Nt_sequential_start = 1` and `Nt_sequential_end = M_I + M_V` reproduces the sequential single spin flip strategy of the above section.

The variable `N_tau_Global` sets the number of global moves carried out on each time slice `ntau`. Each global move is generated in the routine `Global_move_tau`, which is provided by the user in the Hamiltonian file. In order to define this move, one specifies the following variables:

- `Flip_length`: An integer stipulating the number of spins to be flipped.
- `Flip_list(1:Flip_length)`: Integer array containing the indices of the operators to be flipped.
- `Flip_value(1:Flip_length)`: `Flip_value(n)` is an integer containing the new value of the HS field for the operator `Flip_list(n)`.
- `T0_Proposal_ratio`: Real number containing the quotient

$$\frac{T_0(C' \rightarrow C)}{T_0(C \rightarrow C')}, \quad (34)$$

where C' denotes the new configuration obtained by flipping the spins specified in the `Flip_list` array. Since we allow for a stochastic generation of the global move, it may very well be that no change is proposed. In this case, `T0_Proposal_ratio` takes the value 0 upon exit of the routine `Global_move_tau` and no update is carried out.

- `S0_ratio`: Real number containing the ratio $e^{-S_0(C')}/e^{-S_0(C)}$.

2.2.4 Global updates in time and space

The code allows for global updates as well. The user must then provide two additional functions in the module `Hamiltonian_Examples_mod.F90`: `Global_move` and `Delta_S0_global(Nsigma_old)`.

The subroutine `Global_move(T0_Proposal_ratio,nsigma_old,size_clust)` proposes a global move. Its single input is the variable `nsigma_old` of type `Field` (see Section 5.1.3) that contains the full configuration C stored in `nsigma_old%f(M_V + M_I, Ltrot)`. On output, the new configuration C' , determined by the user, is stored in the two-dimensional array `nsigma`, which is a global variable declared in the module `Hamiltonian`. Like for the global move in space (Sec. 2.2.3), `T0_Proposal_ratio` contains the proposal ratio $T_0(C' \rightarrow C)/T_0(C \rightarrow C')$. Since we allow for a stochastic generation of the global move, it may very well be that no change is proposed. In this case, `T0_Proposal_ratio` takes the value 0 upon exit, and `nsigma=nsigma_old`. The real-valued `size_clust` gives the size of the proposed move (e.g., $\frac{\text{Number of flipped spins}}{\text{Total number of spins}}$). This is used to calculate the average sizes of proposed and accepted moves which will be printed in the `info` file. The variable `size_clust` is not necessary for the simulation, but may help the user to estimate the effectiveness of the global update.

In order to compute the acceptance-rejection ratio, the user must also provide a function `Delta_S0_global(nsigma_old)` that computes the ratio $e^{-S_0(C')}/e^{-S_0(C)}$. Again, the configuration C' is given by the field `nsigma`.

The variable `N_Global` determines the number of global updates performed per sweep. Note that global updates are expensive, since they require a complete recalculation of the weight.

2.2.5 Parallel tempering

Exchange Monte Carlo [63], or parallel tempering [64], is a possible route to overcome sampling issues in parts of the parameter space. Let h be a parameter which one can vary without altering the configuration space $\{C\}$ and let us assume that for some values of h one encounters sampling problems. For example, in the realm of spin glasses, h could correspond to the inverse temperature. Here at high temperatures the phase space is easily sampled, but at low temperatures simulations get stuck in local minima. For quantum systems, h could trigger a quantum phase transition where sampling issues are encountered, for example, in the ordered phase and not in the disordered one. As its name suggests, parallel tempering carries out in parallel simulations at consecutive values of h : h_1, h_2, \dots, h_n , with $h_1 < h_2 < \dots < h_n$. One will sample the extended ensemble:

$$P([h_1, C_1], [h_2, C_2], \dots, [h_n, C_n]) = \frac{W(h_1, C_1)W(h_2, C_2) \cdots W(h_n, C_n)}{\sum_{C_1, C_2, \dots, C_n} W(h_1, C_1)W(h_2, C_2) \cdots W(h_n, C_n)} \quad (35)$$

where $W(h, C)$ corresponds to the weight for a given value of h and configuration C . Clearly, one can sample $P([h_1, C_1], [h_2, C_2], \dots, [h_n, C_n])$ by carrying out n independent runs. However, parallel tempering includes the following exchange step:

$$[h_1, C_1], \dots, [h_i, C_i], [h_{i+1}, C_{i+1}] \cdots, [h_n, C_n] \rightarrow [h_1, C_1], \dots, [h_i, C_{i+1}], [h_{i+1}, C_i] \cdots, [h_n, C_n] \quad (36)$$

which, for a symmetric proposal matrix, will be accepted with probability:

$$\min \left(1, \frac{W(h_i, C_{i+1})W(h_{i+1}, C_i)}{W(h_i, C_i)W(h_{i+1}, C_{i+1})} \right). \quad (37)$$

Thereby, a configuration can meander in parameter space h and explore regions where ergodicity is not an issue. In the context of spin-glasses, a low temperature configuration, stuck in a local minima, can heat up, overcome the potential barrier and then cool down again.

A judicious choice of the values h_i is important to obtain a good acceptance rate for the exchange step. With $W(h, C) = e^{-S(h, C)}$, the distribution of the action S reads:

$$\mathcal{P}(h, S) = \sum_C P(h, C) \delta(S(h, C) - S). \quad (38)$$

A given exchange step can only be accepted if the distributions $\mathcal{P}(h, S)$ and $\mathcal{P}(h + \Delta h, S)$ overlap. For $\langle S \rangle_h < \langle S \rangle_{h+\Delta h}$ one can formulate this requirement as:

$$\langle S \rangle_h + \langle \Delta S \rangle_h \simeq \langle S \rangle_{h+\Delta h} - \langle \Delta S \rangle_{h+\Delta h}, \text{ with } \langle \Delta S \rangle_h = \sqrt{\langle (S - \langle S \rangle_h)^2 \rangle_h}. \quad (39)$$

Assuming $\langle \Delta S \rangle_{h+\Delta h} \simeq \langle \Delta S \rangle_h$ and expanding in Δh one obtains:

$$\Delta h \simeq \frac{2\langle \Delta S \rangle_h}{\partial \langle S \rangle_h / \partial h}. \quad (40)$$

The above equation becomes transparent for classical systems with $S(h, C) = hH(C)$. In this case, the above equation reads:

$$\Delta h \simeq 2h \frac{\sqrt{C}}{C + h\langle H \rangle_h}, \text{ with } C = h^2 \langle (H - \langle H \rangle_h)^2 \rangle_h. \quad (41)$$

Several comments are in order.

- i) Let us identify h with the inverse temperature such that C corresponds to the specific heat. This quantity is extensive, as well as the energy, such that $\Delta h \simeq 1/\sqrt{N}$ where N is the system size.
- ii) In the proximity of a phase transition the specific heat can diverge, and h must be chosen with particular care.
- iii) Since the action is formulation dependent, one expects the acceptance of the exchange move to equally depend upon the formulation.

The quantum Monte Carlo code in the ALF project carries out parallel-tempering runs when the script `configure.sh` is called with the argument `Tempering` before compilation, see Sec. 6.1.

2.2.6 Langevin dynamics

For models that includes continuous real fields $\mathbf{s} \equiv \{s_{k,\tau}\}$ there is the option of using Langevin dynamics for the updating scheme, by setting the variable `Langevin` to `.true..` This corresponds to a stochastic differential equation for the fields. They acquire a discrete Langevin time t_l with step width δt_l and satisfy the stochastic differential equation

$$\mathbf{s}(t_l + \delta t_l) = \mathbf{s}(t_l) - \frac{\partial S(\mathbf{C})}{\partial \mathbf{s}(t_l)} \delta t_l + \sqrt{2\delta t_l} \boldsymbol{\eta}(t_l). \quad (42)$$

Here, $\boldsymbol{\eta}(t_l)$ are independent Gaussian stochastic variables satisfying:

$$\langle \eta_{k,\tau}(t_l) \rangle_\eta = 0 \text{ and } \langle \eta_{k,\tau}(t_l) \eta_{k',\tau'}(t'_l) \rangle_\eta = \delta_{k,k'} \delta_{\tau,\tau'} \delta_{t_l,t'_l} \quad (43)$$

We refer the reader to Ref. [65] for a more in depth introduction to stochastic differential equations. To see that the above indeed produces the desired probability distribution in the long Langevin time limit, we can transform the Langevin equation into the corresponding Fokker-Plank one. Let $P(\mathbf{s}, t_l)$ be the distribution of fields at Langevin time t_l . Then,

$$P(\mathbf{s}, t_l + \delta t_l) = \int D\mathbf{s}' P(\mathbf{s}', t_l) \left\langle \delta \left(\mathbf{s} - \left[\mathbf{s}' - \frac{\partial S(\mathbf{s}')}{\partial \mathbf{s}'} \delta t_l + \sqrt{2\delta t_l} \boldsymbol{\eta}(t_l) \right] \right) \right\rangle_\eta, \quad (44)$$

where δ corresponds to the $L_{\text{trot}} M_I$ dimensional Dirac δ -function. Taylor expanding up to order δt_l and averaging over the stochastic variable yields:

$$P(\mathbf{s}, t_l + \delta t_l) = \int D\mathbf{s}' P(\mathbf{s}', t_l) \times \left(\delta(\mathbf{s}' - \mathbf{s}) - \frac{\partial S(\mathbf{s}')}{\partial \mathbf{s}'} \frac{\partial}{\partial \mathbf{s}'} \delta(\mathbf{s}' - \mathbf{s}) \delta t_l + \frac{\partial}{\partial \mathbf{s}'} \frac{\partial}{\partial \mathbf{s}'} \delta(\mathbf{s}' - \mathbf{s}) \delta t_l^2 \right) + \mathcal{O}(\delta t_l^2). \quad (45)$$

Partial integration and taking the limit of infinitesimal time steps gives the Fokker-Plank equation

$$\frac{\partial}{\partial t_l} P(\mathbf{s}, t_l) = \frac{\partial}{\partial \mathbf{s}} \left(P(\mathbf{s}, t_l) \frac{\partial S(\mathbf{s})}{\partial \mathbf{s}} + \frac{\partial P(\mathbf{s}, t_l)}{\partial \mathbf{s}} \right). \quad (46)$$

The stationary, $\frac{\partial}{\partial t_l} P(\mathbf{s}, t_l) = 0$, normalizable, solution to the above equation corresponds to the desired probability distribution:

$$P(\mathbf{s}) = \frac{e^{-S(\mathbf{s})}}{\int D\mathbf{s} e^{-S(\mathbf{s})}}. \quad (47)$$

In order to formulate the Langevin dynamics, we will need to estimate the forces:

$$\frac{\partial S(C)}{\partial s_{k,\tau}} = \frac{\partial S_{0,I}(C)}{\partial s_{k,\tau}} + \frac{\partial S^F(C)}{\partial s_{k,\tau}}, \quad (48)$$

with the fermionic part of the action

$$S^F(C) = -\ln \left\{ \prod_{s=1}^{N_{\text{fl}}} \left[\det \left(\mathbb{1} + \prod_{\tau=1}^{L_{\text{Trotter}}} \prod_{k=1}^{M_V} e^{\sqrt{-\Delta\tau} \bar{U}_k \eta_{k,\tau} \mathbf{V}^{(ks)}} \prod_{k=1}^{M_I} e^{-\Delta\tau s_{k,\tau} \mathbf{I}^{(ks)}} \prod_{k=1}^{M_T} e^{-\Delta\tau \mathbf{T}^{(ks)}} \right) \right]^{N_{\text{col}}} \right\}. \quad (49)$$

The forces must be bounded for Langevin dynamics to work well. If this condition is violated the results produced by the code lose their reliability.

One possible source of divergence is the determinant in the fermionic action. Zeros lead to unbounded forces and, in order to circumvent this problem at least partially, we adopt a variable time step strategy in the code. The user provides an upper bound to the fermion force, **Max_Force** and, if the maximal force in a configuration, **Max_Force_Conf**, is larger than **Max_Force**, then the time step is rescaled as

$$\tilde{\delta t_l} = \frac{\text{Max_Force} * \delta t_l}{\text{Max_Force_Conf}}. \quad (50)$$

With the adaptive time step, averages are computed as:

$$\langle \hat{O} \rangle = \frac{\sum_n (\tilde{\delta t_l})_n \langle \hat{O} \rangle_{(C_n)}}{\sum_n (\tilde{\delta t_l})_n}. \quad (51)$$

In order to use Langevin dynamics the user also has to provide the Langevin time step **Delta_tau_Langevin** and the maximal force **Max_Force** in the **parameter** file. The routine **Langevin_update** in the module **Langevin_update_mod.F90** computes the fermion forces for a general model

$$\frac{\partial S^F(C)}{\partial s_{k,\tau}} = \Delta\tau N_{\text{col}} \sum_{s=1}^{N_{\text{fl}}} \text{Tr} \left[\mathbf{I}^{(ks)} \left(\mathbb{1} - \mathbf{G}^{(s)}(k, \tau) \right) \right]. \quad (52)$$

Here we introduce a Green function that depends on the time slice τ and the interaction term k to which the corresponding field $s_{k,\tau}$ belongs:

$$G_{x,y}^{(s)}(k, \tau) = \frac{\text{Tr} \left[\hat{U}_{(s)}^<(k, \tau) \hat{c}_{x,s} \hat{c}_{y,s}^\dagger \hat{U}_{(s)}^>(k, \tau) \right]}{\text{Tr} \left[\hat{U}_{(s)}^<(k, \tau) \hat{U}_{(s)}^>(k, \tau) \right]}, \quad (53)$$

where the following definitions are used

$$\hat{U}_{(s)}^<(k', \tau') = \prod_{\tau=\tau'+1}^{L_{\text{Trotter}}} \left(\hat{U}_{(s)}(\tau) \right) \prod_{k=1}^{M_V} e^{\sqrt{-\Delta\tau} \bar{U}_k \eta_{k,\tau} \hat{c}_s^\dagger \mathbf{V}^{(ks)} \hat{c}_s} \prod_{k=k'+1}^{M_I} e^{-\Delta\tau s_{k,\tau'} \hat{c}_s^\dagger \mathbf{I}^{(ks)} \hat{c}_s}, \quad (54)$$

$$\hat{U}_{(s)}^>(k', \tau') = \prod_{k=1}^{k'} e^{-\Delta\tau s_{k,\tau'} \hat{c}_s^\dagger \mathbf{I}^{(ks)} \hat{c}_s} \prod_{k=1}^{M_T} e^{-\Delta\tau \hat{c}_s^\dagger \mathbf{T}^{(ks)} \hat{c}_s} \prod_{\tau=1}^{\tau'-1} \left(\hat{U}_{(s)}(\tau) \right), \quad (55)$$

$$\hat{U}_{(s)}(\tau) = \prod_{k=1}^{M_V} e^{\sqrt{-\Delta\tau} \bar{U}_k \eta_{k,\tau} \hat{c}_s^\dagger \mathbf{V}^{(ks)} \hat{c}_s} \prod_{k=1}^{M_I} e^{-\Delta\tau s_{k,\tau} \hat{c}_s^\dagger \mathbf{I}^{(ks)} \hat{c}_s} \prod_{k=1}^{M_T} e^{-\Delta\tau \hat{c}_s^\dagger \mathbf{T}^{(ks)} \hat{c}_s}. \quad (56)$$

The vector \hat{c}_s^\dagger contains all fermionic operators $\hat{c}_{x,s}^\dagger$ of flavor s . The fermion forces are passed to the routine `Ham_Langevin_update` in the Hamiltonian file, where the user has to define the update rule for the fields according to Eq. (42). During each sweep all fields are updated and the Langevin time is incremented by δt_l . All updates are accepted to ensure ergodicity. At the end of a run, the mean and maximal forces encountered during the run are printed out in the info file.

The great advantage the Langevin updating scheme is the absence of update rejection, meaning that all fields are updated at each step. As mentioned above, the price we pay for using Langevin dynamics is ensuring that forces show no singularities, and two other potential issues should be highlighted:

- Langevin dynamics will be carried out at a finite Langevin time step, thereby introducing a further source of systematic error.
- The factor $\sqrt{2\delta t_l}$ multiplying the stochastic variable makes the noise dominant on short time scales. On these time scales Langevin dynamics essentially corresponds to a random walk. This has the advantage of allowing one to circumvent potential barriers, but may render the updating scheme less efficient than the hybrid molecular dynamics approach.

We have tested the code for a 6-site Hubbard chain at half-filling at $U/t = 4$, $\beta t = 4$. The Hubbard interaction can also be decoupled using a continuous HS transformation, where we introduce a real auxiliary field $s_{i,\tau}$ for every lattice site i and time slice τ . When the HS fields are coupled to the z -component of the magnetization (see Sec. 7.2), the partition function can be written as

$$Z = \int \left(\prod_{\tau=1}^{L_{\text{Trotter}}} \prod_{i=1}^{N_{\text{unit-cell}}} \frac{ds_{i,\tau}}{\sqrt{2\pi}} e^{-\frac{1}{2}s_{i,\tau}^2} \right) \times \prod_{s=\uparrow,\downarrow} \det \left(\mathbb{1} + \prod_{\tau=1}^{L_{\text{Trotter}}} \prod_{i=1}^{N_{\text{unit-cell}}} \left(e^{-\sqrt{\Delta\tau} \bar{U} s_{i,\tau} \mathbf{V}^{(is)}} \right) e^{-\Delta\tau \mathbf{T}} \right) + \mathcal{O}(\Delta\tau^2). \quad (57)$$

The flavor dependent interaction matrices have only one non-vanishing entry $V_{x,y}^{(i,s=\uparrow)} = \delta_{x,y} \delta_{x,i}$ and $V_{x,y}^{(i,s=\downarrow)} = -\delta_{x,y} \delta_{x,i}$ respectively. The forces of the Hubbard model are given by:

$$\frac{\partial S(C)}{\partial s_{i,\tau}} = s_{i,\tau} - \sqrt{\Delta\tau} \bar{U} \sum_{s=\uparrow,\downarrow} \text{Tr} \left[\mathbf{V}^{(is)} \left(\mathbb{1} - \mathbf{G}^{(s)}(i, \tau) \right) \right], \quad (58)$$

where the Green function is defined by eq. (53) with

$$\hat{U}_{(s)}^<(i', \tau') = \prod_{\tau=\tau'+1}^{L_{\text{Trotter}}} \left(\hat{U}_{(s)}(\tau) \right) \prod_{i=i'+1}^{N_{\text{unit-cell}}} e^{-\sqrt{\Delta\tau} \bar{U} s_{i,\tau'} \hat{c}_s^\dagger \mathbf{V}^{(is)} \hat{c}_s}, \quad (59)$$

$$\hat{U}_{(s)}^>(i', \tau') = \prod_{i=1}^{i'} \left(e^{-\sqrt{\Delta\tau} \bar{U} s_{i,\tau'} \hat{c}_s^\dagger \mathbf{V}^{(is)} \hat{c}_s} \right) e^{-\Delta\tau \hat{c}_s^\dagger \mathbf{T} \hat{c}_s} \prod_{\tau=1}^{\tau'-1} \left(\hat{U}_{(s)}(\tau) \right), \quad (60)$$

$$\hat{U}_{(s)}(\tau) = \prod_{i=1}^{N_{\text{unit-cell}}} \left(e^{-\sqrt{\Delta\tau} \bar{U} s_{i,\tau} \hat{c}_s^\dagger \mathbf{V}^{(is)} \hat{c}_s} \right) e^{-\Delta\tau \hat{c}_s^\dagger \mathbf{T} \hat{c}_s}. \quad (61)$$

One can show that for periodic boundary conditions the forces are not bounded and to make sure that the program does not crash we have set `Max_Force` = 1.5.

The discrete variable code gives

$$\langle \hat{H} \rangle = -3.4684 \pm 0.0007, \quad (62)$$

while the Langevin code at $\delta t_l = 0.001$ yields

$$\langle \hat{H} \rangle = -3.457 \pm 0.010 \quad (63)$$

and at $\delta t_l = 0.01$

$$\langle \hat{H} \rangle = -3.495 \pm 0.007. \quad (64)$$

At $\delta t_l = 0.001$ the maximal force that occurred during the run was 112, whereas at $\delta t_l = 0.01$ it grew to 524. In both cases the average force was given by 0.45. For larger values of δt_l the maximal force grows and the fluctuations on the energy become larger. ($\langle \hat{H} \rangle = -3.718439 \pm 0.206469$ at $\delta t_l = 0.02$. For this parameter set the maximal force we encountered during the run was of 1658.)

Controlling Langevin dynamics when the action has logarithmic divergences is a challenge, and it is not clear that the results will be satisfying. For our specific problem we can solve this issue by considering open boundary conditions. Following an argument put forward in [49], we can show, using world lines, that the determinant is always positive. In this case the action does not have logarithmic divergences and the Langevin dynamics works beautifully well, see Fig. 1.



Figure 1: Total energy for the 6-site Hubbard chain at $U/t = 4$, $\beta t = 4$ and with open boundary conditions. Here one can show that the determinant is always positive such that no singularities occur in the action, and consequently the Langevin dynamics works very well. The data point at $\delta t_l = 0$ stems from running the discrete field code with coupling of the field to the z-component of the magnetization. The extrapolated value of the energy reads -2.8710 ± 0.0011 and the reference result from the discrete code is -2.8711 ± 0.0004 . Throughout the runs the maximal force was always less than the threshold of 1.5.

2.3 The Trotter error and checkerboard decomposition

2.3.1 Asymmetric Trotter decomposition

In practice, many applications are carried out at finite imaginary time steps, and it is important to understand the consequences of the Trotter error. How does it scale with system size and what symmetries does it break? In particular, if one is investigating a critical point, then one should understand if the potential symmetry breaking associated with the Trotter decomposition generates relevant operators.

To at best describe the workings of the ALF code, we divide the Hamiltonian into hopping terms $\hat{\mathcal{H}}_T$ and interaction terms $\hat{\mathcal{H}}_V + \hat{\mathcal{H}}_I + \hat{\mathcal{H}}_{0,I}$. Let

$$\hat{\mathcal{H}}_T = \sum_{i=1}^{N_T} \sum_{k \in \mathcal{S}_i^T} \hat{T}^{(k)} \equiv \sum_{i=1}^{N_T} \hat{T}_i \quad (65)$$

Here the decomposition follows the rule that if k and k' belong to the same set \mathcal{S}_i^T then $[\hat{T}^{(k)}, \hat{T}^{(k')}] = 0$. As an example, we can mention the checkerboard decomposition. For the square lattice we can decouple the nearest neighbor hopping into $N_T = 4$ groups, each group consisting of two site hopping processes. This type of checkerboard decomposition is activated for a set of predefined lattices by setting the flag `Checkerboard` to `.true`. We will carry out the same decomposition for the interaction:

$$\hat{\mathcal{H}}_V + \hat{\mathcal{H}}_I + \hat{\mathcal{H}}_{0,I} = \sum_{i=1}^{N_I} \hat{\mathcal{O}}_i \quad (66)$$

where each $\hat{\mathcal{O}}_i$ contains a set of commuting terms. For instance, for the Hubbard model, the above reduces to $U \sum_i \hat{n}_{i,\uparrow} \hat{n}_{i,\downarrow}$ such the $N_T = 1$ and $\hat{\mathcal{O}}_1 = U \sum_i \hat{n}_{i,\uparrow} \hat{n}_{i,\downarrow}$.

The default Trotter decomposition in the ALF code is based on the equation:

$$e^{-\Delta\tau(\hat{A}+\hat{B})} = e^{-\Delta\tau\hat{A}}e^{-\Delta\tau\hat{B}} + \frac{\Delta\tau^2}{2} [\hat{B}, \hat{A}] + \mathcal{O}(\Delta\tau^3) \quad (67)$$

Using iteratively the above the single time step is given by:

$$e^{-\Delta\tau\mathcal{H}} = \prod_{i=1}^{N_O} e^{-\Delta\tau\hat{\mathcal{O}}_i} \prod_{j=1}^{N_T} e^{-\Delta\tau\hat{T}_j} + \underbrace{\frac{\Delta\tau^2}{2} \left(\sum_{i=1}^{N_O} \sum_{j=1}^{N_T} [\hat{T}_j, \hat{\mathcal{O}}_i] + \sum_{j'}^{N_T-1} [\hat{T}_{j'}, \hat{T}_{j'}^>] + \sum_{i'=1}^{N_O-1} [\hat{\mathcal{O}}_{i'}, \hat{\mathcal{O}}_{i'}^>] \right)}_{\equiv \Delta\tau\hat{\lambda}_1} + \mathcal{O}(\Delta\tau^3). \quad (68)$$

In the above, we have introduced the short hand notation

$$\hat{T}_n^> = \sum_{j=n+1}^{N_T} \hat{T}_j, \text{ and } \hat{\mathcal{O}}_n^> = \sum_{j=n+1}^{N_O} \hat{\mathcal{O}}_j. \quad (69)$$

The full propagation then reads

$$\hat{U}_{\text{Approx}} = \left(\prod_{i=1}^{N_O} e^{-\Delta\tau\hat{\mathcal{O}}_i} \prod_{j=1}^{N_T} e^{-\Delta\tau\hat{T}_j} \right) = e^{-\beta(\hat{H}+\hat{\lambda}_1)} + \mathcal{O}(\Delta\tau^2) = e^{-\beta\hat{H}} - \int_0^\beta d\tau e^{-(\beta-\tau)\hat{H}} \hat{\lambda}_1 e^{-\tau\hat{H}} + \mathcal{O}(\Delta\tau^2). \quad (70)$$

The last step follows from time-dependent perturbation theory. The following comments are in order:

- The error is anti-Hermitian since $\hat{\lambda}_1^\dagger = -\hat{\lambda}_1$. This has for consequence that if all the operators as well as the quantity being measured are all simultaneously real representable, then the prefactor of the linear in $\Delta\tau$ error vanishes since it ultimately corresponds to computing the trace of a anti-symmetric matrix. This *lucky* cancellation was put forward in Ref. [55]. Hence, under this assumption – which is certainly valid for the Hubbard model considered in Fig. 2 – the systematic error is of order $\Delta\tau^2$.
- The biggest drawback of the above decomposition is that the imaginary-time propagation is not Hermitian. This can lead to acausal features in imaginary-time correlation functions [66]. To be more precise, the eigenvalues of $H_{\text{Approx}} = -\frac{1}{\beta} \log U_{\text{Approx}}$ need not be real such that imaginary-time displaced correlation functions can have oscillatory behavior as a function of imaginary time. This is shown in Fig. 2 (a) that plots the absolute value of local time-displaced Green function for the Honeycomb lattice at $U/t = 2$. Sign changes of this quantity involve zeros that, on the considered log-scale, correspond to negative divergences. As we will see now, this issue can be solved by considering a symmetric Trotter decomposition.

2.3.2 Symmetric Trotter decomposition

To address the issue described above, the ALF library provides the possibility of using a symmetric Trotter decomposition,

$$e^{-\Delta\tau(\hat{A}+\hat{B})} = e^{-\Delta\tau\hat{A}/2} e^{-\Delta\tau\hat{B}} e^{-\Delta\tau\hat{A}/2} + \frac{\Delta\tau^3}{12} [2\hat{A} + \hat{B}, [\hat{B}, \hat{A}]] + \mathcal{O}(\Delta\tau^5), \quad (71)$$

which is activated with the `Symm` flag. In order to apply the expression above to our time step, we first write

$$e^{-\Delta\tau\mathcal{H}} = e^{-\frac{\Delta\tau}{2}\sum_{j=1}^{N_T}\hat{T}_j} e^{-\Delta\tau\sum_{i=1}^{N_I}\hat{O}_i} e^{-\frac{\Delta\tau}{2}\sum_{j=1}^{N_T}\hat{T}_j} + \underbrace{\frac{\Delta\tau^3}{12}\left[2\hat{T}_0^> + \hat{O}_0^>, [\hat{O}_0^>, \hat{T}_0^>]\right]}_{\equiv \Delta\tau\hat{\lambda}_{TO}} + \mathcal{O}(\Delta\tau^5). \quad (72)$$

Then, using,

$$e^{-\Delta\tau\sum_{i=1}^{N_I}\hat{O}_i} = \left(\prod_{i=1}^{N_O-1} e^{-\frac{\Delta\tau}{2}\hat{O}_i}\right) e^{-\Delta\tau\hat{O}_{N_O}} \left(\prod_{i=N_O-1}^1 e^{-\frac{\Delta\tau}{2}\hat{O}_i}\right) + \underbrace{\frac{\Delta\tau^3}{12}\sum_{i=1}^{N_O-1}\left[2\hat{O}_i + \hat{O}_i^>, [\hat{O}_i^>, \hat{O}_i]\right]}_{\equiv \Delta\tau\hat{\lambda}_O} + \mathcal{O}(\Delta\tau^5) \quad (73)$$

and

$$e^{-\frac{\Delta\tau}{2}\sum_{j=1}^{N_T}\hat{T}_j} = \left(\prod_{j=1}^{N_T-1} e^{-\frac{\Delta\tau}{4}\hat{T}_j}\right) e^{-\frac{\Delta\tau}{2}\hat{T}_{N_T}} \left(\prod_{j=N_T-1}^1 e^{-\frac{\Delta\tau}{4}\hat{T}_j}\right) + \underbrace{\frac{\Delta\tau^3}{96}\sum_{j=1}^{N_T-1}\left[2\hat{T}_j + \hat{T}_j^>, [\hat{T}_j^>, \hat{T}_j]\right]}_{\equiv \Delta\tau\hat{\lambda}_T} + \mathcal{O}(\Delta\tau^5) \quad (74)$$

we can derive a closed equation for the free energy density:

$$\begin{aligned} f_{\text{Approx}} &= -\frac{1}{\beta V} \log \text{Tr} \left[\left(\prod_{j=1}^{N_T-1} e^{-\frac{\Delta\tau}{4}\hat{T}_j} \right) e^{-\frac{\Delta\tau}{2}\hat{T}_{N_T}} \left(\prod_{j=N_T-1}^1 e^{-\frac{\Delta\tau}{4}\hat{T}_j} \right) \right. \\ &\quad \left(\prod_{i=1}^{N_O-1} e^{-\frac{\Delta\tau}{2}\hat{O}_i} \right) e^{-\Delta\tau\hat{O}_{N_O}} \left(\prod_{i=N_O-1}^1 e^{-\frac{\Delta\tau}{2}\hat{O}_i} \right) \\ &\quad \left. \left(\prod_{j=1}^{N_T-1} e^{-\frac{\Delta\tau}{4}\hat{T}_j} \right) e^{-\frac{\Delta\tau}{2}\hat{T}_{N_T}} \left(\prod_{j=N_T-1}^1 e^{-\frac{\Delta\tau}{4}\hat{T}_j} \right) \right]^{L_{\text{Trotter}}} \\ &= f - \frac{1}{V} \langle \hat{\lambda}_{TO} + \hat{\lambda}_O + 2\hat{\lambda}_T \rangle + \mathcal{O}(\Delta\tau^5). \end{aligned} \quad (75)$$

The following comments are in order:

- The approximate imaginary-time propagation from which the f_{Approx} is derived is Hermitian. Hence no spurious effects in imaginary-time correlation functions are to be expected. This is explicitly shown in Fig. 2(a).
- In Fig. 2(b) we have used the ALF-library with `Symm=.true.` with and without checkerboard decomposition. We still expect the systematic error to be of order $\Delta\tau^2$. However its prefactor is much smaller than that of the aforementioned anti-symmetric decomposition.
- We have taken the burden to evaluate explicitly the prefactor of the $\Delta\tau^2$ error on the free energy density. One can see that for Hamiltonians that are sums of local operators, $\langle \hat{\lambda}_{TO} + \hat{\lambda}_O + 2\hat{\lambda}_T \rangle$ will scale as the volume V of the system, such that the systematic error on the free energy density (and on correlations functions that can be computed by adding source terms) will be volume independent. For model Hamiltonians that are not sums of local terms, care must be taken. A conservative upper bound on the error is $\langle \hat{\lambda}_{TO} + \hat{\lambda}_O + 2\hat{\lambda}_T \rangle \propto \Delta\tau^2 V^3$, which means that, in order to maintain a constant systematic error for the free energy density, we have to keep $\Delta\tau V$ constant. Such a situation has been observed in Ref. [67].

2.3.3 The `Symm` flag

If the `Symm` flag is set to true, then the program will automatically – for the set of predefined lattices and models – use the symmetric $\Delta\tau$ time step of the interaction and hopping terms.



Figure 2: Analysis of Trotter systematic error. Left: We consider a 6×6 Hubbard model on the Honeycomb lattice, $U/t = 2$, half-band filling, inverse temperature $\beta t = 40$, and we have used Hubbard-Stratonovich transformation that couples to the density. The figure plots the local-time displaced Green function. Right: Here we consider the 6×6 Hubbard model at $U/t = 4$, half-band filling, inverse temperature $\beta t = 5$, and we have used the Hubbard Stratonovich transformation that couples to the z-component of spin. We provide data for the four combinations of the logical variables **Symm** and **Checkerboard**, where **Symm=.true.** (**.false.**) indicates a symmetric (asymmetric) Trotter decomposition has been used, and **Checkerboard=.true.** (**.false.**) that the checkerboard decomposition for the hopping matrix has (not) been used.

To save CPU time when the **Symm** flag is on we carry out the following approximation:

$$\left[\left(\prod_{j=1}^{N_T-1} e^{-\frac{\Delta\tau}{4} \hat{T}_j} \right) e^{-\frac{\Delta\tau}{2} \hat{T}_{N_T}} \left(\prod_{j=N_T-1}^1 e^{-\frac{\Delta\tau}{4} \hat{T}_j} \right) \right]^2 \simeq \left(\prod_{j=1}^{N_T-1} e^{-\frac{\Delta\tau}{2} \hat{T}_j} \right) e^{-\Delta\tau \hat{T}_{N_T}} \left(\prod_{j=N_T-1}^1 e^{-\frac{\Delta\tau}{2} \hat{T}_j} \right). \quad (76)$$

The above is consistent with the overall precision of the Trotter decomposition and more importantly conserves the Hermiticity of the propagation.

2.4 Stabilization - a peculiarity of the BSS algorithm

From the partition function in Eq. (15) it can be seen that, for the calculation of the Monte Carlo weight and of the observables, a long product of matrix exponentials has to be formed. In addition to that, we need to be able to extract the single-particle Green function for a given flavor index at, say, time slice $\tau = 0$. As mentioned above (cf. Eq. (19)), this quantity is given by:

$$\mathbf{G} = \left(\mathbb{1} + \prod_{\tau=1}^{L_{\text{Trotter}}} \mathbf{B}_{\tau} \right)^{-1}, \quad (77)$$

which can be recast as the more familiar linear algebra problem of finding a solution for the linear system

$$\left(\mathbb{1} + \prod_{\tau} \mathbf{B}_{\tau} \right) x = b. \quad (78)$$

The matrices $\mathbf{B}_{\tau} \in \mathbb{C}^{n \times n}$ depend on the lattice size as well as other physical parameters that can be chosen such that a matrix norm of \mathbf{B}_{τ} can be unbound in size. From standard perturbation theory for linear systems, the computed solution \tilde{x} would contain a relative error

$$\frac{|\tilde{x} - x|}{|x|} = \mathcal{O} \left(\epsilon \kappa_p \left(\mathbb{1} + \prod_{\tau} \mathbf{B}_{\tau} \right) \right), \quad (79)$$

where ϵ denotes the machine precision, which is 2^{-53} for IEEE double-precision numbers, and $\kappa_p(\mathbf{M})$ is the condition number of the matrix \mathbf{M} with respect to the matrix p -norm. Due to $\prod_{\tau} \mathbf{B}_{\tau}$ containing exponentially large and small scales, as can be seen in Eq. (15), a straightforward inversion turns out

to be completely ill-suited. That would lead the condition number, as a function of increasing inverse temperature, to grow exponentially, rendering the computed solution \tilde{x} meaningless.

In order to circumvent this, more sophisticated methods have to be employed. As a first step, assuming that the multiplication of **NWrap** \mathbf{B} matrices has an acceptable condition number and, for simplicity, that **NWrap** is a divisor of L_{Trotter} , we can write:

$$\mathbf{G} = \left(\mathbb{1} + \prod_{i=1}^{\frac{L_{\text{Trotter}}}{\text{NWrap}}} \underbrace{\prod_{\tau=1}^{\text{NWrap}} \mathbf{B}_{(i-1) \cdot \text{NWrap} + \tau}}_{\equiv \mathcal{B}_i} \right)^{-1}. \quad (80)$$

The default stabilization strategy in the auxiliary-field QMC implementation of the ALF project, is then to form a product of QR-decompositions, which was proven to be weakly backwards stable in [68]. The key idea is to efficiently separate the scales of a matrix from the orthogonal part of a matrix. This can be achieved using a QR decomposition of a matrix \mathbf{A} in the form $\mathbf{A}_i = \mathbf{Q}_i \mathbf{R}_i$. The matrix \mathbf{Q}_i is unitary and hence in the usual 2-norm it holds that $\kappa_2(\mathbf{Q}_i) = 1$. To get a handle on the condition number of \mathbf{R}_i we will form the diagonal matrix

$$(\mathbf{D}_i)_{n,n} = |(\mathbf{R}_i)_{n,n}| \quad (81)$$

and set $\tilde{\mathbf{R}}_i = \mathbf{D}_i^{-1} \mathbf{R}_i$. This gives the decomposition

$$\mathbf{A}_i = \mathbf{Q}_i \mathbf{D}_i \tilde{\mathbf{R}}_i. \quad (82)$$

\mathbf{D}_i now contains the row norms of the original \mathbf{R}_i matrix and hence attempts to separate off the total scales of the problem from \mathbf{R}_i . This is similar in spirit to the so-called matrix equilibration which tries to improve the condition number of a matrix through suitably chosen column and row scalings. Due to a theorem by van der Sluis [69] we know that the choice in Eq. (81) is almost optimal among all diagonal matrices \mathbf{D} from the space of diagonal matrices \mathcal{D} , in the sense that

$$\kappa_p((\mathbf{D}_i)^{-1} \mathbf{R}_i) \leq n^{1/p} \min_{\mathbf{D} \in \mathcal{D}} \kappa_p(\mathbf{D}^{-1} \mathbf{R}_i).$$

Now, given an initial decomposition of $\mathbf{A}_{j-1} = \prod_i \mathcal{B}_i = \mathbf{Q}_{j-1} \mathbf{D}_{j-1} \mathbf{T}_{j-1}$ an update $\mathcal{B}_j \mathbf{A}_{j-1}$ is formed in the following three steps:

1. Form $\mathbf{M}_j = (\mathcal{B}_j \mathbf{Q}_{j-1}) \mathbf{D}_{j-1}$. Note the parentheses.
2. Do a QR decomposition of $\mathbf{M}_j = \mathbf{Q}_j \mathbf{D}_j \mathbf{R}_j$. This gives the final \mathbf{Q}_j and \mathbf{D}_j .
3. Form the updated \mathbf{T} matrices $\mathbf{T}_j = \mathbf{R}_j \mathbf{T}_{j-1}$.

The effectiveness of the stabilization *has* to be judged for every simulation from the output file **info** (Sec. 5.4.2). For most simulations there are two values to look out for:

- **Precision Green**
- **Precision Phase**

The Green function, as well as the average phase, are usually numbers with a magnitude of $\mathcal{O}(1)$. For that reason we recommend that **NWrap** is chosen such that the mean precision is of the order of 10^{-8} or better (or further recommendations see Sec. 6.3). We include typical values of **Precision Phase** and of the mean and the maximal values of **Precision Green** in the example simulations discussed in Sec. 7.1.3 and Sec. 7.2.3.

3 Auxiliary Field Quantum Monte Carlo: projective algorithm

The projective approach is the method of choice if one is interested in ground-state properties. The starting point is a pair of trial wave functions, $|\Psi_{T,L/R}\rangle$, that are not orthogonal to the ground state $|\Psi_0\rangle$:

$$\langle \Psi_{T,L/R} | \Psi_0 \rangle \neq 0. \quad (83)$$

The ground-state expectation value of any observable \hat{O} can then be computed by propagation along the imaginary time axis:

$$\frac{\langle \Psi_0 | \hat{O} | \Psi_0 \rangle}{\langle \Psi_0 | \Psi_0 \rangle} = \lim_{\theta \rightarrow \infty} \frac{\langle \Psi_{T,L} | e^{-\theta \hat{H}} e^{-(\beta-\tau) \hat{H}} \hat{O} e^{-\tau \hat{H}} e^{-\theta \hat{H}} | \Psi_{T,R} \rangle}{\langle \Psi_{T,L} | e^{-(2\theta+\beta) \hat{H}} | \Psi_{T,R} \rangle}, \quad (84)$$

where β defines the imaginary time range where observables (time displaced and equal time) are measured and τ varies from 0 to β in the calculation of time-displace observables. The simulations are carried out at large but finite values of θ so as to guarantee convergence to the ground state within the statistical uncertainty. The trial wave functions are determined up to a phase, and the program uses this gauge choice to guarantee that

$$\langle \Psi_{T,L} | \Psi_{T,R} \rangle > 0. \quad (85)$$

In order to use the projective version of the code, the model's namespace in the `parameter` file must set `projector=.true.` and specify the value of the projection parameter `Theta`, as well as the imaginary time interval `Beta` in which observables are measured.

Note that time-displaced correlation functions are computed for a τ ranging from 0 to β . The implicit assumption in this formulation is that the projection parameter `Theta` suffices to reach the ground state. Since the computational time scales linearly with `Theta` large projections parameters are computationally not expensive.

3.1 Specification of the trial wave function

For each flavor, one needs to specify a left and a right trial wave function. In the ALF, they are assumed to be the ground state of single-particle trial Hamiltonians $\hat{H}_{T,L/R}$ and hence correspond to a single Slater determinant each. More specifically, we consider a single-particle Hamiltonian with the same symmetries (color and flavor) as the original Hamiltonian:

$$\hat{H}_{T,L/R} = \sum_{\sigma=1}^{N_{\text{col}}} \sum_{s=1}^{N_{\text{fl}}} \sum_{x,y}^{N_{\text{dim}}} \hat{c}_{x\sigma s}^\dagger h_{xy}^{(s,L/R)} \hat{c}_{y\sigma s}. \quad (86)$$

Ordering the eigenvalues of the Hamiltonian in ascending order yields the ground state

$$|\Psi_{T,L/R}\rangle = \prod_{\sigma=1}^{N_{\text{col}}} \prod_{s=1}^{N_{\text{fl}}} \prod_{n=1}^{N_{\text{part},s}} \left(\sum_{x=1}^{N_{\text{dim}}} \hat{c}_{x\sigma s}^\dagger U_{x,n}^{(s,L/R)} \right) |0\rangle, \quad (87)$$

where

$$U^{\dagger,(s,L/R)} h^{(s,L/R)} U^{(s,L/R)} = \text{Diag} \left(\epsilon_1^{(s,L/R)}, \dots, \epsilon_{N_{\text{dim}}}^{(s,L/R)} \right). \quad (88)$$

The trial wave function is hence completely defined by the set of orthogonal vectors $U_{x,n}^{(s,L/R)}$ for n ranging from 1 to the number of particles in each flavor sector, $N_{\text{part},s}$. This information is stored in the `WaveFunction` type defined in the module `WaveFunction_mod`. Note that owing to the $\text{SU}(N_{\text{col}})$ symmetry the color index is not necessary to define the trial wave function. The user will have to specify the trial wave function in the following way:

```
Do s = 1, N_fl
  Do x = 1, Ndim
    Do n = 1, N_part(s)
      WF_L(s)%P(x,n) = U^{(s,L)}_{x,n}
      WF_R(s)%P(x,n) = U^{(s,R)}_{x,n}
    Enddo
  Enddo
Enddo
```

In the above `WF_L` and `WF_R` are arrays of length N_{fl} and of type `WaveFunction`. ALF comes with a set of predefined trial wave functions, see Sec. 8.5.

Generically, the unitary matrix will be generated by a diagonalization routine such that if the ground state for the given particle number is degenerate, the trial wave function has a degree of ambiguity and

does not necessarily share the symmetries of the Hamiltonian $\hat{H}_{T,L/R}$. Since symmetries are the key for guaranteeing the absence of the negative sign problem, violating them in the choice of the trial wave function can very well lead to a sign problem. It is hence recommended to define the trial Hamiltonians $\hat{H}_{T,L/R}$ such that the ground state for the given particle number is non-degenerate. That can be checked using the value of `WL_L/R(s)%Degen`, which stores the energy difference between the last occupied and first un-occupied single particle state. If this value is greater than zero, then the trial wave function is non-degenerate and hence has all the symmetry properties of the trial Hamiltonians, $\hat{H}_{T,L/R}$. When the `projector` variable is set to `.true.`, this quantity is listed in the `info` file.

3.2 Some technical aspects of the projective code.

If one is interested solely in zero-temperature properties, the projective code offers many advantages. This comes from the related facts that the Green function matrix is a projector, and that scales can be omitted.

In the projective algorithm, it is known [6] that

$$G(x, \sigma, s, \tau | x', \sigma, s, \tau) = \left[1 - U_{(s)}^>(\tau) \left(U_{(s)}^<(\tau) U_{(s)}^>(\tau) \right)^{-1} U_{(s)}^<(\tau) \right]_{x, x'} \quad (89)$$

with

$$U_{(s)}^>(\tau) = \prod_{\tau'=1}^{\tau} \mathbf{B}_{\tau'}^{(s)} P^{(s),R} \quad \text{and} \quad U_{(s)}^<(\tau) = P^{(s),L,\dagger} \prod_{\tau'=L_{\text{Trotter}}}^{\tau+1} \mathbf{B}_{\tau'}^{(s)}, \quad (90)$$

where $\mathbf{B}_{\tau}^{(s)}$ is given by Eq. (20) and $P^{(s),L/R}$ correspond to the $N_{\text{dim}} \times N_{\text{part},s}$ submatrices of $U^{(s),L/R}$. To see that scales can be omitted, we carry out a singular value decomposition:

$$U_{(s)}^>(\tau) = \tilde{U}_{(s)}^>(\tau) d^> v^> \quad \text{and} \quad U_{(s)}^<(\tau) = v^< d^< \tilde{U}_{(s)}^<(\tau) \quad (91)$$

such that $\tilde{U}_{(s)}^>(\tau)$ corresponds to a set of column-wise orthogonal vectors. It can be readily seen that scales can be omitted, since

$$G(x, \sigma, s, \tau | x', \sigma, s, \tau) = \left[1 - \tilde{U}_{(s)}^>(\tau) \left(\tilde{U}_{(s)}^<(\tau) \tilde{U}_{(s)}^>(\tau) \right)^{-1} \tilde{U}_{(s)}^<(\tau) \right]_{x, x'}. \quad (92)$$

Hence, stabilization is never an issue for the projective code, and arbitrarily large projection parameters can be reached.

The form of the Green function matrix implies that it is a projector: $G^2 = G$. This property has been used in Ref. [78] to very efficiently compute imaginary-time-displaced correlation functions.

3.3 Comparison of finite and projective codes.

The finite temperature code operates in the grand canonical ensemble, whereas in the projective approach the particle number is fixed. On finite lattices, the comparison between both approaches can only be made at a temperature scale below which a finite-sized charge gap emerges. In Fig. 3 we consider a semi-metallic phase as realized by the Hubbard model on the Honeycomb lattice at $U/t = 2$. It is evident that, at a scale below which charge fluctuations are suppressed, both algorithms yield identical results.

4 Monte Carlo sampling

Error estimates in Monte Carlo simulations are based on the central limit theorem [70] and can be delicate. This theorem requires independent measurements and a finite variance. In this subsection we will give examples of the issues that a user will have to look out for while using a Monte Carlo code. Those effects are part of the common lore of the field and we can only cover them briefly in this text. For a deeper understanding of the inherent issues of Markov-chain Monte Carlo methods we refer the reader to the pedagogical introduction in chapter 1.3.5 of Krauth [71], the overview article of Sokal [42], the more specialized literature by Geyer [72] and chapter 6.3 of Neal [73].

In general, one distinguishes local from global updates. As the name suggest, the local update corresponds to a small change of the configuration, e.g., a single spin flip of one of the $L_{\text{Trotter}}(M_I + M_V)$ field

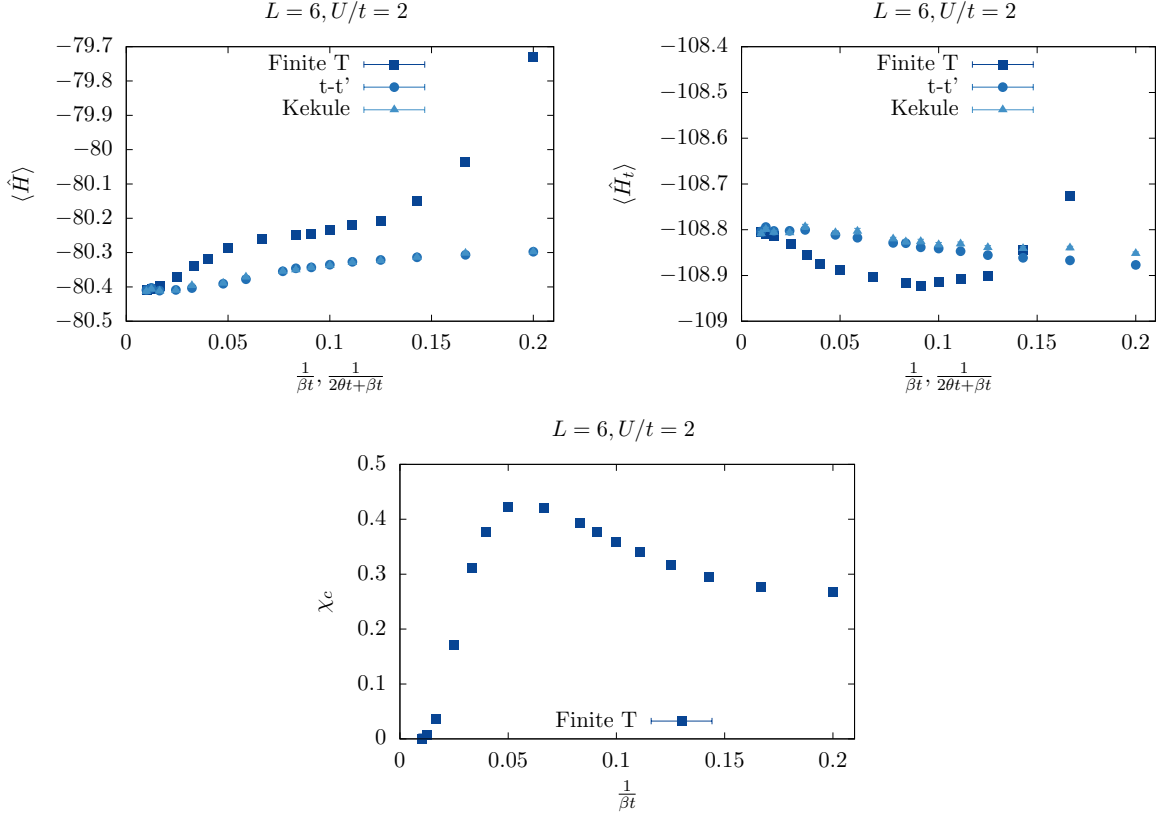


Figure 3: Comparison between the finite-temperature and projective codes for the Hubbard model on a 6×6 Honeycomb lattice at $U/t = 2$ and with periodic boundary conditions. For the projective code (blue and black symbols) $\beta t = 1$ is fixed, while θ is varied. In all cases we have $\Delta\tau t = 0.1$, no checkerboard decomposition, and a symmetric Trotter decomposition. For this lattice size and choice of boundary conditions, the non-interacting ground state is degenerate, since the Dirac points belong to the discrete set of crystal momenta. In order to generate the trial wave function we have lifted this degeneracy by either including a K ekul e mass term [25] that breaks translation symmetry (blue symbols), or by adding a next-next nearest neighbor hopping (black symbols) that breaks the symmetry nematically and shifts the Dirac points away from the zone boundary [79]. As apparent, both choices of trial wave functions yield the same answer, which compares very well with the finite temperature code at temperature scales below the finite-size charge gap.

entries (see Sec. 2.2), whereas a global update changes a significant part of the configuration. The default update scheme of the ALF implementation are local updates, such that there is a minimum number of moves required for generating an independent configuration. The associated time scale is called the autocorrelation time, T_{auto} , and is generically dependent upon the choice of the observables.

Our unit of *sweeps* is defined such that each field is visited twice in a sequential propagation from $\tau = 0$ to $\tau = L_{\text{Trotter}}$ and back. A single sweep will generically not suffice to produce an independent configuration. In fact, the autocorrelation time T_{auto} characterizes the required time scale to generate independent values of $\langle\langle\hat{O}\rangle\rangle_C$ for the observable O . This has several consequences for the Monte Carlo simulation:

- First of all, we start from a randomly chosen field configuration, such that one has to invest a time of *at least* one T_{auto} , but typically many more, in order to generate relevant, equilibrated configurations before reliable measurements are possible. This phase of the simulation is known as the warm-up or burn-in phase. In order to keep the code as flexible as possible (as different simulations might have different autocorrelation times), measurements are taken from the very beginning and, in the analysis phase, the parameter `n_skip` controls the number of initial bins that are ignored.
- Second, our implementation averages over bins with `NSWEEPS` measurements before storing the results on disk. The error analysis requires statistically independent bins in order to generate reliable confidence estimates. If the bins are instead too small (averaged over a period shorter than T_{auto}), then the error bars are typically underestimated. Most of the time, however, the autocorrelation time is unknown before the simulation is started and, sometimes, single runs long enough to generate appropriately sized bins are not feasible. For this reason, we provide a rebinning facility controlled by the parameter `N_rebin` that specifies the number of bins recombined into each new bin during the error analysis. One can test the suitability of a given bin size by verifying whether a increase in size changes the error estimate (For an explicit example, see Sec. 4.2 and the appendix of Ref. [52]).

The `N_rebin` variable can be used to control a further issue. The distribution of the Monte Carlo estimates $\langle\langle\hat{O}\rangle\rangle_C$ is unknown, while a result in the form (mean \pm error) assumes a Gaussian distribution. Every distribution with a finite variance turns into a Gaussian one once it is folded often enough (central limit theorem). Due to the internal averaging (folding) within one bin, many observables are already quite Gaussian. Otherwise one can increase `N_rebin` further, even if the bins are already independent [74].

- The third issue concerns time-displaced correlation functions. Even if the configurations are independent, the fields within the configuration are still correlated. Hence, the data for $S_{\alpha,\beta}(\mathbf{k}, \tau)$ (see Sec. 5.2; Eq. (119)) and $S_{\alpha,\beta}(\mathbf{k}, \tau + \Delta\tau)$ are also correlated. Setting the switch `N_Cov=1` triggers the calculation of the covariance matrix in addition to the usual error analysis. The covariance is defined by

$$COV_{\tau\tau'} = \frac{1}{N_{\text{Bin}}} \langle (S_{\alpha,\beta}(\mathbf{k}, \tau) - \langle S_{\alpha,\beta}(\mathbf{k}, \tau) \rangle) (S_{\alpha,\beta}(\mathbf{k}, \tau') - \langle S_{\alpha,\beta}(\mathbf{k}, \tau') \rangle) \rangle. \quad (93)$$

An example where this information is necessary is the calculation of mass gaps extracted by fitting the tail of the time-displaced correlation function. Omitting the covariance matrix will underestimate the error.

4.1 The Jackknife resampling method

For each observable $\hat{A}, \hat{B}, \hat{C} \dots$ the Monte Carlo program computes a data set of N_{Bin} (ideally) independent values where for each observable the measurements belong to the same statistical distribution. In the general case, we would like to evaluate a function of expectation values, $f(\langle\hat{A}\rangle, \langle\hat{B}\rangle, \langle\hat{C}\rangle \dots)$ – see for example the expression (24) for the observable including reweighting – and are interested in the statistical estimates of its mean value and the standard error of the mean. A numerical method for the statistical analysis of a given function f which properly handles error propagation and correlations among the observables is the Jackknife method, which is, like the related Bootstrap method, a resampling scheme [75]. Here we briefly review the *delete-1 Jackknife* scheme, which consists in generating N_{bin} new data sets of size $N_{\text{bin}} - 1$ by consecutively removing one data value from the original set. By $A_{(i)}$ we denote

the arithmetic mean for the observable \hat{A} , without the i -th data value A_i , namely

$$A_{(i)} \equiv \frac{1}{N_{\text{Bin}} - 1} \sum_{k=1, k \neq i}^{N_{\text{Bin}}} A_k. \quad (94)$$

As the corresponding quantity for the function $f(\langle \hat{A} \rangle, \langle \hat{B} \rangle, \langle \hat{C} \rangle \dots)$, we define

$$f_{(i)}(\langle \hat{A} \rangle, \langle \hat{B} \rangle, \langle \hat{C} \rangle \dots) \equiv f(A_{(i)}, B_{(i)}, C_{(i)} \dots). \quad (95)$$

Following the convention in the literature, we will denote the final Jackknife estimate of the mean by $f_{(\cdot)}$ and its standard error by Δf . The Jackknife mean is given by

$$f_{(\cdot)}(\langle \hat{A} \rangle, \langle \hat{B} \rangle, \langle \hat{C} \rangle \dots) = \frac{1}{N_{\text{Bin}}} \sum_{i=1}^{N_{\text{Bin}}} f_{(i)}(\langle \hat{A} \rangle, \langle \hat{B} \rangle, \langle \hat{C} \rangle \dots), \quad (96)$$

and the standard error, including bias correction, is given by

$$(\Delta f)^2 = \frac{N_{\text{Bin}} - 1}{N_{\text{Bin}}} \sum_{i=1}^{N_{\text{Bin}}} \left[f_{(i)}(\langle \hat{A} \rangle, \langle \hat{B} \rangle, \langle \hat{C} \rangle \dots) - f_{(\cdot)}(\langle \hat{A} \rangle, \langle \hat{B} \rangle, \langle \hat{C} \rangle \dots) \right]^2. \quad (97)$$

In case of $f = \langle \hat{A} \rangle$, the results (96) and (97) reduce to the plain sample average and the standard, bias corrected, estimate of the error.

4.2 An explicit example of error estimation

In the following we use one of our examples, the Hubbard model on a square lattice in the M_z Hubbard-Stratonovich decoupling (see Sec. 7.2), to show explicitly how to estimate errors. We will show as well that the autocorrelation time is dependent upon the choice of the observable. In fact, different observables within the same run can have different autocorrelation times and, of course, this time scale depends on the parameter choice. Hence, the user has to check autocorrelations of individual observables for each simulation! Typical regions of the phase diagram that require special attention are critical points where length scales diverge.

In order to determine the autocorrelation time, we calculate the correlation function

$$S_{\hat{O}}(t_{\text{QMC}}) = \sum_{i=0}^{N_{\text{Bin}} - t_{\text{QMC}}} \frac{(O_i - \langle \hat{O} \rangle) (O_{i+t_{\text{QMC}}} - \langle \hat{O} \rangle)}{(O_i - \langle \hat{O} \rangle) (O_i - \langle \hat{O} \rangle)}, \quad (98)$$

where O_i refers to the Monte Carlo estimate of the observable \hat{O} in the i^{th} bin. This function typically shows an exponential decay and the decay rate defines the autocorrelation time. Figure 4(a) shows the autocorrelation functions $S_{\hat{O}}(t_{\text{QMC}})$ for three spin-spin-correlation functions [Eq. (119)] at momentum $\mathbf{k} = (\pi, \pi)$ and at $\tau = 0$:

$\hat{O} = S_{\hat{S}_z}$ for the z spin direction, $\hat{O} = (S_{\hat{S}_x} + S_{\hat{S}_y})/2$ for the xy plane, and $\hat{O} = (S_{\hat{S}_x} + S_{\hat{S}_y} + S_{\hat{S}_z})/3$ for the total spin. The Hubbard model has a $SU(2)$ spin symmetry. However, we chose a HS field which couples to the z -component of the magnetization, M_z , such that each configuration breaks this symmetry. Of course, after Monte Carlo averaging one expects restoration of the symmetry. The model, on bipartite lattices, shows spontaneous spin-symmetry breaking at $T = 0$ and in the thermodynamic limit. At finite temperatures, and within the so-called renormalized classical regime, quantum antiferromagnets have a length scale that diverges exponentially with decreasing temperatures [76]. The parameter set chosen for Fig. 4 is non-trivial in the sense that it places the Hubbard model in this renormalized classical regime where the correlation length is substantial. Figure 4 clearly shows a very short autocorrelation time for the xy -plane whereas we detect a considerably longer autocorrelation time for the z -direction. This is a direct consequence of the *long* magnetic length scale and the chosen decoupling. The physical reason for the long autocorrelation time corresponds to the restoration of the $SU(2)$ spin symmetry. This insight can be used to define an improved, $SU(2)$ symmetric estimator for the spin-spin correlation function, namely $(S_{\hat{S}_x} + S_{\hat{S}_y} + S_{\hat{S}_z})/3$. Thereby, global spin rotations are no longer an issue and this improved estimator shows the shortest autocorrelation time, as can be clearly seen in Fig. 4(b). Other ways to tackle large autocorrelations are global updates and parallel tempering.



Figure 4: The autocorrelation function $S_{\hat{O}}(t_{QMC})$ (a) and the scaling of the error with effective bin size (b) of three equal-time, spin-spin correlation functions \hat{O} of the Hubbard model in the M_z decoupling (see Sec. 7.2). Simulations were done on a 6×6 square lattice, with $U/t = 4$ and $\beta t = 6$. The original bin contained only one sweep and we calculated around one million bins on a single core. The different autocorrelation times for the xy -plane compared to the z -direction can be detected from the decay rate of the autocorrelation function (a) and from the point where saturation of the error sets in (b), which defines the required effective bin size for independent measurements. The improved estimator $(S_{\hat{S}_x} + S_{\hat{S}_y} + S_{\hat{S}_z})/3$ appears to have the smallest autocorrelation time, as argued in the text.

A simple method to obtain estimates of the mean and its standard error from the time series of Monte Carlo samples is provided by the aforementioned facility of rebinning. Also known in the literature as rebatching, it consists in aggregating a fixed number N_{rebin} of adjacent original bins into a new effective bin. In addition to measuring the decay rate of the autocorrelation function (Eq. (98)), a measure for the autocorrelation time can be also obtained by the rebinning method. For a comparison to other methods of estimating the autocorrelation time we refer the reader to the literature [77, 72, 73]. A reliable error analysis requires independent bins, otherwise the error is typically underestimated. This behavior is observed in Fig. 4 (b), where the effective bin size is systematically increased by rebinning. If the effective bin size is smaller than the autocorrelation time the error will be underestimated. When the effective bin size becomes larger than the autocorrelation time, converging behavior sets in and the error estimate becomes reliable.

For the analysis of the Monte Carlo data (see Sec. 6.2), the user can provide a finite value for N_{auto} to trigger the computation of autocorrelation functions $S_{\hat{O}}(t_{QMC})$ in the range $t_{QMC} = [0, N_{auto}]$. Since these computations are quite time consuming and require many Monte Carlo bins, the default value is $N_{auto}=0$. For Fig. 4, we set $N_{auto} = 500$ and used a total of approximately one million bins.

4.3 Pseudo code description

Basic structure of the auxiliary-field QMC implementation (Prog/main.F90):

Set the Hamiltonian and the lattice:

Call ham_set

Read in an auxiliary-field configuration or generate it randomly:

Call field%in

This loop fills the storage needed for the first actual Monte Carlo sweep:

Do ntau from 1 to 1

 Compute propagation matrices and store them at the stabilization points:

Call wrapul

Enddo

Loop over bins:

```

Do nbc from 1 to nbin
  Loop over sweeps. Each sweep updates twice (upward and downward in time) the whole
  space-time lattice of auxiliary fields. The sweep defines the unit of Monte Carlo time:
  Do nsweep from 1 to nsweep
    Upward sweep:
    Do ntau from 1 to ltrot
      Propagate the Green function from time ntau-1 to ntau, and compute a new
      estimate (using sequential update scheme) of the Green function at ntau:
      Call wrapgrup

      Stabilization:
      If ntau equals stabilization point in imaginary time then
        Compute propagation matrix from previous stabilization point to ntau:
        Call wrapur
        Read from storage: propagation from ltrot to ntau
        Write to storage: the just-computed propagation
        Recalculate the Green function at time ntau in a stable way:
        Call cgr
        Check the precision between propagated and recalculated Green functions:
        Call control_precisionG
      Endif

      Measure the equal-time observables:
      If ntau is in the intervall [LOBS_ST, LOBS_EN] then
        Call obser
      Endif
    Enddo

    Downward sweep:
    Do ntau from ltrot to 1
      Repeat the above steps (update, propagation, stabilization, equal-time measurements)
      for the downward direction in imaginary time
    Enddo

    Measure the time-displaced observables:
    Call tau_m
  Enddo (loop over sweeps)

  Calculate measurement averages for current bin and write them to disk:
  Call pr_obs
  Write auxiliary-field configuration to disk:
  Call field%out
Enddo (loop over bins)

```

5 Data Structures and Input/Output

We have to restructure this section. As it stands it is a chaos. We have to separate more clearly data structures, specification of the model, and the Input output.

5.1 Implementation of the Hamiltonian and the lattice

The module `Hamiltonian` defines the model Hamiltonian, the lattice under consideration and the desired observables (Table 2). This module can be found in the file `Hamiltonian_Examples_mod.F90`, which also contains a number of example Hamiltonians, lattices and observables. The examples are described in Sec. 12. In order to implement a user-defined model, only the module `Hamiltonian` has to be set up. Accordingly, this documentation focuses almost entirely on this module and the subprograms it includes. The remaining parts of the code may hence be treated as a black box.

In order to specify the Hamiltonian, one needs an **Operator** and a **Lattice** types, as well as a type for the observables. These three data structures are described in the following sections.

Subprogram	Description	Section
Ham_Set	Reads in model and lattice parameters from the file <code>parameters</code> ; sets the Hamiltonian calling the necessary subprograms.	5.1
Ham_V	Sets the interaction term $\hat{\mathcal{H}}_V$ (i.e., operator <code>Op_V</code> , Sec. 5.1.1).	5.1.2
S0	Returns an update ratio for the Ising term $\hat{\mathcal{H}}_{I,0}$.	2.2.1
Setup_Ising_action	Sets bonds and median lattice for the Ising bond fields.	12.1
Global_move	Generates a global move and returns <code>T0_Proposal_ratio</code> .	2.2.3
Delta_S0_global	Computes the ratio $e^{-S_0(C')}/e^{-S_0(C)}$.	2.2.3
Global_move_tau	Generates a global move on a given time slice τ and returns <code>T0_Proposal_ratio</code> (see Eq. (34)).	2.2.4
Alloc_obs	Assigns memory storage to the observables.	
Obser	Computes the scalar and equal-time observables.	5.2
ObserT	Computes time-displaced correlation functions.	5.2
<code>Hamiltonian_set_</code>		
<code>nsigma</code>	Sets the initial field.	
<code>Override_global_tau_</code>		
<code>sampling_parameters</code>	Allows setting <code>global_tau</code> parameters at run time.	
<code>Init_obs</code>	Initializes the observables to zero.	
<code>Pr_obs</code>	Writes the observables to disk by calling <code>Print_bin</code> .	

Table 2: Overview of the subprograms of the module `Hamiltonian`, contained in `Hamiltonian_Examples_mod.F90`, used to define the Hamiltonian, the lattice and the observables. The highlighted subroutines may have to be modified by the user.

5.1.1 The Operator type

The fundamental data structure in the code is the **Operator**. It is implemented as a Fortran derived data type designed to efficiently define the Hamiltonian (2).

Let the matrix \mathbf{X} of dimension $N_{\text{dim}} \times N_{\text{dim}}$ stand for any of the typically sparse, Hermitian matrices $\mathbf{T}^{(ks)}$, $\mathbf{V}^{(ks)}$ and $\mathbf{I}^{(ks)}$ that define the Hamiltonian. Furthermore, let $\{z_1, \dots, z_N\}$ denote a subset of N indices for which

$$X_{x,y} \begin{cases} \neq 0 & \text{if } x, y \in \{z_1, \dots, z_N\} \\ = 0 & \text{otherwise.} \end{cases} \quad (99)$$

Usually, we have $N \ll N_{\text{dim}}$. We define the $N \times N_{\text{dim}}$ matrices \mathbf{P} as

$$P_{i,x} = \delta_{z_i,x} , \quad (100)$$

where $i \in [1, \dots, N]$ and $x \in [1, \dots, N_{\text{dim}}]$. The matrix \mathbf{P} selects the non-vanishing entries of \mathbf{X} , which are contained in the rank- N matrix \mathbf{O} defined by:

$$\mathbf{X} = \mathbf{P}^T \mathbf{O} \mathbf{P} , \quad (101)$$

and

$$X_{x,y} = \sum_{i,j} P_{i,x} O_{i,j} P_{j,y} = \sum_{i,j} \delta_{z_i,x} O_{ij} \delta_{z_j,y} . \quad (102)$$

Since the \mathbf{P} matrices have only one non-vanishing entry per column, they can conveniently be stored as a vector \mathbf{P} , with entries

$$P_i = z_i . \quad (103)$$

There are many useful identities which emerge from this structure. For example:

$$e^{\mathbf{X}} = e^{\mathbf{P}^T \mathbf{O} \mathbf{P}} = \sum_{n=0}^{\infty} \frac{(\mathbf{P}^T \mathbf{O} \mathbf{P})^n}{n!} = \mathbb{1} + \mathbf{P}^T (e^{\mathbf{O}} - \mathbb{1}) \mathbf{P}, \quad (104)$$

since

$$\mathbf{P} \mathbf{P}^T = \mathbb{1}_{N \times N}. \quad (105)$$

In the code, we define a structure called `Operator` to capture the above. This type `Operator` bundles several components, listed in Table 3, that are needed to define and use an operator matrix in the program.

5.1.2 Specification of the model

Variable	Type	Description
<code>Op_X%N</code>	Integer	Effective dimension N
<code>Op_X%O</code>	Complex	Matrix \mathbf{O} of dimension $N \times N$
<code>Op_X%P</code>	Integer	Matrix \mathbf{P} encoded as a vector of dimension N
<code>Op_X%g</code>	Complex	Coupling strength g
<code>Op_X%alpha</code>	Complex	Constant α
<code>Op_X%type</code>	Integer	Sets the type of HS transformation (1: Ising; 2: discrete HS for perfect-square term; 3: continuous real field.)
<code>Op_X%diag</code>	Logical	True if \mathbf{O} is diagonal
<code>Op_X%U</code>	Complex	Matrix containing the eigenvectors of \mathbf{O}
<code>Op_X%E</code>	Real	Eigenvalues of \mathbf{O}
<code>Op_X%N_non_zero</code>	Integer	Number of non-vanishing eigenvalues of \mathbf{O}
<code>Op_X%M_exp</code>	Complex	Stores $\mathbf{M_exp}(:, :, s) = e^{g\phi(s, \text{type})\mathbf{O}(:, :)}$
<code>Op_X%E_exp</code>	Complex	Stores $\mathbf{E_exp}(:, s) = e^{g\phi(s, \text{type})\mathbf{E}(:)}$

Table 3: Member variables of the `Operator` type. In the left column, the letter **X** is a placeholder for the letters **T** and **V**, indicating hopping and interaction operators, respectively. The highlighted variables must be specified by the user. `M_exp` and `E_exp` are allocated only if `type` = 1, 2.

In this section we show how the Hamiltonian (2) is specified in the code. Notice that ALF comes with predefined structures (Sec. 8) which the user can combine together or use as templates for defining new Hamiltonians.

In order to specify a Hamiltonian, we have to set the matrix representation of the imaginary-time propagators, $e^{-\Delta\tau \mathbf{T}^{(ks)}}$, $e^{\sqrt{-\Delta\tau} \mathbf{U}_k \eta_{k\tau} \mathbf{V}^{(ks)}}$ and $e^{-\Delta\tau s_{k\tau} \mathbf{I}^{(ks)}}$, that appear in the partition function (15). For each pair of indices (k, s) , these terms have the general form

$$\text{Matrix Exponential} = e^{g\phi(\text{type})\mathbf{X}}. \quad (106)$$

In case of the perfect-square term, we additionally have to set the constant α , see the definition of the operators $\hat{\mathbf{V}}^{(k)}$ in Eq. (4). The data structures which hold all the above information are variables of the type `Operator` (see Table 3). For each pair of indices (k, s) , we store the following parameters in an `Operator` variable:

- \mathbf{P} and \mathbf{O} defining the matrix \mathbf{X} [see Eq. (101)],
- the constants g , α ,
- optionally: the type `type` of the discrete fields ϕ .

The latter parameter can take one of three values: Ising (1), discrete HS (2), and real (3), as detailed in Sec. 5.1.3. Note that we have dropped the color index σ , since the implementation uses the $SU(N_{\text{col}})$ invariance of the Hamiltonian.

Accordingly, the following data structures fully describe the Hamiltonian (2):

- For the hopping Hamiltonian (3), we have to set the exponentiated hopping matrices $e^{-\Delta\tau \mathbf{T}^{(ks)}}$: In this case $\mathbf{X}^{(ks)} = \mathbf{T}^{(ks)}$, and a single variable `Op_T` describes the operator matrix

$$\left(\sum_{x,y}^{N_{\text{dim}}} \hat{c}_x^\dagger T_{xy}^{(ks)} \hat{c}_y \right), \quad (107)$$

where $k = [1, M_T]$ and $s = [1, N_{\text{fl}}]$. In the notation of the general expression (106), we set $g = -\Delta\tau$ (and $\alpha = 0$). In case of the hopping matrix, the type variable `Op_T%type` is neglected by the code. All in all, the corresponding array of structure variables is `Op_T(M_T, N_fl)`.

- For the interaction Hamiltonian (4), which is of perfect-square type, we have to set the exponentiated matrices $e^{\sqrt{-\Delta\tau U_k} \eta_{k\tau} \mathbf{V}^{(ks)}}$: In this case, $\mathbf{X} = \mathbf{V}^{(ks)}$ and a single variable `Op_V` describes the operator matrix:

$$\left[\left(\sum_{x,y}^{N_{\text{dim}}} \hat{c}_x^\dagger V_{x,y}^{(ks)} \hat{c}_y \right) + \alpha_{ks} \right], \quad (108)$$

where $k = [1, M_V]$ and $s = [1, N_{\text{fl}}]$, $g = \sqrt{-\Delta\tau U_k}$ and $\alpha = \alpha_{ks}$. The discrete Hubbard-Stratonovich decomposition which is used for the perfect-square interaction, is selected by setting the type variable to `Op_V%type = 2`. All in all, the required structure variables `Op_V` are defined using the array `Op_V(M_V, N_fl)`.

- For the Ising interaction Hamiltonian (5), we have to set the exponentiated matrices $e^{-\Delta\tau s_{k\tau} \mathbf{I}^{(ks)}}$: In this case, $\mathbf{X} = \mathbf{I}^{(k,s)}$ and a single variable `Op_V` then describes the operator matrix:

$$\left(\sum_{x,y}^{N_{\text{dim}}} \hat{c}_x^\dagger I_{xy}^{(ks)} \hat{c}_y \right), \quad (109)$$

where $k = [1, M_I]$ and $s = [1, N_{\text{fl}}]$ and $g = -\Delta\tau$ (and $\alpha = 0$). The Ising interaction is specified by setting the type variable `Op_V%type=1`. All in all, the required structure variables are contained in the array `Op_V(M_I, N_fl)`.

- In case of a full interaction [perfect-square term (4) and Ising term (5)], we define the corresponding doubled array `Op_V(M_V+M_I, N_fl)` and set the variables separately for both ranges of the array according to the above.

5.1.3 Handling of the fields: the `Fields` type

The partition function (see Sec. 2.1) consists of terms which, in general, can be written as $\gamma e^{g\phi \mathbf{X}}$, where \mathbf{X} denotes an arbitrary operator, g is a constant, and γ and ϕ are fields. For such auxiliary fields a dedicated type `Fields` is defined, whose components, listed in Table 5.1.3, include the variables `Field%f` and `Field%t`, which store the field values and types, respectively, and functions such as `Field%flip`, which flips the field values randomly (as there are only two Ising states, $s_{k,\tau} = \pm 1$, it simply inverts the sign for those).

For an Ising term, we store type `t=1`, which sets $\gamma_{k,\tau} = 1$ and $\phi_{k,\tau} = s_{k,\tau} = \pm 1$. In the case of a perfect-square term, the fields results from the discrete HS transformation (10) and we store `t=2`, which sets $\gamma_{k,\tau} = s_{k,\tau}$ and $\phi_{k,\tau} = \eta_{k,\tau}$ (see Eq. 11). For continuous real fields f we store `t=3`, which sets $\gamma_{k,\tau} = 1$ and $\phi_{k,\tau} = f$.

5.1.4 The `Lattice` and `Unit_cell` types

ALF's lattice module can generate one- and two-dimensional Bravais lattices. Both the lattice and the unit cell are defined in the module `Lattices_v3_mod.F90` and their components are detailed in Tables 5 and 6. Note that the orbital structure of each unit cell has to be specified by the user in the Hamiltonian module – however, the `Predefined_Latt_mod.F90` also provides, as its name suggests, predefined lattices, described in Sec. 8.1. The user who wishes to defined their own lattice also has to specify unit vectors \mathbf{a}_1 and \mathbf{a}_2 , as well as the size of the lattice, characterized by the vectors \mathbf{L}_1 and \mathbf{L}_2 . The lattice is placed on a torus (periodic boundary conditions):

$$\hat{c}_{\mathbf{i}+\mathbf{L}_1} = \hat{c}_{\mathbf{i}+\mathbf{L}_2} = \hat{c}_{\mathbf{i}}. \quad (110)$$

The function call

Component	Description	
Variable	Type	
Field%f(:,:)	Real	Defines the auxiliary fields. The first index runs through the operator sequence and the second through the time slices.
Field%t(:)	Integer	Sets the HS transformation type (1: Ising; 2: discrete HS for perfect-square term; 3: continuous real field). The index denotes the operator.
Field%del	Real	Width Δx of the uniform random initial configuration for fields of type t=3 , with a default value of 1.
Field%amplitude	Real	Width of a random flip for fields of type t=3 , defaults to 1.
Method(arguments)		
Fields_init(del)		Initializes internal variables such as $s_{k,\tau}$ and $\eta_{k,\tau}$, the variable del = Δx (see above) is optional.
Field%make(n_op,n_tau)		Reserves memory for the field.
Field%clear()		Clears field from memory.
Field%set()		Sets a random configuration.
Field%flip(n_op,n_tau)		Flips the field values randomly.
Field%phi(n_op,n_tau)		Returns $\phi_{k\tau}$ for the k -th operator at the time slice τ .
Field%gamma(n_op,n_tau)		Returns $\gamma_{k\tau}$ for the k -th operator at the time slice τ .
Field%i(n_op,n_tau)		Returns Field%f rounded to nearest integer (for t=1 or 2).
Field%in(Group_Comm,In_field)		Reads in the initial field configuration from the file confin_0 , if present, otherwise reads seeds (see Table 10) and the configuration In_field – if provided, otherwise calls Field%set() .
Field%out(Group_Comm)		Writes out the field configuration.

Table 4: Components of a variable of type **Fields** named **Field**, where **del** (real) denotes the **Field%del**, **n_op** and **n_tau** (integers) are the number of operators and time slices, respectively, **Group_Comm** (integer) defines an MPI communicator, and the optional **In_field** stores the initial field configuration.

Call Make_Lattice(L1, L2, a1, a2, Latt)

generates the lattice **Latt** of type **Lattice**. Note again that the orbital structure of the unit cell has to be provided by the user. The reciprocal lattice vectors \mathbf{g}_i are defined by:

$$\mathbf{a}_i \cdot \mathbf{g}_i = 2\pi\delta_{i,j}, \quad (111)$$

and the Brillouin zone BZ corresponds to the Wigner-Seitz cell of the lattice. With $\mathbf{k} = \sum_i \alpha_i \mathbf{g}_i$, the k -space quantization follows from:

$$\begin{bmatrix} \mathbf{L}_1 \cdot \mathbf{g}_1 & \mathbf{L}_1 \cdot \mathbf{g}_2 \\ \mathbf{L}_2 \cdot \mathbf{g}_1 & \mathbf{L}_2 \cdot \mathbf{g}_2 \end{bmatrix} \begin{bmatrix} \alpha_1 \\ \alpha_2 \end{bmatrix} = 2\pi \begin{bmatrix} n \\ m \end{bmatrix} \quad (112)$$

such that

$$\mathbf{k} = n\mathbf{b}_1 + m\mathbf{b}_2, \text{ with } \begin{aligned} \mathbf{b}_1 &= \frac{2\pi}{(\mathbf{L}_1 \cdot \mathbf{g}_1)(\mathbf{L}_2 \cdot \mathbf{g}_2) - (\mathbf{L}_1 \cdot \mathbf{g}_2)(\mathbf{L}_2 \cdot \mathbf{g}_1)} [(\mathbf{L}_2 \cdot \mathbf{g}_2)\mathbf{g}_1 - (\mathbf{L}_2 \cdot \mathbf{g}_1)\mathbf{g}_2], \\ \mathbf{b}_2 &= \frac{2\pi}{(\mathbf{L}_1 \cdot \mathbf{g}_1)(\mathbf{L}_2 \cdot \mathbf{g}_2) - (\mathbf{L}_1 \cdot \mathbf{g}_2)(\mathbf{L}_2 \cdot \mathbf{g}_1)} [(\mathbf{L}_1 \cdot \mathbf{g}_1)\mathbf{g}_2 - (\mathbf{L}_1 \cdot \mathbf{g}_2)\mathbf{g}_1] \end{aligned} \quad (113)$$

The **Lattice** module also handles the Fourier transformation. For example, the subroutine **Fourier_R_to_K** carries out the transformation:

$$S(\mathbf{k}, :, :, :) = \frac{1}{N_{\text{unit-cell}}} \sum_{\mathbf{i}, \mathbf{j}} e^{-i\mathbf{k} \cdot (\mathbf{i} - \mathbf{j})} S(\mathbf{i} - \mathbf{j}, :, :, :) \quad (114)$$

Variable	Type	Description
Latt%a1_p, Latt%a2_p	Real	Unit vectors $\mathbf{a}_1, \mathbf{a}_2$.
Latt%L1_p, Latt%L2_p	Real	Vectors $\mathbf{L}_1, \mathbf{L}_2$ that define the topology of the lattice. Tilted lattices are thereby possible to implement.
Latt%N	Integer	Number of lattice points, $N_{\text{unit-cell}}$.
Latt%list	Integer	Maps each lattice point $i = 1, \dots, N_{\text{unit-cell}}$ to a real space vector denoting the position of the unit cell: $\mathbf{R}_i = \text{list}(i,1)\mathbf{a}_1 + \text{list}(i,2)\mathbf{a}_2 \equiv i_1\mathbf{a}_1 + i_2\mathbf{a}_2$.
Latt%invlist	Integer	Return lattice point from position: $\text{Invlist}(i_1, i_2) = i$.
Latt%nnlist	Integer	Nearest neighbor indices: $j = \text{nnlist}(i, n_1, n_2)$, $n_1, n_2 \in [-1, 1]$, $\mathbf{R}_j = \mathbf{R}_i + n_1\mathbf{a}_1 + n_2\mathbf{a}_2$.
Latt%imj	Integer	$\mathbf{R}_{\text{imj}(i,j)} = \mathbf{R}_i - \mathbf{R}_j$, with $\text{imj}, i, j \in 1, \dots, N_{\text{unit-cell}}$.
Latt%BZ1_p, Latt%BZ2_p	Real	Reciprocal space vectors \mathbf{g}_i (See Eq. 111).
Latt%b1_p, Latt%b1_p	Real	k -quantization (See Eq. 113).
Latt%listk	Integer	Maps each reciprocal lattice point $k = 1, \dots, N_{\text{unit-cell}}$ to a reciprocal space vector $\mathbf{k}_k = \text{listk}(k,1)\mathbf{b}_1 + \text{listk}(k,2)\mathbf{b}_2 \equiv k_1\mathbf{b}_1 + k_2\mathbf{b}_2$.
Latt%invlistk	Integer	$\text{Invlistk}(k_1, k_2) = k$.
Latt%b1_perp_p, Latt%b2_perp_p	Real	Orthonormal vectors to \mathbf{b}_i . For internal use.

Table 5: Components of the `Lattice` type for two-dimensional lattices using as example the default lattice name `Latt`. The **highlighted** variables must be specified by the user. Other components of the `Lattice` are generated upon calling: `Call Make_Lattice(L1, L2, a1, a2, Latt)`.

and `Fourier_K_to_R` the inverse Fourier transform

$$S(\mathbf{r}, :, :, :) = \frac{1}{N_{\text{unit-cell}}} \sum_{\mathbf{k} \in BZ} e^{i\mathbf{k} \cdot \mathbf{r}} S(\mathbf{k}, :, :, :). \quad (115)$$

In the above, the unspecified dimensions of the structure factor can refer to imaginary-time and orbital indices.

Variable	Type	Description
Norb	Integer	Number of orbitals.
N_coord	Integer	Coordination number.
Orb_pos(1..Norb, 2[3])	Real	Positions of the orbitals as measured from the lattice site.

Table 6: Components of an instance `Latt_unit` of the `Unit_cell` type. The **highlighted** variables have to be specified by the user. Note that for bilayer lattices the second index of the `Orb_pos` array ranges from 1 to 3.

5.2 The observable types `Obser_Vec` and `Obser_Latt`

Our definition of the model includes observables [Eq. (24)]. We have defined two observable types: `Obser_vec` for an array of *scalar* observables such as the energy, and `Obser_Latt` for correlation functions that have the lattice symmetry. In the latter case, translation symmetry can be used to provide improved estimators and to reduce the size of the output. We also obtain improved estimators by taking measurements in the imaginary-time interval `[LOBS_ST, LOBS_EN]` (see the parameter file in Sec. 5.4.1) thereby exploiting the invariance under translation in imaginary-time. Note that the translation symmetries in space and in time are *broken* for a given configuration C but restored by the Monte Carlo sampling. In general, the user defines size and number of bins in the parameter file, each bin containing a given amount of sweeps. Within a sweep we run sequentially through the HS and Ising fields, from time slice 1 to time slice L_{Trotter} and back. The results of each bin are written to a file and analyzed at the end of the run.

To accomplish the reweighting of observables (see Sec. 2.1.3), for each configuration the measured value of an observable is multiplied by the factors ZS and ZP:

$$\text{ZS} = \text{sign}(C) , \quad (116)$$

$$\text{ZP} = \frac{e^{-S(C)}}{\text{Re}[e^{-S(C)}]} . \quad (117)$$

They are computed from the Monte Carlo phase of a configuration,

$$\text{phase} = \frac{e^{-S(C)}}{|e^{-S(C)}|} , \quad (118)$$

which is provided by the main program. Note that each observable structure also includes the average sign [Eq. (25)].

5.2.1 Scalar observables

Scalar observables are stored in the data type `Obser_vec`, described in Table 7. Consider a variable `Obs` of type `Obser_vec`. At the beginning of each bin, a call to `Obser_Vec_Init` in the module `observables_mod.F90` will set `Obs%N=0`, `Obs%Ave_sign=0` and `Obs%Obs_vec(:)=0`. Each time the main program calls the routine `Obser` in the `Hamiltonian` module, the counter `Obs%N` is incremented by one, the sign (see Eq. 23) is accumulated in the variable `Obs%Ave_sign`, and the desired observables (multiplied by the sign and $\frac{e^{-S(C)}}{\text{Re}[e^{-S(C)}]}$, see Sec. 2.1.2) are accumulated in the vector `Obs%Obs_vec`. At the end

Variable	Type	Description	Contribution of configuration C
<code>Obs%N</code>	Int.	Number of measurements	+1
<code>Obs%Ave_sign</code>	Real	Cumulated average sign [Eq. (25)]	$\text{sign}(C)$
<code>Obs%Obs_vec(:)</code>	Comp.	Cumul. vector of observables [Eq. (24)]	$\langle\langle\hat{O}(\cdot)\rangle\rangle_C \frac{e^{-S(C)}}{\text{Re}[e^{-S(C)}]} \text{sign}(C)$
<code>Obs%File_Vec</code>	Char.	Name of output file	

Table 7: Components of a variable of type `Obser_vec` named `Obs`.

of the bin, a call to `Print_bin_Vec` in module `observables_mod.F90` will append the result of the bin in the file `File_Vec_scal`. Note that this subroutine will automatically append the suffix `_scal` to the filename `File_Vec`. This suffix is important to allow automatic analysis of the data at the end of the run.

5.2.2 Equal-time and time-displaced correlation functions

The data type `Obser_latt` (see Table 8) is useful for dealing with both equal-time and imaginary-time-displaced correlation functions of the form:

$$S_{\alpha,\beta}(\mathbf{k}, \tau) = \frac{1}{N_{\text{unit-cell}}} \sum_{\mathbf{i}, \mathbf{j}} e^{-i\mathbf{k} \cdot (\mathbf{i} - \mathbf{j})} \left(\langle \hat{O}_{\mathbf{i},\alpha}(\tau) \hat{O}_{\mathbf{j},\beta} \rangle - \langle \hat{O}_{\mathbf{i},\alpha} \rangle \langle \hat{O}_{\mathbf{j},\beta} \rangle \right) , \quad (119)$$

where α and β are orbital indices and \mathbf{i} and \mathbf{j} lattice positions. Here, translation symmetry of the Bravais lattice is explicitly taken into account. The correlation function splits in a correlated part $S_{\alpha,\beta}^{(\text{corr})}(\mathbf{k}, \tau)$ and a background part $S_{\alpha,\beta}^{(\text{back})}(\mathbf{k})$:

$$S_{\alpha,\beta}^{(\text{corr})}(\mathbf{k}, \tau) = \frac{1}{N_{\text{unit-cell}}} \sum_{\mathbf{i}, \mathbf{j}} e^{-i\mathbf{k} \cdot (\mathbf{i} - \mathbf{j})} \langle \hat{O}_{\mathbf{i},\alpha}(\tau) \hat{O}_{\mathbf{j},\beta} \rangle , \quad (120)$$

$$\begin{aligned} S_{\alpha,\beta}^{(\text{back})}(\mathbf{k}) &= \frac{1}{N_{\text{unit-cell}}} \sum_{\mathbf{i}, \mathbf{j}} e^{-i\mathbf{k} \cdot (\mathbf{i} - \mathbf{j})} \langle \hat{O}_{\mathbf{i},\alpha}(\tau) \rangle \langle \hat{O}_{\mathbf{j},\beta} \rangle \\ &= N_{\text{unit-cell}} \langle \hat{O}_{\alpha} \rangle \langle \hat{O}_{\beta} \rangle \delta(\mathbf{k}) , \end{aligned} \quad (121)$$

Variable	Type	Description	Contribution of configuration C
Obs%N	Int.	Number of measurements	+1
Obs%Ave_sign	Real	Cumulated sign [Eq. (25)]	$\text{sign}(C)$
Obs%Obs_latt($i - j, \tau, \alpha, \beta$)	Compl.	Cumul. correl. funct. [Eq. (24)]	$\langle \langle \hat{O}_{i,\alpha}(\tau) \hat{O}_{j,\beta} \rangle \rangle_C \frac{e^{-S(C)}}{\text{Re}[e^{-S(C)}]} \text{sign}(C)$
Obs%Obs_latt0(α)	Compl.	Cumul. expect. value [Eq. (24)]	$\langle \langle \hat{O}_{i,\alpha} \rangle \rangle_C \frac{e^{-S(C)}}{\text{Re}[e^{-S(C)}]} \text{sign}(C)$
Obs%File_Latt	Char.	Name of output file	

Table 8: Components of a variable of type `Obser_latt` named `Obs`.

where translation invariance in space and time has been exploited to obtain the last line. The background part depends only on the expectation value $\langle \hat{O}_\alpha \rangle$, for which we use the following estimator

$$\langle \hat{O}_\alpha \rangle \equiv \frac{1}{N_{\text{unit-cell}}} \sum_i \langle \hat{O}_{i,\alpha} \rangle. \quad (122)$$

Consider a variable `Obs` of type `Obser_latt`. At the beginning of each bin a call to `Obser_Latt_Init` in the module `observables_mod.F90` will initialize the elements of `Obs` to zero. Each time the main program calls the `Obser` or `ObserT` routines one accumulates $\langle \langle \hat{O}_{i,\alpha}(\tau) \hat{O}_{j,\beta} \rangle \rangle_C \frac{e^{-S(C)}}{\text{Re}[e^{-S(C)}]} \text{sign}(C)$ in `Obs%Obs_latt($i - j, \tau, \alpha, \beta$)` and $\langle \langle \hat{O}_{i,\alpha} \rangle \rangle_C \frac{e^{-S(C)}}{\text{Re}[e^{-S(C)}]} \text{sign}(C)$ in `Obs%Obs_latt0(α)`. At the end of each bin, a call to `Print_bin_Latt` in the module `observables_mod.F90` will append the result of the bin in the specified file `Obs%File_Latt`. Note that the routine `Print_bin_Latt` carries out the Fourier transformation and prints the results in k -space. We have adopted the following naming conventions. For equal-time observables, defined by having the second dimension of the array `Obs%Obs_latt($i - j, \tau, \alpha, \beta$)` set to unity, the routine `Print_bin_Latt` attaches the suffix `_eq` to `Obs%File_Latt`. For time-displaced correlation functions we use the suffix `_tau`.

5.3 The trial wave function type

This still has to be done @Jefferson could you please start this.

5.4 File structure

Directory	Description
<code>Prog/</code>	Main program and subroutines.
<code>Libraries/</code>	Collection of mathematical routines.
<code>Analysis/</code>	Routines for error analysis.
<code>Scripts_and_Parameters_files/</code>	Helper scripts and the <code>Start/</code> directory, which contains the files required to start a run.
<code>Documentation/</code>	This documentation.
<code>testsuite/</code>	A suite for automatic testing various parts of the code.

Table 9: Overview of the directories included in the ALF package.

The code package, summarized in Table 9, consists of the program directories `Prog/`, `Libraries/`, and `Analysis/`, as well as the directory `Scripts_and_Parameters_files/`, which contains supporting scripts and, in its subdirectory `Start`, the input files necessary for a run, described in the Sec. 5.4.1. The routines available in the directory `Analysis/` are described in Sec. 6.2, and the testsuite in Sec. 6.1.

Below we describe the structure of the input and output files of the QMC. Notice that the input/output files for the `Analysis` routines are described in Sec. 6.2.

5.4.1 Input files

The input files are listed in Table 10. The parameter file `Start/parameters` has the following form – using as an example the Mz-Hubbard model on a square lattice (see Sec. 7.1 for a detailed walkthrough):

```

=====
!   Input variables for a general ALF run
=====

&VAR_lattice                !! Parameters defining the specific lattice and base model
L1                          = 6                ! Length in direction a_1
L2                          = 6                ! Length in direction a_2
Lattice_type                = "Square"        ! Sets a_1 = (1,0), a_2=(0,1), Norb=1, N_coord=2
Model                      = "Hubbard"        ! Sets the Hubbard model, to be specified in &VAR_Hubbard
/

&VAR_Model_Generic          !! Common model parameters
Checkerboard                = .T.             ! Whether checkerboard decomposition is used
Symm                        = .T.             ! Whether symmetrization takes place
N_SUN                       = 2               ! Number of colors
N_FL                        = 1               ! Number of flavors
Phi_X                      = 0.d0            ! Twist along the L_1 direction, in units of the flux quanta
Phi_Y                      = 0.d0            ! Twist along the L_2 direction, in units of the flux quanta
Bulk                        = .T.             ! Twist as a vector potential (.T.), or at the boundary (.F.)
N_Phi                      = 0               ! Total number of flux quanta traversing the lattice
Dtau                       = 0.1d0           ! Thereby Ltrot=Beta/dtau
Beta                        = 5.d0           ! Inverse temperature
Projector                   = .F.            ! Whether the projective algorithm is used
Theta                      = 10.d0          ! Projection parameter
/

&VAR_QMC                    !! Variables for the QMC run
Nwrap                      = 10              ! Stabilization. Green functions will be computed from
                                     ! scratch after each time interval Nwrap*Dtau
NSweep                     = 20              ! Number of sweeps
NBin                       = 5               ! Number of bins
Ltau                       = 1               ! 1 to calculate time-displaced Green functions; 0 otherwise
LOBS_ST                    = 0               ! Start measurements at time slice LOBS_ST
LOBS_EN                    = 0               ! End measurements at time slice LOBS_EN
CPU_MAX                    = 0.0             ! Code stops after CPU_MAX hours, if 0 or not
                                     ! specified, the code stops after Nbin bins
Propose_S0                 = .F.            ! Proposes single spin flip moves with probability exp(-S0)
Global_moves               = .F.            ! Allows for global moves in space and time
N_Global                   = 1               ! Number of global moves per sweep
Global_tau_moves           = .F.            ! Allows for global moves on a single time slice.
N_Global_tau               = 1               ! Number of global moves that will be carried out on a
                                     ! single time slice
Nt_sequential_start        = 0               ! One can combine sequential and global moves on a time slice
Nt_sequential_end          = -1             ! The program then carries out sequential local moves in the
                                     ! range [Nt_sequential_start, Nt_sequential_end] followed by
                                     ! N_Global_tau global moves
/

&VAR_errors                !! Variables for analysis programs
n_skip                     = 1               ! Number of bins that to be skipped.
N_rebin                    = 1               ! Rebinning
N_Cov                      = 0               ! If set to 1 covariance computed for non-equal-time
                                     ! correlation functions
/

&VAR_TEMP                  !! Variables for parallel tempering
N_exchange_steps           = 6               ! Number of exchange moves [see Eq. (36)]
N_Tempering_frequency      = 10             ! The frequency in units of sweeps at which the
                                     ! exchange moves are carried out

```

```

mpi_per_parameter_set = 2      ! Number of mpi-processes per parameter set
Tempering_calc_det     = .T.   ! Specifies whether the fermion weight has to be taken
                                ! into account while tempering. The default is .true.,
                                ! and it can be set to .F. if the parameters that
                                ! get varied only enter the Ising action S_0
/

&VAR_Max_Stoch          !! Variables for Stochastic Maximum entropy
Ngamma      = 400        ! Number of Dirac delta-functions for parametrization
Om_st       = -10.d0     ! Frequency range lower bound
Om_en       = 10.d0      ! Frequency range upper bound
NDis        = 2000       ! Number of boxes for histogram
Nbins       = 250        ! Number of bins for Monte Carlo
Nsweeps     = 70         ! Number of sweeps per bin
NWarm       = 20         ! The Nwarm first bins will be ommitted
N_alpha     = 14         ! Number of temperatures
alpha_st    = 1.d0       ! Smallest inverse temperature increment for inverse
R           = 1.2d0      ! temperature (see above)
Channel     = "P"        ! Options: zero temperature (T0), and finite temperature
                                ! particle (P), particle-hole (PH), or particle-particle (PP)
Checkpoint  = .F.        ! Whether to produce dump files, allowing the simulation
                                ! to be resumed later on
Tolerance   = 0.1d0      ! Data points for which the relative error exceeds the
                                ! tolerance threshold will be omitted.
/

&VAR_Hubbard          !! Variables for the specific model
Mz           = .T.       ! When true, sets the M_z-Hubbard model: Nf=2, N_sun=1, HS field
                                ! couples to the z-component of magnetization; otherwise, HS field
                                ! couples to the density
ham_T        = 1.d0      ! Hopping parameter
ham_chem     = 0.d0      ! Chemical potential
ham_U        = 4.d0      ! Hubbard interaction
ham_T2       = 1.d0      ! For bilayer systems
ham_U2       = 4.d0      ! For bilayer systems
ham_Tperp    = 1.d0      ! For bilayer systems
/

```

File	Description
parameters	Sets the parameters for lattice, model, QMC process, and the error analysis.
seeds	List of integer numbers to initialize the random number generator and to start a simulation from scratch.

Table 10: [To be removed, at least after the file seeds is no longer necessary.] Overview of the input files required for a simulation, which can be found in the subdirectory Scripts_and_Parameters_files/Start/.

The program allows for a number of different updating schemes. If no other variables are specified in the VAR_QMC name space, then the program will run in its default mode, namely the sequential single spin-flip mode. In particular, note that if Nt_sequential_start and Nt_sequential_end are not specified and that the variable Global_tau_moves is set to true, then the program will carry out only global moves, by setting Nt_sequential_start=1 and Nt_sequential_end=0.

If the program is not compiled with the parallel tempering flag, then the VAR_TEMP name space can be omitted from the parameter file.

5.4.2 Output files – observables

The standard output files are listed in Table 11. The output of the measured data is organized in bins. One bin corresponds to the arithmetic average over a fixed number of individual measurements which

File	Description
info	After completion of the simulation, this file documents the parameters of the model, as well as the QMC run and simulation metrics (precision, acceptance rate, wallclock time).
X_scal	Results of equal-time measurements of scalar observables. The placeholder X stands for the observables Kin , Pot , Part , and Ener .
Y_eq,Y_tau	Results of equal-time and time-displaced measurements of correlation functions. The placeholder Y stands for Green , SpinZ , SpinXY , and Den .
confout_<threadnumber>	Output files (one per MPI instance) for the HS and Ising configuration.

Table 11: Overview of the standard output files. See Sec. 5.2 for the definitions of observables and correlation functions.

depends on the chosen measurement interval [LOBS_ST, LOBS_EN] on the imaginary-time axis and on the number **NSweep** of Monte Carlo sweeps. If the user runs an MPI parallelized version of the code, the average also extends over the number of MPI threads. The formatting of a single bin's output depends on the observable type, **Obs_vec** or **Obs_Latt**:

- Observables of type **Obs_vec**: For each additional bin, a single new line is added to the output file. In case of an observable with **N_size** components, the formatting is

```
N_size + 1    <measured value, 1> ... <measured value, N_size>    <measured sign>
```

The counter variable **N_size+1** refers to the number of measurements per line, including the phase measurement. This format is required by the error analysis routine (see Sec. 6.2). Scalar observables like kinetic energy, potential energy, total energy and particle number are treated as a vector of size **N_size=1**.

- Observables of type **Obs_Latt**: For each additional bin, a new data block is added to the output file. The block consists of the expectation values [Eq. (122)] contributing to the background part [Eq. (121)] of the correlation function, and the correlated part [Eq. (120)] of the correlation function. For imaginary-time displaced correlation functions, the formatting of the block is given by:

```
<measured sign> <N_orbital> <N_unit_cell> <N_time_slices> <dtau>
do alpha = 1, N_orbital
  <O_alpha>
enddo
do i = 1, N_unit_cell
  <reciprocal lattice vector k(i)>
  do tau = 1, N_time_slices
    do alpha = 1, N_orbital
      do beta = 1, N_orbital
        <S_alpha,beta^(corr)(k(i), tau)>
      enddo
    enddo
  enddo
enddo
enddo
```

The same block structure is used for equal-time correlation functions, except for the entries **<N_time_slices>** and **<dtau>**, which are then omitted. Using this structure for the bins as input, the full correlation function $S_{\alpha,\beta}(\mathbf{k}, \tau)$ [Eq. (119)] is then calculated by calling the error analysis routine (see Sec. 6.2).

6 Using the Code

In this section we describe the steps for compiling and running the code, and describe how to search for optimal parameter values as well as how to perform the error analysis of the data.

6.1 Compiling and running

The necessary environment variables and the directives for compiling the code are set by the script `configure.sh`:

```
source configure.sh [MACHINE] [MODE] [STAB]
```

If run with no arguments, it lists the available options and sets a generic, serial GNU compiler with minimal flags `-cpp -O3 -ffree-line-length-none -ffast-math`. The predefined machine configurations and parallelization modes available, as well as the options for stabilization schemes for the matrix multiplications (see Sec. 2.4) are shown Table 12. The stabilization scheme choice, in particular, is critical for performance and is discussed further in Sec. 6.3.

Argument	Selected feature
MACHINE	
Intel	Intel compiler for a generic machine ⁴ .
GNU	GNU compiler for a generic machine (<i>default</i>).
PGI	PGI compiler for a generic machine.
MAC	GNU compiler for a generic MAC computer.
SuperMUC-NG	Intel compiler and loading the necessary modules for SuperMUC-NG ⁵ .
JUWELS	Intel compiler and loading the necessary modules for JUWELS ⁶ .
Devel Development	GNU compiler, and flags appropriate for debugging.
MODE	
noMPI serial	No parallelization.
MPI	MPI parallelization (<i>default</i> – if a machine is selected).
Tempering	Parallel tempering (Sec. 2.2.5) and the required MPI as well.
STAB	
STAB1	Simplest stabilization, with UDV (QR-, not SVD-based) decompositions.
STAB2	QR-based UDV decompositions with additional normalizations.
STAB3	Newest stabilization, additionally separates large and small scales (<i>default</i>).
LOG	Log storage for internal scales, increases accessible ranges.

Table 12: Available arguments for the script `configure.sh`, called before compilation of the package: predefined machines, parallelization modes, and stabilization schemes (see also Sec. 6.3).

In order to compile the libraries, the analysis routines and the QMC program at once, just execute the single command:

```
make
```

Related directories, object files and executables can be removed by executing the command `make clean`. The accompanying `Makefile` also provides rules for compiling and cleaning up the library, the analysis routines and the QMC program separately.

A suite of tests for individual parts of the code (subroutines, functions, operations, etc.) is available at the directory `testsuite`. The tests can be run by executing the following sequence of commands (the script `configure.sh` sets environment variables as described above.):

```
source configure.sh Devel serial
gfortran -v
make lib
make ana
```

⁴A known issue with the alternative Intel Fortran compiler `ifort` is the handling of automatic, temporary arrays which `ifort` allocates on the stack. For large system sizes and/or low temperatures this may lead to a runtime error. One solution is to demand allocation of arrays above a certain size on the heap instead of the stack. This is accomplished by the `ifort` compiler flag `-heap-arrays [n]` where `[n]` is the minimal size (in kilobytes, for example `n=1024`) of arrays that are allocated on the heap.

⁵Supercomputer at the Leibniz Supercomputing Centre.

⁶Supercomputer at the Jülich Supercomputing Centre.

```

make Examples
cd testsuite
cmake -E make_directory tests
cd tests
cmake -G "Unix Makefiles" -DCMAKE_Fortran_FLAGS_RELEASE=${F90OPTFLAGS} \
-DCMAKE_BUILD_TYPE=RELEASE ..
cmake --build . --target all --config Release
ctest -VV -O log.txt

```

which will output test results and total success rate.

Starting a simulation

In order to start a simulation from scratch, the following files have to be present: `parameters` and `seeds` (see Sec. 5.4.1). To run serially the simulation for a given model, for instance one of the Hubbard models included in `Hamiltonian_Examples_mod.F90`, described in Sec. 12, issue the command

```
./Prog/Examples.out
```

In order to run a different model, the corresponding executable should be used and, for running with parallelization, the appropriate MPI execution command should be called. For instance, a GNU-compiled Kondo model (Sec. 13.1.1) can be run in parallel by issuing

```
orterun ./Prog/Kondo_Honey.out
```

@Jefferson. This cannot really be, since somewhere you have to specify the number of mpi process. I think that it would be good to use the standards defined by pyALF.

To restart the code using the configuration from a previous simulation as a starting point, first run the script `out_to_in.sh`, which copies outputted field configurations into input files, before calling the ALF executable.

6.2 Error analysis

The ALF package includes a few bash scripts for performing simple error analysis and correlation function calculations, as listed in Table 13. To perform an error analysis based on the Jackknife resampling method [75] (Sec. 4.1) of the Monte Carlo bins for all observables run

```
./analysis.sh
```

In case that the parameter `N_auto` is set to a finite value the script will also trigger the computation of autocorrelation functions (Sec. 4.2).

Note that the error analysis script requires the presence of the environment variable `ALF_DIR`, which stores the package's path and can be set by running `source configure.sh`. The files taken by `analysis.sh` as input, as well as its output files are listed in Table 14.

The error analysis is based on the central limit theorem, which requires bins to be statistically independent, and also the existence of a well-defined variance for the observable under consideration (see Sec. 4). The former will be the case if bins are longer than the autocorrelation time. The latter has to be checked by the user. In the parameter file described in Sec. 5.4.1, the user can specify how many initial bins should be omitted (variable `n_skip`). This number should be comparable to the autocorrelation time. The rebinning variable `N_rebin` will merge `N_rebin` bins into a single new bin. If the autocorrelation time is smaller than the effective bin size, the error should become independent of the bin size and thereby of the variable `N_rebin`. The analysis output files listed in Table 14 and are formatted in the following way:

- For the scalar quantities `X`, the output files `X_scalJ` have the following formatting:

Effective number of bins, and bins:	<N_bin - n_skip>	<N_bin>
OBS : 1	<mean(X)>	<error(X)>
OBS : 2	<mean(sign)>	<error(sign)>

- For the equal-time correlation functions `Y`, the formatting of the output files `Y_eqJR` and `Y_eqJK` follows the structure:

Program	Description
cov_scal.F90	In combination with the script <code>analysis.sh</code> , the bin files with suffix <code>_scal</code> are read in, and the corresponding files with suffix <code>_scalJ</code> are produced. They contain the result of the Jackknife rebinning analysis (see Sec. 4).
cov_eq.F90	In combination with the script <code>analysis.sh</code> , the bin files with suffix <code>_eq</code> are read in, and the corresponding files with suffix <code>_eqJR</code> and <code>_eqJK</code> are produced. They correspond to correlation functions in real and Fourier space, respectively.
cov_tau.F90	In combination with the script <code>analysis.sh</code> , the bin files <code>X_tau</code> are read in, and the directories <code>X_kx_ky</code> are produced for all <code>kx</code> and <code>ky</code> greater or equal to zero. Here <code>X</code> is a place holder from <code>Green</code> , <code>SpinXY</code> , etc., as specified in <code>Alloc_obs(Ltau)</code> (See section 7.1.2.1). Each directory contains a file <code>g_kx_ky</code> containing the time-displaced correlation function traced over the orbitals. It also contains the covariance matrix if <code>N_cov</code> is set to unity in the parameter file (see Sec. 5.4.1). Also, a directory <code>X_R0</code> for the local time displaced correlation function is generated.
cov_tau_ph.F90	At compilation time the file <code>cov_tau_ph.F90</code> is generated, and should be used to compute particle-hole, imaginary-time correlation functions such as Spin and Charge. Here we use the fact that these correlation functions are symmetric around $\tau = \beta/2$ so that we can define an improved estimator by averaging over τ and $\beta - \tau$.

Table 13: Overview of analysis programs that are called within the script `analysis.sh`.

File	Description
Input	
<code>parameters</code>	Includes error analysis variables <code>n_skip</code> , <code>N_rebin</code> , and <code>N_Cov</code> (see Sec. 5.4.1).
<code>X_scal</code> , <code>Y_eq</code> , <code>Y_tau</code>	Monte Carlo bins (see Table 11).
Output	
<code>X_scalJ</code>	Jackknife mean and error of <code>X</code> , where <code>X</code> stands for <code>Kin</code> , <code>Pot</code> , <code>Part</code> , or <code>Ener</code> .
<code>Y_eqJR</code> and <code>Y_eqJK</code>	Jackknife mean and error of <code>Y</code> , which stands for <code>Green</code> , <code>SpinZ</code> , <code>SpinXY</code> , or <code>Den</code> . The suffixes <code>R</code> and <code>K</code> refer to real and reciprocal space, respectively.
<code>Y_R0/g_R0</code>	Time-resolved and spatially local Jackknife mean and error of <code>Y</code> , where <code>Y</code> stands for <code>Green</code> , <code>SpinZ</code> , <code>SpinXY</code> , and <code>Den</code> .
<code>Y_kx_ky/g_kx_ky</code>	Time resolved and \mathbf{k} -dependent Jackknife mean and error of <code>Y</code> , where <code>Y</code> stands for <code>Green</code> , <code>SpinZ</code> , <code>SpinXY</code> , and <code>Den</code> .

Table 14: Standard input and output files of the error analysis script `analysis.sh`.

```

do i = 1, N_unit_cell
  <k_x(i)>   <k_y(i)>
  do alpha = 1, N_orbital
    do beta  = 1, N_orbital
      alpha  beta  Re<mean(Y)>  Re<error(Y)>  Im<mean(Y)>  Im<error(Y)>
    enddo
  enddo
enddo

```

where `Re` and `Im` refer to the real and imaginary part, respectively.

- The imaginary-time displaced correlation functions `Y` are written to the output files `g_R0` inside folders `Y_R0`, when measured locally in space; and to the output files `g_kx_ky` inside folders `Y_kx_ky` when they are measured \mathbf{k} -resolved (where $\mathbf{k} = (\mathbf{kx}, \mathbf{ky})$). The first line of the file prints the number of time slices, the number of bins and the inverse temperature. Both output files have the following formatting:

```

do i = 0, Ltau

```

```

    tau(i)    <mean( Tr[Y] )>    <error( Tr[Y])>
enddo

```

where Tr corresponds to the trace over the orbital degrees of freedom. For particle-hole quantities at finite temperature, τ runs from 0 to $\beta/2$. In all other cases it runs from 0 to β .

6.3 Performance & parameter optimization

The finite-temperature, auxiliary-field QMC algorithm is known to be numerically unstable, as discussed in Sec. 2.4. The numerical instabilities arise from the imaginary-time propagation, which invariably leads to exponentially small and exponentially large scales. As shown in Ref. [6], scales can be omitted in the ground state algorithm – thus rendering it very stable – but have to be taken into account in the finite-temperature code.

Numerical stabilization of the code is a delicate procedure that has been pioneered in Ref. [2] for the finite-temperature algorithm and in Refs. [3, 4] for the zero-temperature, projective algorithm. It is important to be aware of the fragility of the numerical stabilization and that there is no guarantee that it will work for a given model. It is therefore crucial to always check the file `info`, which, apart from runtime data, contains important information concerning the stability of the code, in particular **Precision Green**. If the numerical stabilization fails, one possible measure is to reduce the value of the parameter `Nwrap` in the parameter file, which will however also impact performance – see Table. 15 for further optimization tips for the Monte Carlo algorithm (Sec. 4). Typical values for the numerical precision ALF can achieve can be found in the examples in Sec. 12 (see Sec. 7.1.3 and 7.2.3).

Element	Suggestion
Precision Green , Precision Phase	should be found to be <i>small</i> , of order $< 10^{-8}$ (see Sec. 2.4).
theta	should be <i>large</i> enough to guarantee convergence to ground state.
dtau	should be set <i>small</i> enough to limit Trotter errors.
Nwrap	should be set <i>small</i> enough to keep Precisions small .
Nsweep	should be set <i>large</i> enough for bins to be of the order of the auto-correlation time.
Nbin	should be set <i>large</i> enough to provide good statistics (recommended minimum: $\sim 10^2$; note: there are <code>Nbin</code> bins per MPI process).
nskip	should be set <i>large</i> enough to allow for equilibration (\sim autocorrelation time).
Nrebin	can be set to 1 when <code>Nsweep</code> is large enough; otherwise, and for testing, larger values can be used.
Stabilization scheme	use the default STAB3 – newest and fastest, if it works for your model; alternatives are: STAB1 – simplest, for reference only; STAB2 – with additional normalizations; and LOG – for dealing with more extreme scales (see also Tab. 12).
Parallelism	for some models and systems, restricting parallelism in OpenBLAS can improve performance: try setting <code>OPENBLAS_NUM_THREADS=1</code> in the shell.

Table 15: Rules of thumb for obtaining best results and performance from ALF. It is important to fine tune the parameters to the specific model under consideration and perform sanity checks throughout. Most suggestions can severely impact performance and numerical stability if overdone.

In particular, for the stabilization of the involved matrix multiplications we rely on routines from LAPACK. Notice that results are very likely to change depending on the specific implementation of the library used⁷. In order to deal with this possibility, we offer a simple baseline which can be used as a quick check as to whether results depend on the library used for linear algebra routines. Namely, we have included QR-decomposition related routines of the LAPACK-3.6.1 reference implementation from <http://www.netlib.org/lapack/>, which you can use by running the script `configure.sh`, (described in Sec. 6), with the flag **STAB1** and recompiling ALF⁸. The stabilization flags available are described in Tables 12 and 15. The performance of the package is further discussed in Sec. 10.6.

⁷The linked library should implement at least the LAPACK-3.4.0 interface.

⁸This flag may trigger compiling issues, in particular, the Intel ifort compiler version 10.1 fails for all optimization levels.

7 The plain vanilla Hubbard model on the square and honeycomb lattices

The Hubbard model without predefined structures

7.1 The square lattice

To implement a Hamiltonian, the user has to provide a module which specifies the lattice, the model, as well as the observables they wish to compute. In this section, we describe the module `Hamiltonian_Examples_mod.F90` which contains an implementation of the Hubbard model on the square lattice. A sample run for this model can be found in `Examples/Hubbard_SU2_Square/`.

The Hamiltonian reads

$$\mathcal{H} = \sum_{\sigma=1}^2 \sum_{x,y=1}^{N_{\text{unit-cell}}} c_{x\sigma}^\dagger T_{x,y} c_{y\sigma} + \frac{U}{2} \sum_x \left[\sum_{\sigma=1}^2 (c_{x\sigma}^\dagger c_{x\sigma} - 1/2) \right]^2. \quad (123)$$

We can make contact with the general form of the Hamiltonian by setting: $N_{\text{fl}} = 1$, $N_{\text{col}} \equiv N_{\text{SUN}} = 2$, $M_T = 1$, $T_{xy}^{(ks)} = T_{x,y}$, $M_V = N_{\text{unit-cell}}$, $U_k = -\frac{U}{2}$, $V_{xy}^{(ks)} = \delta_{x,y} \delta_{x,k}$, $\alpha_{ks} = -\frac{1}{2}$ and $M_I = 0$.

7.1.1 Setting the Hamiltonian: `Ham_set`

The main program will call the subroutine `Ham_set` in the module `Hamiltonian_Hub_mod.F90`. The latter subroutine defines the public variables

```
Type (Operator), dimension(:,,:), allocatable :: Op_V
Type (Operator), dimension(:,,:), allocatable :: Op_T
Integer, allocatable :: nsigma(:, :)
Integer :: Ndim, N_FL, N_SUN, Ltrot
```

which specify the model. The array `nsigma` contains the HS field. The routine `Ham_set` will first read the parameter file, then set the lattice, Call `Ham_latt`, set the hopping, Call `Ham_hop`, and set the interaction, call `Ham_V`. The parameters are read in from the file `parameters`, see Sec. 5.4.1.

7.1.1.1 The lattice: Call `Ham_latt`

Superseded by Predefined Structures.

7.1.1.2 The hopping term: Call `Ham_hop`

The hopping matrix is implemented as follows. We allocate an array of dimension 1×1 of type operator called `Op_T` and set the dimension for the hopping matrix to $N = N_{\text{dim}}$. One allocates and initializes this type by a single call to the subroutine `Op_make`:

```
call Op_make(Op_T(1,1),Ndim)
```

Since the hopping does not break down into small blocks, we have $\mathbf{P} = \mathbb{1}$ and

```
Do i= 1,Ndim
  Op_T(1,1)%P(i) = i
Enddo
```

We set the hopping matrix with

```
DO I = 1, Latt%N
  Ix = Latt%nnlist(I,1,0)
  Iy = Latt%nnlist(I,0,1)
  Op_T(1,1)%O(I ,Ix) = cmplx(-Ham_T, 0.d0,kind(0.D0))
  Op_T(1,1)%O(Ix,I ) = cmplx(-Ham_T, 0.d0,kind(0.D0))
  Op_T(1,1)%O(I ,Iy) = cmplx(-Ham_T, 0.d0,kind(0.D0))
  Op_T(1,1)%O(Iy, I ) = cmplx(-Ham_T, 0.d0,kind(0.D0))
  Op_T(1,1)%O(I ,I ) = cmplx(-Ham_chem,0.d0,kind(0.D0))
ENDDO
```

Here, the integer function `j= Latt%nnlist(I,n,m)` is defined in the lattice module and returns the index of the lattice site $I + na_1 + ma_2$. Note that periodic boundary conditions are already taken into account. The hopping parameter `Ham_T` as well as the chemical potential `Ham_chem` are read from the parameter file. To completely define the hopping we further set: `Op_T(1,1)%g = -Dtau , Op_T(1,1)%alpha = cmplx(0.d0,0.d0, kind(0.D0))` and call the routine `Op_set(Op_T(1,1))` so as to generate the unitary transformation and eigenvalues as specified in Table 3. Recall that for the hopping, the variable `Op_set(Op_T(1,1))%type` is not required. Note that although a checkerboard decomposition is not used here, it can be implemented by considering a larger number of sparse hopping matrices.

7.1.1.3 The interaction term: Call `Ham_V`

Superseded by Predefined Structures.

7.1.2 Observables

At this point, all the information for the simulation to start has been provided. The code will sequentially go through the operator list `Op_V` and update the fields. Between time slices `LOBS_ST` and `LOBS_EN` the main program will call the routine `Obser(GR,Phase,Ntau)` which is provided by the user and handles equal-time correlation functions. If `Ltau=1` the main program will call the routine `ObserT(NT, GTO,GOT,G00,GTT, PHASE)` which is again provided by the user and handles imaginary-time displaced correlation functions.

The user will have to implement the observables they want to compute. Here we will describe how to proceed.

7.1.2.1 Allocating space for the observables: Call `Alloc_obs(Ltau)`

For four scalar or vector observables, the user will have to declare the following:

```
Allocate ( Obs_scal(4) )
Do I = 1,Size(Obs_scal,1)
  select case (I)
    case (1)
      N = 2;  Filename = "Kin"
    case (2)
      N = 1;  Filename = "Pot"
    case (3)
      N = 1;  Filename = "Part"
    case (4)
      N = 1,  Filename = "Ener"
    case default
      Write(6,*) ' Error in Alloc_obs '
  end select
  Call Obser_Vec_make(Obs_scal(I),N,Filename)
enddo
```

Here, `Obs_scal(1)` contains a vector of two observables so as to account for the x - and y -components of the kinetic energy for example.

For equal-time correlation functions we allocate `Obs_eq` of type `Obser_Latt`. Here we include the calculation of spin-spin and density-density correlation functions alongside equal-time Green functions.

```
Allocate ( Obs_eq(4) )
Do I = 1,Size(Obs_eq,1)
  select case (I)
    case (1)
      Ns = Latt%N; No = Norb;  Filename = "Green"
    case (2)
      Ns = Latt%N; No = Norb;  Filename = "SpinZ"
    case (3)
      Ns = Latt%N; No = Norb;  Filename = "SpinXY"
    case (4)
      Ns = Latt%N; No = Norb;  Filename = "Den"
    case default
      Write(6,*) ' Error in Alloc_obs '
  end select
```



```

Nt = 1
Call Obser_Latt_make(Observe_eq(I),Ns,Nt,No,Filename)
enddo

```

For the Hubbard model $N_{orb} = 1$ and for equal-time correlation functions $N_t = 1$. If $L_{tau} = 1$ then the code will allocate space for time displaced quantities. The same structure as for equal-time correlation functions will be used, albeit with $N_t = L_{trot} + 1$. At the beginning of each bin, the main program will set the bin observables to zero by calling the routine `Init_obs(Ltau)`. The user does not have to edit this routine.

7.1.2.2 Measuring equal-time observables: `Observe(GR,Phase,Ntau)`

The equal-time Green function,

$$GR(x, y, \sigma) = \langle c_{x,\sigma} c_{y,\sigma}^\dagger \rangle, \quad (124)$$

the phase factor `phase` [Eq. (118)], and time slice N_{tau} are provided by the main program.

Here, x and y label both unit cell as well as the orbital within the unit cell. For the Hubbard model described here, x corresponds to the unit cell. The Green function does not depend on the color index, and is diagonal in flavor. For the $SU(2)$ symmetric implementation there is only one flavor, $\sigma = 1$ and the Green function is independent on the spin index. This renders the calculation of the observables particularly easy.

An explicit calculation of the potential energy $\langle U \sum_i \hat{n}_{i,\uparrow} \hat{n}_{i,\downarrow} \rangle$ reads

```

Obs_scal(2)%N      = Obs_scal(2)%N + 1
Obs_scal(2)%Ave_sign = Obs_scal(2)%Ave_sign + Real(ZS,kind(0.d0))
Do i = 1,Ndim
  Obs_scal(2)%Obs_vec(1) = Obs_scal(2)%Obs_vec(1) + (1-GR(i,i,1))*2 * Ham_U * ZS * ZP
Enddo

```

Here $ZS = \text{sign}(C)$ [see Eq. (23)], $ZP = \frac{e^{-S(C)}}{\text{Re}[e^{-S(C)}]}$ [see Eq. (118)] and Ham_U corresponds to the Hubbard- U term.

Equal-time correlations are also computed in this routine. As an explicit example, we consider the equal-time density-density correlation:

$$\langle n_{i,\alpha} n_{j,\beta} \rangle - \langle n_{i,\alpha} \rangle \langle n_{j,\beta} \rangle. \quad (125)$$

For the calculation of such quantities, it is convenient to define:

$$GRC(x, y, s) = \delta_{x,y} - GR(y, x, s) \quad (126)$$

such that $GRC(x, y, s)$ corresponds to $\langle \langle \hat{c}_{x,s}^\dagger \hat{c}_{y,s} \rangle \rangle$. In the program code, the calculation of the equal-time density-density correlation function looks as follows:

```

Obs_eq(4)%N = Obs_eq(4)%N + 1          ! Even if it is redundant, each observable
                                         ! carries its own counter and sign.
Obs_eq(4)%Ave_sign = Obs_eq(4)%Ave_sign + Real(ZS,kind(0.d0))
Do I1 = 1,Ndim
  I = List(I1,1)                        ! = I1 (The Hubbard model on the square
  no_I = List(I1,2)                     ! = 1 lattice has one orbital per unit-cell)
  Do J1 = 1,Ndim
    J = List(J1,1)
    no_J = List(J1,2)
    imj = latt%imj(I,J)
    Obs_eq(4)%Obs_Latt(imj,1,no_I,no_J) = Obs_eq(4)%Obs_Latt(imj,1,no_I,no_J) + &
                                         & ( GRC(I1,I1,1) * GRC(J1,J1,1) * N_SUN * N_SUN + &
                                         & GRC(I1,J1,1) * GR(I1,J1,1) * N_SUN ) * ZP * ZS
  Enddo
  Obs_eq(4)%Obs_Latt0(no_I) = Obs_eq(4)%Obs_Latt0(no_I) + GRC(I1,I1,1) * N_SUN*ZP*ZS
Enddo

```

Note that we consider the square lattice of the single site Hubbard model as a special case of a multi-orbital problem as described in Sec. 7.3.1 At the end of each bin the main program will call the routine `Pr_obs(LTAU)`. This routine will append the result of the bins in the specified file, with appropriate suffix.

7.1.2.3 Measuring time displaced observables: `ObserT(NT, GT0, GOT, G00, GTT, PHASE)`

This subroutine is called by the main program at the beginning of each sweep, provided that `LTAU` is set to unity. `NT` runs from 0 to `Ltrot` and denotes the imaginary time difference. For a given time displacement, the main program provides:

$$\begin{aligned}
\text{GT0}(\mathbf{x}, \mathbf{y}, \mathbf{s}) &= \langle \langle \hat{c}_{x,s}(Nt\Delta\tau) \hat{c}_{y,s}^\dagger(0) \rangle \rangle = \langle \langle \mathcal{T} \hat{c}_{x,s}(Nt\Delta\tau) \hat{c}_{y,s}^\dagger(0) \rangle \rangle \\
\text{GOT}(\mathbf{x}, \mathbf{y}, \mathbf{s}) &= -\langle \langle \hat{c}_{y,s}^\dagger(Nt\Delta\tau) \hat{c}_{x,s}(0) \rangle \rangle = \langle \langle \mathcal{T} \hat{c}_{x,s}(0) \hat{c}_{y,s}^\dagger(Nt\Delta\tau) \rangle \rangle \\
\text{G00}(\mathbf{x}, \mathbf{y}, \mathbf{s}) &= \langle \langle \hat{c}_{x,s}(0) \hat{c}_{y,s}^\dagger(0) \rangle \rangle \\
\text{GTT}(\mathbf{x}, \mathbf{y}, \mathbf{s}) &= \langle \langle \hat{c}_{x,s}(Nt\Delta\tau) \hat{c}_{y,s}^\dagger(Nt\Delta\tau) \rangle \rangle
\end{aligned} \tag{127}$$

In the above we have omitted the color index since the Green functions are color independent. The time displaced spin-spin correlations $4\langle \langle \hat{S}_i^z(\tau) \hat{S}_j^z(0) \rangle \rangle$ are thereby given by:

$$4\langle \langle \hat{S}_i^z(\tau) \hat{S}_j^z(0) \rangle \rangle = -2 \text{GOT}(\mathbf{J1}, \mathbf{I1}, 1) \text{GT0}(\mathbf{I1}, \mathbf{J1}, 1) \quad . \tag{128}$$

Note that the above holds for the $SU(2)$ HS transformation discussed in this chapter. The handling of time displaced correlation functions is identical to that of equal-time correlations.

7.1.3 Numerical precision

The directory `Examples/Hubbard_SU2_Square` contains an example simulation of the 4×4 Hubbard model at $U/t = 4$ and $\beta t = 10$. Information on the numerical stability is included in the following lines of the corresponding file `info`:

```

Precision Green   Mean, Max :    1.2918865817224671E-014    4.0983018995027644E-011
Precision Phase, Max      :    5.0272908791449966E-012
Precision tau      Mean, Max :    8.4596701790588625E-015    3.5033530012121281E-011

```

showing the mean and maximum difference between the *wrapped* and from scratch computed equal and time displaced Green functions [6]. A stable code should produce results where the mean difference is smaller than the stochastic error. The above example shows a very stable simulation since the Green function is of order one.

7.2 The M_z -Hubbard model on a square lattice

The Hubbard Hamiltonian can equally be written as:

$$\mathcal{H} = \sum_{\sigma=1}^2 \sum_{x,y=1}^{N_{\text{unit cells}}} c_{x\sigma}^\dagger T_{x,y} c_{y\sigma} - \frac{U}{2} \sum_x \left[c_{x,\uparrow}^\dagger c_{x\uparrow} - c_{x,\downarrow}^\dagger c_{x\downarrow} \right]^2. \tag{129}$$

We can make contact with the general form of the Hamiltonian (see Eq. 2) by setting: $N_{\text{fl}} = 2$, $N_{\text{col}} \equiv N_{\text{SUN}} = 1$, $M_T = 1$, $T_{xy}^{(ks)} = T_{x,y}$, $M_V = N_{\text{unit-cell}}$, $U_k = \frac{U}{2}$, $V_{xy}^{(k,s=1)} = \delta_{x,y} \delta_{x,k}$, $V_{xy}^{(k,s=2)} = -\delta_{x,y} \delta_{x,k}$, $\alpha_{ks} = 0$ and $M_I = 0$. The coupling of the HS fields to the z -component of the magnetization breaks the $SU(2)$ spin symmetry. Nevertheless the z -component of the spin remains a good quantum number such that the imaginary-time propagator – for a given HS field – is block diagonal in this quantum number. This corresponds to the flavor index which runs from one to two labelling spin up and spin down degrees of freedom. In the parameter file listed in Sec. 5.4.1 setting the model variable to `Hubbard_Mz` will carry out the simulation in the above representation. With respect to the $SU(2)$ case, the changes required in the `Hamiltonian_Examples_mod.F90` module are minimal and essentially effect only the interaction term, and the calculation of observables. We note that in this formulation the hopping matrix can be flavor dependent such that a Zeeman magnetic field can be introduced. If the chemical potential is set to zero, this will not generate a negative sign problem [34, 81, 82]. A sample run for this model can be found in `Examples/Hubbard_Mz_Square/`.

7.2.1 The interaction term: `Call Ham_V`

Superseded by `Predefined Structures`.

7.2.2 The measurements: Call Obser, Call ObserT

Since the spin up and spin down Green functions differ for a given HS configuration, the Wick decomposition will take a different form. In particular, the equal-time spin-spin correlation functions $4\langle\langle\hat{S}_i^z\hat{S}_j^z\rangle\rangle$ calculated in the subroutine `Obser` will take the form:

$$4\langle\langle\hat{S}_x^z\hat{S}_y^z\rangle\rangle = \text{GRC}(x,y,1) * \text{GR}(x,y,1) + \text{GRC}(x,y,2) * \text{GR}(x,y,2) + \\ (\text{GRC}(x,x,2) - \text{GRC}(x,x,1)) * (\text{GRC}(y,y,2) - \text{GRC}(y,y,1))$$

Here, `GRC` is defined in Eq. 126. Equivalent changes will have to be carried out for other equal-time and time displaced observables.

Apart from these modifications, the program will run in exactly the same manner as for the $SU(2)$ case.

7.2.3 Numerical precision

The directory `Examples/Hubbard_Mz_Square` contains an example simulation of the 4×4 Hubbard model at $U/t = 4$ and $\beta t = 10$. Information on the numerical stability is included in the following lines of the corresponding file `info`:

```
Precision Green   Mean, Max :    5.0823874429126405E-011    5.8621144596315844E-006
Precision Phase, Max      :    0.00000000000000000
Precision tau      Mean, Max :    1.5929357848647394E-011    1.0985132530727526E-005
```

This is still an excellent precision but nevertheless choosing a HS field which couples to the z-component of the magnetization apparently leads to numerical results that are a couple of order of magnitudes less precise than a HS decomposition coupling to the charge (compare with Sec. 7.1.3).

7.3 The $SU(2)$ -Hubbard model on the honeycomb lattice

The Hamilton module `Hamiltonian_Examples_mod.F90` can also carry out simulations for the Hubbard model on the Honeycomb lattice by setting in the parameter file `Lattice_type="Honeycomb"` (see Sec. 5.4.1). A sample run for this model can be found in `Examples/Hubbard_SU2_Honeycomb/`.

7.3.1 Working with multi-orbital unit cells: Call Ham_Latt

Superseded by [Predefined Structures](#).

7.3.2 The hopping term: Call Ham_Hop

Some care has to be taken when setting the hopping matrix. In the Hamilton module `Hamiltonian_Examples_mod.F90` we do this in the following way:

```
DO I = 1, Latt%N                                ! Loop over unit cell
  do no = 1, Norb                                ! Runs over orbitals and
                                                ! sets the chemical potential

    I1 = invlist(I,no)
    Op_T(nc,n)%0(I1,I1) = cmplx(-Ham_chem, 0.d0, kind(0.D0))
  enddo
  I1 = Invlist(I,1)                                ! Orbital A of unit cell I
  Do nc1 = 1, N_coord                            ! Loop over coordination number
    select case (nc1)
      case (1)
        J1 = invlist(I,2)                        ! Orbital B of unit cell i
      case (2)
        J1 = invlist(Latt%nnlist(I,1,-1),2)      ! Orbital B of unit cell i + a_1 - a_2
      case (3)
        J1 = invlist(Latt%nnlist(I,0,-1),2)      ! Orbital B of unit cell i - a_2
      case default
        Write(6,*) ' Error in Ham_Hop '
    end select
    Op_T(nc,n)%0(I1,J1) = cmplx(-Ham_T, 0.d0, kind(0.D0))
    Op_T(nc,n)%0(J1,I1) = cmplx(-Ham_T, 0.d0, kind(0.D0))
  enddo
```

```
Enddo
Enddo
```

As apparent from the above, hopping matrix elements are non-zero only between the A and B sublattices.

7.3.3 Observables: Call Obser, Call ObserT

In the multi-orbital case, the correlation functions have additional orbital indices. This is automatically taken care of in the routines `Call Obser` and `Call ObserT` since we have already considered the Hubbard model on the square lattice to correspond to a multi-orbital unit cell albeit with the special choice of one orbital per unit cell.

8 Predefined Structures

ALF includes modules providing predefined structures which the user can combine together or use as templates for defining new structures, namely:

- lattices and unit cells – `Predefined_Latt_mod.F90`
- hopping Hamiltonians – `Predefined_Hop_mod.F90`
- interaction Hamiltonians – `Predefined_Int_mod.F90`
- observables – `Predefined_Obs_mod.F90`
- trial wave functions – `Predefined_Trial_mod.F90`

which are defined using the data structures defined in the Sec. 5, as described in this section.

8.1 Predefined lattices

The types `Lattice` and `Unit_cell`, described in Section 5.1.4, allow us to define arbitrary one- and two-dimensional Bravais lattices. The subroutine `Predefined_Latt` provides some of the most common lattices, as described bellow.

The subroutine is called as:

```
Predefined_Latt(Lattice_type, L1, L2, Ndim, List, Invlist, Latt, Latt_Unit)
```

which returns a lattice of size $L1 \times L2$ of the given `Lattice_type`, as detailed in Table 16. Notice that the orbital position `Latt_Unit%Orb_pos_p(1,:)` is set to zero unless otherwise specified.

In order to easily keep track of the orbital and unit cell, `List` and `Invlist` make use of a super-index, defined as shown below:

```
nc = 0
Do I = 1,Latt%N
  Do no = 1,Norb
    nc = nc + 1
    List(nc,1) = I
    List(nc,2) = no
    Invlist(I,no) = nc
  Enddo
Enddo
```

! Super-index labeling unit cell and orbital
! Unit-cell index
! Orbital index
! Unit-cell of super index nc
! Orbital of super index nc
! Super-index for given unit cell and orbital

With the above lists one can run through all the orbitals and at each time keep track of the unit-cell and orbital index. We note that when translation symmetry is completely absent one can work with a single unit cell, and the number of orbitals will then correspond to the number of lattice sites.

8.1.1 Square lattice, Fig. 5(a)

The choice `Lattice_type = "Square"` sets $\mathbf{a}_1 = (1,0)$ and $\mathbf{a}_2 = (0,1)$ and for an $L_1 \times L_2$ lattice $L_1 = L_1 \mathbf{a}_1$ and $L_2 = L_2 \mathbf{a}_2$:



Figure 5: Predefined lattices in ALF: (a) square, (b) bilayer square, (c) 3-leg ladder (d) honeycomb and (e) bilayer honeycomb. Nontrivial unit cells are shown as gray regions, while gray sites belong to the second layer in bilayer systems. The links between the orbitals denote the hopping matrix elements and we have assumed, for the purpose of the plot, the absence of hopping in the second layer for bilayer systems. The color coding of the links denotes the checkerboard decomposition.

```
Latt_Unit%N_coord = 2
Latt_Unit%Norb = 1
Latt_Unit%Orb_pos_p(1,:) = 0.d0
a1_p(1) = 1.0 ; a1_p(2) = 0.d0
a2_p(1) = 0.0 ; a2_p(2) = 1.d0
L1_p = dble(L1)*a1_p
L2_p = dble(L2)*a2_p
Call Make_Lattice( L1_p, L2_p, a1_p, a2_p, Latt )
```

Also, the number of orbitals per unit cell is given by $NORB=1$ such that $N_{dim} \equiv N_{unit-cell} \cdot NORB = Latt\%N \cdot NORB$, since $N_{unit-cell} = Latt\%N$.

8.1.2 Bilayer Square lattice, Fig. 5(b)

The "Bilayer_square" configuration sets:

```
Latt_Unit%Norb = 2
Latt_Unit%N_coord = 2
do no = 1,2
  Latt_Unit%Orb_pos_p(no,1) = 0.d0
  Latt_Unit%Orb_pos_p(no,2) = 0.d0
  Latt_Unit%Orb_pos_p(no,3) = real(1-no,kind(0.d0))
enddo
Latt%a1_p(1) = 1.0 ; Latt%a1_p(2) = 0.d0
Latt%a2_p(1) = 0.0 ; Latt%a2_p(2) = 1.d0
Latt%L1_p = dble(L1)*a1_p
Latt%L2_p = dble(L2)*a2_p
Call Make_Lattice( L1_p, L2_p, a1_p, a2_p, Latt )
```

8.1.3 N-leg Ladder lattice, Fig. 5(c)

The "N_leg_ladder" configuration sets:

Argument	Type	Role	Description
Lattice_type	String	Input	lattice configuration, which can take the values: <ul style="list-style-type: none"> - Square - Honeycomb - Pi_Flux (deprecated) - N_leg_ladder - Bilayer_square - Bilayer_honeycomb
L1, L2	Integer	Input	lattice sizes (set L2=1 for 1D lattices)
Ndim	Integer	Output	total number of orbitals
List	Integer	Output	for every site index $I \in [1, Ndim]$, stores the corresponding lattice position, <code>List(I,1)</code> , and the (local) orbital index, <code>List(I,2)</code>
Invlist	Integer	Output	for every <code>lattice_position</code> $\in [1, Latt\%N]$ and <code>orbital</code> $\in [1, Norb]$ stores the corresponding site index <code>I(lattice_position,orbital)</code>
Latt	Lattice	Output	sets the lattice
Latt_Unit	Unit_cell	Output	sets the unit cell

Table 16: Arguments of the subroutine `Predefined_Latt`. Note that the `Pi_Flux` lattice is deprecated for the moment since it can be emulated with the `Square` lattice with half a flux quanta piercing each plaquette.

```

Latt_Unit%Norb      = L2
Latt_Unit%N_coord   = 1
do no = 1,L2
  Latt_Unit%Orb_pos_p(no,1) = 0.d0
  Latt_Unit%Orb_pos_p(no,2) = real(no-1,kind(0.d0))
enddo
a1_p(1) = 1.0 ; a1_p(2) = 0.d0
a2_p(1) = 0.0 ; a2_p(2) = 1.d0
L1_p    = dble(L1)*a1_p
L2_p    =          a2_p
Call Make_Lattice( L1_p, L2_p, a1_p, a2_p, Latt )

```

8.1.4 Honeycomb lattice, Fig. 5(d)

In order to carry out simulations on the Honeycomb lattice, which is a triangular Bravais lattice with two orbitals per unit cell, we choose `Lattice_type="Honeycomb"` , which sets

```

a1_p(1) = 1.D0 ; a1_p(2) = 0.d0
a2_p(1) = 0.5D0 ; a2_p(2) = sqrt(3.D0)/2.D0
L1_p    = Dble(L1) * a1_p
L2_p    = dble(L2) * a2_p
Call Make_Lattice( L1_p, L2_p, a1_p, a2_p, Latt )
Latt_Unit%Norb      = 2
Latt_Unit%N_coord   = 3
Latt_Unit%Orb_pos_p(1,:) = 0.d0
Latt_Unit%Orb_pos_p(2,:) = (a2_p(:) - 0.5D0*a1_p(:) ) * 2.D0/3.D0

```

The coordination number of this lattice is `N_coord=3` and the number of orbitals per unit cell, `NORB=2`. The total number of orbitals is therefore $N_{dim}=Latt\%N*NORB$.

8.1.5 Bilayer Honeycomb lattice, Fig. 5(e)

The "`Bilayer_honeycomb`" configuration sets:

```

Latt_Unit%Norb      = 4

```

```

Latt_Unit%N_coord = 3
Latt_unit%Orb_pos_p = 0.d0
do n = 1,2
  Latt_Unit%Orb_pos_p(1,n) = 0.d0
  Latt_Unit%Orb_pos_p(2,n) = (a2_p(n) - 0.5D0*a1_p(n) ) * 2.D0/3.D0
  Latt_Unit%Orb_pos_p(3,n) = 0.d0
  Latt_Unit%Orb_pos_p(4,n) = (a2_p(n) - 0.5D0*a1_p(n) ) * 2.D0/3.D0
enddo
Latt_Unit%Orb_pos_p(3,3) = -1.d0
Latt_Unit%Orb_pos_p(4,3) = -1.d0
a1_p(1) = 1.D0 ; a1_p(2) = 0.d0
a2_p(1) = 0.5D0 ; a2_p(2) = sqrt(3.D0)/2.D0
L1_p = dble(L1)*a1_p
L2_p = dble(L2)*a2_p
Call Make_Lattice( L1_p, L2_p, a1_p, a2_p, Latt )

```

8.1.6 π -Flux lattice (deprecated)

The Pi_Flux lattice has been deprecated, since it can be emulated with the Square lattice with half a flux quanta piercing each plaquette. Nonetheless, the configuration is still available, and sets:

```

Latt_Unit%Norb = 2
Latt_Unit%N_coord = 4
a1_p(1) = 1.D0 ; a1_p(2) = 1.d0
a2_p(1) = 1.D0 ; a2_p(2) = -1.d0
Latt_Unit%Orb_pos_p(1,:) = 0.d0
Latt_Unit%Orb_pos_p(2,:) = (a1_p(:) - a2_p(:))/2.d0
L1_p = dble(L1) * (a1_p - a2_p)/2.d0
L2_p = dble(L2) * (a1_p + a2_p)/2.d0

```

8.2 Generic hopping matrices on bravais lattices

8.2.1 Setting up the hopping matrix: the Hopping_Matrix_type

The module `Predefined_Hopping` provides a generic way to specify a hopping matrix on a multi-orbital Bravais lattice. The only assumption that we make is translation symmetry. We allow for twisted boundary conditions in the L_1 and L_2 lattice directions. The twist is given by Φ_X and Φ_Y respectively. If the flag `bulk=.true.`, then the twist is implemented with a vector potential. Otherwise, if `bulk=.false.`, the twist is imposed at the boundary. The routine also accounts for the inclusion of a total number of N_Φ flux quanta traversing the lattice. All phase factors mentioned above can be flavor dependent. The checkerboard decomposition can also be specified in this module. All information, including the checkerboard decomposition is specified in the `Hopping_Matrix_type` type (see below) from which the array of operator type `OP_T`, accounting for the single particle propagation in one time step, as well as the Kinetic energy can be derived.

Generic hopping matrices

The generic Hopping Hamiltonian reads:

$$\hat{H}_T = \sum_{(i,\delta),(j,\delta'),s,\sigma} T_{(i,\delta),(j,\delta'),s,\sigma}^{(s)} c_{(i,\delta),s,\sigma}^\dagger e^{\frac{2\pi i}{\Phi_0} \int_{i+\delta}^{j+\delta'} \mathbf{A}^{(s)}(l) dl} c_{(j,\delta'),s,\sigma} \quad (130)$$

with boundary conditions

$$c_{(i+L_i,\delta),s,\sigma}^\dagger = e^{-2\pi i \frac{\Phi^{(s)}}{\Phi_0}} e^{\frac{2\pi i}{\Phi_0} \chi_{L_i}^{(s)}(i+\delta)} c_{(i,\delta),s,\sigma}^\dagger. \quad (131)$$

Both the twist and vector potential can have a flavor dependency. For now onwards we will mostly omit the flavor index s .

Phase factors. The vector potential accounts for an orbital magnetic field that is implemented in the Landau gauge: $\mathbf{A}(\mathbf{x}) = -B(y, 0, 0)$ with $\mathbf{x} = (x, y, z)$. Φ_0 corresponds to the flux quanta and the scalar function χ is defined through as:

$$\mathbf{A}(\mathbf{x} + \mathbf{L}_i) = \mathbf{A}(\mathbf{x}) + \nabla \chi_{L_i}(\mathbf{x}). \quad (132)$$

Provided that the bare hopping Hamiltonian, T , is invariant under lattice translations, \hat{H}_T commutes with magnetic translations that satisfy the Algebra:

$$\hat{T}_{\mathbf{a}} \hat{T}_{\mathbf{b}} = e^{\frac{2\pi i}{\Phi_0} \mathbf{B} \cdot (\mathbf{a} \times \mathbf{b})} \hat{T}_{\mathbf{b}} \hat{T}_{\mathbf{a}}. \quad (133)$$

On the torus, the uniqueness of the wave functions requires that $\hat{T}_{\mathbf{L}_1} \hat{T}_{\mathbf{L}_2} = \hat{T}_{\mathbf{L}_2} \hat{T}_{\mathbf{L}_1}$ such that

$$\frac{\mathbf{B} \cdot (\mathbf{a} \times \mathbf{b})}{\Phi_0} = N_\Phi \quad (134)$$

with N_Φ an integer. The variable `N_Phi`, specified in the parameter file, denotes the number of flux quanta piercing the lattice. The variables `Phi_X` and `Phi_Y` also in the parameter file denote the twists – in units of the flux quanta – along the \mathbf{L}_1 and \mathbf{L}_2 directions. There are gauge equivalent ways to insert the twist in the boundary conditions. In the above we have inserted twist as a boundary condition such that for example setting `Phi_1=0.5` corresponds to anti-periodic boundary conditions along the L_1 axis. Alternatively we can consider the Hamiltonian:

$$\hat{H}_T = \sum_{(i,\delta),(j,\delta'),s,\sigma} T_{(i,\delta),(j,\delta'),s,\sigma}^{(s)} \tilde{c}_{(i,\delta),s,\sigma}^\dagger e^{\frac{2\pi i}{\Phi_0} \int_{i+\delta}^{j+\delta'} (\mathbf{A}(\mathbf{l}) + \mathbf{A}_\phi) d\mathbf{l}} \tilde{c}_{(j,\delta'),s,\sigma} \quad (135)$$

with boundary conditions

$$\tilde{c}_{(i+\mathbf{L}_i,\delta),s,\sigma}^\dagger = e^{\frac{2\pi i}{\Phi_0} \chi_{L_i}(i+\delta)} \tilde{c}_{(i,\delta),s,\sigma}^\dagger. \quad (136)$$

Here

$$\mathbf{A}_\phi = \frac{\phi_1 |\mathbf{a}_1|}{2\pi |\mathbf{L}_1|} \mathbf{b}_1 + \frac{\phi_2 |\mathbf{a}_2|}{2\pi |\mathbf{L}_2|} \mathbf{b}_2 \quad (137)$$

and \mathbf{b}_i correspond to the reciprocal lattice vectors satisfying $\mathbf{a}_i \cdot \mathbf{b}_j = 2\pi \delta_{i,j}$. The logical variable `bulk` chooses between these two gauge equivalent ways of inserting the twist angle. If `bulk=true` then we use periodic boundary conditions – in the absence of an orbital field – otherwise twisted boundaries are used. The above phase factors are computed in the module function:

```
complex function Generic_hopping(i,no_i, n_1, n_2, no_j, N_Phi, Phi_1,Phi_2, Bulk,
Latt, Latt_Unit)
```

that returns the phase factor involved in the hopping of a hole from lattice site $\mathbf{i} + \delta_{\text{no}_i}$ to $\mathbf{i} + n_1 \mathbf{a}_1 + n_2 \mathbf{a}_2 + \delta_{\text{no}_j}$. Here δ_{no_i} is the position of the no_i orbital in the unit cell \mathbf{i} . As we will see below, the information for the phases is encoded in the type `Hopping_matrix_type`.

The Hopping matrix elements. The hopping matrix is specified assuming only translation invariance. (The point group symmetry of the lattice can be broken). That is, we assume that for each flavor index:

$$T_{(\mathbf{i},\delta),(\mathbf{i}+n_1\mathbf{a}_1+n_2\mathbf{a}_2,\delta')}^{(s)} = T_{(\mathbf{0},\delta),(n_1\mathbf{a}_1+n_2\mathbf{a}_2,\delta')}^{(s)}. \quad (138)$$

The right hand side of the above equation is given the type `Hopping_matrix_type`.

The checkerboard decomposition. Aside from the hopping phases and hopping matrix elements, the `Hopping_matrix_type` type, contains information concerning the checkerboard decomposition. In Eq. 65 we wrote the hopping Hamiltonian as:

$$\hat{H}_T = \sum_{i=1}^{N_T} \sum_{k \in S_i^T} \hat{T}^{(k)}, \quad (139)$$

with the rule that if k and k' belong to the same set \mathcal{S}_i^T then $[\hat{T}^{(k)}, \hat{T}^{(k')}] = 0$. In the checkerboard decomposition, $\hat{T}^{(k)}$ corresponds to hopping on a bond. The checkerboard decomposition depends on the lattice type, as well as on the hopping matrix elements. The required information is stored in `Hopping_matrix_type`. In this data type, `N_FAM` corresponds to the number of sets (or families) (N_T in the above equation). `L_FAM(1:N_FAM)` corresponds to the number of bonds in the set, and finally, `LIST_FAM(1:N_FAM, 1:max(L_FAM(:)), 2)` contains information concerning the two legs of the bonds. In the checkerboard decomposition, care has to be taken for local terms: each site occurs multiple times in the list of bonds. Since we have postulated translation symmetry, a one-dimensional array, `Multiplicity`, of length given by the number of orbitals per unit cell suffices to encode the required information. Finally, to be able to generate the imaginary time step of length $\Delta\tau$ we have to know by which fraction of $\Delta\tau$ we have to propagate each set. This information is given in the array `Prop_Fam`.

As an example we can consider the three leg ladder lattice of Figure 5(c). Here the number of sets (or families) `N_FAM` is equal to four corresponding to the red, green, black and blue bonds. As apparent, bonds in a given set do not have common legs such that hopping instances on the bonds of a given set commute. For this three leg ladder it is apparent that the second orbital in a unit cell appears in each set or family. It hence has a multiplicity of four. On the other hand, the top and bottom orbitals have a multiplicity of 3 since they appear in only three of the four sets.

Usage: the `Hopping_Matrix_type`

There are `N_bonds` hopping matrix elements emanating from a given unit cell. For each bond, the array `List` contains the full information to define the RHS of Eq. (138). The hopping amplitudes are stored in the array `T` and the local potentials in the array `T_loc` (See Table 17). The `Hopping_Matrix_type` type also contains the information for the checkerboard decomposition.

Variable	Type	Description
<code>N_bonds</code>	Integer	Number of hopping matrix elements within and emanating from a unit cell
<code>List(N_bonds,4)</code>	Integer	$\text{List}(\bullet,1) = \delta$ $\text{List}(\bullet,2) = \delta'$ $\text{List}(\bullet,3) = n_1$ $\text{List}(\bullet,4) = n_2$
<code>T(N_bonds)</code>	Complex	Hopping amplitude
<code>T_loc(Norb)</code>	Complex	On site potentials (e.g., chemical potential, Zeeman field)
<code>N_Phi</code>	Integer	Number of flux quanta piercing the lattice
<code>Phi_X</code>	Real	Twist in \mathbf{a}_1 direction
<code>Phi_Y</code>	Real	Twist in \mathbf{a}_2 direction
<code>Bulk</code>	Logical	Twist as vector potential (T) or boundary condition (F).
<code>N_Fam</code>	Integer	Number of sets, N_T in Eq. (65)
<code>L_Fam(N_FAM)</code>	Integer	Number of bonds per set \mathcal{S}^T
<code>List_Fam(N_FAM,L_FAM,2)</code>	Integer	$\text{List Fam}(\bullet,\bullet,1) = \text{Unit cell}$ $\text{List Fam}(\bullet,\bullet,2) = \text{Bond number}$
<code>Multiplicity(Norb)</code>	Integer	Number of times a given orbital occurs in the list of bonds
<code>Prop_Fam</code>	Real	The fraction of $\Delta\tau$ with which the set will be propagated

Table 17: Member variables of the `Hopping_Matrix_type` type.

The data in the `Hopping_matrix_type` type suffices to uniquely define the unit step propagation for the kinetic energy, and for any combinations of the `Checkerboard` and `Symm` options (see Sec. 2.3). This is carried by the call:

```
Call Predefined_Hoppings_set_OPT(Hopping_Matrix, List, Invlist, Latt, Latt_unit, Dtau,
Checkerboard, Symm, OP_T)
```

in which the operator array `OP_T(*,N_FL)` is allocated and defined. In the simplest case, where no checkerboard is used, the first dimension is unity.

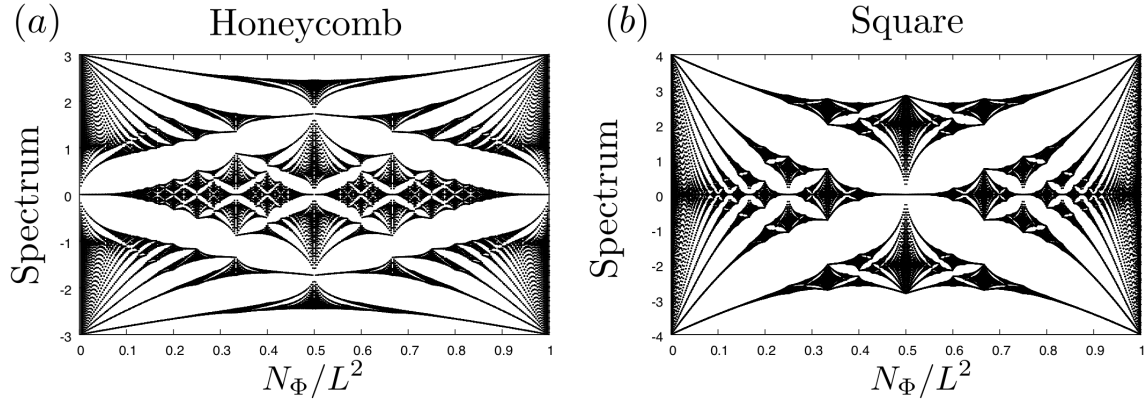


Figure 6: The single particle spectrum of the tight binding model on the honeycomb (a) and square (b) lattices as a function of the flux N_Φ . This corresponds to the well known Hofstadter butterflies.

The data in the `Hopping_matrix_type` type equally suffices to compute the kinetic energy. This is carried out in the routine `Predefined_Hoppings_Compute_Kin`.

8.2.2 An example: nearest neighbor hopping on the honeycomb lattice

For the honeycomb lattice of Fig. 5(d) the number of bond within and emanating from a unit cell is $N_{\text{bonds}} = 3$. The list array of the `Hopping_matrix_type` reads:

```
list(1,1) = 1; list(1,2) = 2; list(1,3) = 0; list(1,4) = 0 ! Intra unit-cell hopping
list(2,1) = 2; list(2,2) = 1; list(2,3) = 0; list(2,4) = 1 ! Inter unit-cell hopping
list(3,1) = 1; list(3,2) = 2; list(3,3) = 1; list(3,4) = -1 ! Inter unit-cell hopping
T(1) = -1.0; T(2) = -1.0; T(3) = -1.0 ! Hopping
T_loc(1) = 0.0; T_loc(2) = 0.0 ! Chemical potential
```

In the last two lines, we have set the hopping matrix element for each bond to -1 and the chemical potential to zero. The fields, can then be specified with the variables N_{phi} , Φ_x , Φ_y . Setting the twists, Φ_x , Φ_y to zero and looping over N_{phi} from $1 \cdots L^2$ produces the single particle spectrum of Fig. 6(a).

For the Honeycomb lattice the checkerboard decomposition for the nearest neighbor hopping consists of three sets: $N_{\text{Fam}} = 3$ each of length corresponding to the number of unit cells. In Fig. 5(d) the bond elements of these three sets are color coded. In the code, the element of the sets are specified as:

```
do I = 1,Latt%N
  Do nf = 1,N_FAM
    List_Fam(nf,I,1) = I ! Unit cell
    List_Fam(nf,I,2) = nf ! The bond
  Enddo
enddo
Multiplicity = 3
```

Since each site of the honeycomb lattice occurs in the three sets, the multiplicity is equal to 3.

8.2.3 Predefined hoppings

The module provides hopping and checkerboard decompositions, defining a `Hopping_Matrix` (an array of length N_{FL} of type `Hopping_Matrix_type`, see Sec. 8.2.1) for each of the following predefined lattices.

Square

The call:

```
Call Set_Default_hopping_parameters_square(Hopping_Matrix, T_vec, Chem_vec, Phi_X_vec,
  Phi_Y_vec, Bulk, N_Phi_vec, N_FL, List, Invlist, Latt, Latt_unit)
```

defines the `Hopping_Matrix` for the square lattice:

$$\hat{H}_T = \sum_{i,\sigma,s} \left(\left[\sum_{\delta=\{\mathbf{a}_1,\mathbf{a}_2\}} -t^{(s)} \hat{c}_{i,s,\sigma}^\dagger e^{\frac{2\pi i}{\Phi_0} \int_i^{i+\delta} \mathbf{A}^{(s)}(l) dl} \hat{c}_{i+\delta,s,\sigma} + H.c. \right] - \mu^{(s)} \hat{c}_{i,s,\sigma}^\dagger \hat{c}_{i,s,\sigma} \right). \quad (140)$$

The vectors `T_vec` and `Chem_vec` have length `N_FL` and specify the hopping and the chemical potentials, while the vectors `Phi_X_vec`, `Phi_Y_vec` and `N_Phi_vec`, also of length `N_FL`, define the vector potential.

Honeycomb

The call:

```
Call Set_Default_hopping_parameters_honeycomb(Hopping_Matrix, T_vec, Chem_vec, Phi_X_vec,
Phi_Y_vec, Bulk, N_Phi_vec, N_FL, List, Invlist, Latt, Latt_unit)
```

defines the `Hopping_Matrix` for the honeycomb lattice:

$$\hat{H}_T = \sum_{i,\sigma,s} \left(\left[\sum_{\delta=\{\delta_1,\delta_2,\delta_3\}} -t^{(s)} \hat{c}_{i,s,\sigma}^\dagger e^{\frac{2\pi i}{\Phi_0} \int_i^{i+\delta} \mathbf{A}^{(s)}(l) dl} \hat{c}_{i+\delta,s,\sigma} + H.c. \right] - \mu^{(s)} \hat{c}_{i,s,\sigma}^\dagger \hat{c}_{i,s,\sigma} \right), \quad (141)$$

where the `T_vec` and `Chem_vec` have length `N_FL` and specify the hopping and the chemical potentials, while the vectors `Phi_X_vec`, `Phi_Y_vec` and `N_Phi_vec`, also of length `N_FL`, define the vector potential. Here i runs over sublattice A, and $i + \delta$ over the three nearest neighbors of site i .

Square bilayer

The call:

```
Call Set_Default_hopping_parameters_Bilayer_square(Hopping_Matrix, T1_vec, T2_vec, Tperp_vec,
Chem_vec, Phi_X_vec, Phi_Y_vec, Bulk, N_Phi_vec, N_FL, List, Invlist, Latt, Latt_unit)
```

defines the `Hopping_Matrix` for the bilayer square lattice:

$$\hat{H}_T = \sum_{i,\sigma,s,n} \left(\left[\sum_{\delta=\{\mathbf{a}_1,\mathbf{a}_2\}} -t_n^{(s)} \hat{c}_{i,s,\sigma,n}^\dagger e^{\frac{2\pi i}{\Phi_0} \int_i^{i+\delta} \mathbf{A}^{(s)}(l) dl} \hat{c}_{i+\delta,s,\sigma,n} + H.c. \right] - \mu^{(s)} \hat{c}_{i,s,\sigma,n}^\dagger \hat{c}_{i,s,\sigma,n} \right) + \sum_{i,\sigma,s} -t_\perp^{(s)} \left(\hat{c}_{i,s,\sigma,1}^\dagger \hat{c}_{i,s,\sigma,2} + H.c. \right), \quad (142)$$

where the additional index n labels the layers.

Square honeycomb

The call:

```
Call Set_Default_hopping_parameters_Bilayer_honeycomb(Hopping_Matrix, T1_vec, T2_vec, Tperp_vec,
Chem_vec, Phi_X_vec, Phi_Y_vec, Bulk, N_Phi_vec, N_FL, List, Invlist, Latt, Latt_unit)
```

defines the `Hopping_Matrix` for the bilayer honeycomb lattice:

$$\hat{H}_T = \sum_{i,\sigma,s,n} \left(\left[\sum_{\delta=\{\delta_1,\delta_2,\delta_3\}} -t_n^{(s)} \hat{c}_{i,s,\sigma,n}^\dagger e^{\frac{2\pi i}{\Phi_0} \int_i^{i+\delta} \mathbf{A}^{(s)}(l) dl} \hat{c}_{i+\delta,s,\sigma,n} + H.c. \right] - \mu^{(s)} \hat{c}_{i,s,\sigma,n}^\dagger \hat{c}_{i,s,\sigma,n} \right) + \sum_{i,\sigma,s} -t_\perp^{(s)} \left(\hat{c}_{i,s,\sigma,1}^\dagger \hat{c}_{i,s,\sigma,2} + \hat{c}_{i+\delta_1,s,\sigma,1}^\dagger \hat{c}_{i+\delta_1,s,\sigma,2} + H.c. \right). \quad (143)$$

Here, the additional index n labels the layer.

N-leg ladder

The call:

```
Call Set_Default_hopping_parameters_n_lag_ladder(Hopping_Matrix, T_vec, Tperp_vec, Chem_vec,
Phi_X_vec, Phi_Y_vec, Bulk, N_Phi_vec, N_FL, List, Invlist, Latt, Latt_unit)
```

defines the `Hopping_Matrix` for the the N-leg ladder lattice:

$$\hat{H}_T = \sum_{\mathbf{i}, \sigma, s} \sum_{n=1}^{\text{Norb}} \left(-t^{(s)} \hat{c}_{\mathbf{i}, s, \sigma, n}^\dagger e^{\frac{2\pi i}{\Phi_0} \int_{\mathbf{i}}^{i+a_1} \mathbf{A}^{(s)}(l) dl} \hat{c}_{\mathbf{i}+\mathbf{a}_1, s, \sigma, n} + H.c. - \mu^{(s)} \hat{c}_{\mathbf{i}, s, \sigma, n}^\dagger \hat{c}_{\mathbf{i}, s, \sigma, n} \right) + \sum_{\mathbf{i}, \sigma, s} \sum_{n=1}^{\text{Norb}-1} -t_\perp^{(s)} \left(\hat{c}_{\mathbf{i}+\boldsymbol{\delta}_1, s, \sigma, n}^\dagger e^{\frac{2\pi i}{\Phi_0} \int_{(n-1)\mathbf{a}_2}^{(n)\mathbf{a}_2} \mathbf{A}^{(s)}(l) dl} \hat{c}_{\mathbf{i}+\boldsymbol{\delta}_1, s, \sigma, n+1} + H.c. \right). \quad (144)$$

Here, the additional index n defines the orbital. Note that this lattice has open boundary conditions in the \mathbf{a}_2 direction.

8.3 Predefined interaction vertices

In its most general form, an interaction Hamiltonian expressed in terms of sums of perfect squares can be written, as presented in Section 1, as a sum of M_V vertices:

$$\hat{H}_V = \sum_{k=1}^{M_V} U_k \left\{ \sum_{\sigma=1}^{N_{\text{col}}} \sum_{s=1}^{N_{\text{fl}}} \left[\left(\sum_{x,y} \hat{c}_{x\sigma s}^\dagger V_{xy}^{(ks)} \hat{c}_{y\sigma s} \right) + \alpha_{ks} \right] \right\}^2 \equiv \sum_{k=1}^{M_V} U_k \left(\hat{V}^{(k)} \right)^2 \quad (4)$$

$$\equiv \sum_{k=1}^{M_V} \hat{H}_V^{(k)},$$

which are encoded in one or more variables of type `Operator`, described in Sec. 5.1.1. We often use arrays of `Operator` type, which should be initialized by repeatedly calling the subroutine `Op_make`.

The module `Predefined_Int_mod.F90` implements some of the most common of such interaction vertices $\hat{H}_V^{(k)}$, as detailed in the remaining of this section, where we drop the superscript (k) when unambiguous.

8.3.1 $SU(N)$ Hubbard interaction

The $SU(N)$ Hubbard interaction on a given site i is given by

$$\hat{H}_{V,i} = + \frac{U}{N_{\text{col}}} \left[\sum_{\sigma=1}^{N_{\text{col}}} \left(c_{i\sigma}^\dagger c_{i\sigma} - 1/2 \right) \right]^2. \quad (145)$$

Assuming that no other term in the Hamiltonian breaks the $SU(N)$ color symmetry, then this interaction term conveniently corresponds to a single operator, obtained by calling, for each of the N_{dim} sites i :

```
Call Predefined_Int_U_SUN( OP, I, N_SUN, DTAU, U )
```

which defines:

```
Op%P(1)      = I
Op%O(1,1)    = cmplx(1.d0, 0.d0, kind(0.D0))
Op%alpha     = cmplx(-0.5d0, 0.d0, kind(0.D0))
Op%g         = SQRT(CMPLX(-DTAU*U/(DBLE(N_SUN)), 0.D0, kind(0.D0)))
Op%type      = 2
```

To relate to Eq. (4) we have, $V_{xy}^{(is)} = \delta_{x,y} \delta_{x,i}$, $\alpha_{is} = -\frac{1}{2}$ and $U_k = \frac{U}{N_{\text{col}}}$. Here the flavor index, s , plays no role.

8.3.2 M_z -Hubbard interaction

```
Call Predefined_Int_U_MZ( OP_up, Op_do, I, DTAU, U )
```

The M_z -Hubbard interaction is given by

$$\hat{\mathcal{H}}_V = -\frac{U}{2} \sum_i \left[c_{i\uparrow}^\dagger c_{i\uparrow} - c_{i\downarrow}^\dagger c_{i\downarrow} \right]^2, \quad (146)$$

which corresponds to the general form of Eq. (4) by setting: $N_{\text{fl}} = 2$, $N_{\text{col}} \equiv N_{\text{SUN}} = 1$, $M_V = N_{\text{unit-cell}}$, $U_k = \frac{U}{2}$, $V_{xy}^{(i,s=1)} = \delta_{x,y} \delta_{x,i}$, $V_{xy}^{(i,s=2)} = -\delta_{x,y} \delta_{x,i}$, and $\alpha_{is} = 0$; and which is defined in the subroutine `Predefined_Int_U_MZ` by two operators:

```
Op_up%P(1) = I
Op_up%O(1,1) = cmplx(1.d0, 0.d0, kind(0.D0))
Op_up%alpha = cmplx(0.d0, 0.d0, kind(0.D0))
Op_up%g = SQRT(CMPLX(DTAU*U/2.d0, 0.D0, kind(0.D0)))
Op_up%type = 2

Op_do%P(1) = I
Op_do%O(1,1) = cmplx(1.d0, 0.d0, kind(0.D0))
Op_do%alpha = cmplx(0.d0, 0.d0, kind(0.D0))
Op_do%g = -SQRT(CMPLX(DTAU*U/2.d0, 0.D0, kind(0.D0)))
Op_do%type = 2
```

8.3.3 $SU(N)$ V -interaction

```
Call Predefined_Int_V_SUN( OP, I, J, N_SUN, DTAU, V )
```

The interaction term of the generalized t-V model, given by

$$\hat{\mathcal{H}}_{V,i,j} = -\frac{V}{N_{\text{col}}} \left[\sum_{\sigma=1}^{N_{\text{col}}} \left(c_{i\sigma}^\dagger c_{j\sigma} + c_{j\sigma}^\dagger c_{i\sigma} \right) \right]^2, \quad (147)$$

is coded in the subroutine `Predefined_Int_V_SUN` by a single symmetric operator:

```
Op%P(1) = I
Op%P(2) = J
Op%O(1,2) = cmplx(1.d0, 0.d0, kind(0.D0))
Op%O(2,1) = cmplx(1.d0, 0.d0, kind(0.D0))
Op%g = SQRT(CMPLX(DTAU*V/real(N_SUN,kind(0.d0)), 0.D0, kind(0.D0)))
Op%alpha = cmplx(0.d0, 0.d0, kind(0.D0))
Op%type = 2
```

8.3.4 Fermion-Ising coupling

```
Call Predefined_Int_Ising_SUN( OP, I, J, DTAU, XI )
```

The interaction between the Ising and a fermion degree of freedom, given by

$$\hat{\mathcal{H}}_{V,i,j} = \hat{Z}_{i,j} \xi \sum_{\sigma=1}^{N_{\text{col}}} \left(c_{i\sigma}^\dagger c_{j\sigma} + c_{j\sigma}^\dagger c_{i\sigma} \right), \quad (148)$$

where ξ determines the coupling strength, is implemented in the subroutine `Predefined_Int_Ising_SUN`:

```
Op%P(1) = I
Op%P(2) = J
Op%O(1,2) = cmplx(1.d0, 0.d0, kind(0.D0))
Op%O(2,1) = cmplx(1.d0, 0.d0, kind(0.D0))
Op%g = cmplx(-DTAU*XI, 0.D0, kind(0.D0))
Op%alpha = cmplx(0.d0, 0.d0, kind(0.D0))
Op%type = 1
```

8.3.5 Long-Range Coulomb repulsion

Call `Predefined_Int_LRC(OP, I, DTAU)`

The Long-Range Coulomb (LRC) interaction can be written as

$$\hat{H}_V = \frac{1}{N} \sum_{i,j} \left(\hat{n}_i - \frac{N}{2} \right) V_{i,j} \left(\hat{n}_j - \frac{N}{2} \right), \quad (149)$$

where

$$\hat{n}_i = \sum_{\sigma=1}^N \hat{c}_{i,\sigma}^\dagger \hat{c}_{i,\sigma} \quad (150)$$

and

$$V_{i,j} = U \begin{cases} 1 & \text{if } i - j = 0 \\ \frac{\alpha d_{\min}}{|i-j|} & \text{otherwise} \end{cases}. \quad (151)$$

Here d_{\min} is the minimal distance between two orbitals. The code uses the following HS decomposition:

$$e^{-\Delta\tau \hat{H}_{V,k}} = \int \prod_i d\phi_i e^{-\frac{N\Delta\tau}{4} \phi_i V_{i,j}^{-1} \phi_j - \sum_i i \Delta\tau \phi_i (n_i - \frac{N}{2})}. \quad (152)$$

The implementation follows Ref. [26] but now supports various lattice geometries. The definition of the Coulomb repulsion is as follows. A general lattice site `I,n` where `I: 1...Latt%N` is the unit cell and `n = 1 ...Latt_unit%NORB` the orbital is given by:

```
X_p(:) = Latt%list(I,1)*latt%a1_p(:) + Latt%list(I,2)*latt%a2_p(:)
+ Latt_unit%Orb_pos_p(no_j,:)
```

or in more compact notation $i + \delta_i$. By definition `Latt_unit%Orb_pos_p(1,:)=0`. The Coulomb repulsion between points $i + \delta_i$ and $j + \delta_j$ reads:

$$V(i + \delta_i, j + \delta_j) = \frac{U d_{\min} \alpha}{|\overline{i - j} + \delta_i - \delta_j|}. \quad (153)$$

Here we use periodic boundary conditions such that $\overline{i - j}$ is an element of the real space lattice. Note that this is encoded in the array `Latt%imj(I,J)`.

The LRC interaction is implemented in the subroutine `Predefined_Int_LRC`:

```
Op%P(1) = I
Op%O(1,1) = cmplx(1.d0, 0.d0, kind(0.D0))
Op%alpha = cmplx(-0.5d0, 0.d0, kind(0.D0))
Op%g = cmplx(0.d0, DTAU, kind(0.D0))
Op%type = 3
```

8.3.6 J_z - J_z interaction

Call `Predefined_Int_Jz(OP_up, Op_do, I, J, DTAU, Jz)`

Another predefined vertex is:

$$\hat{H}_{V,i,j} = -\frac{|J_z|}{2} (S_i^z - \text{sgn}|J_z|S_j^z)^2 = J_z S_i^z S_j^z - \frac{|J_z|}{2} (S_i^z)^2 - \frac{|J_z|}{2} (S_j^z)^2 \quad (154)$$

which, if particle fluctuations are frozen on the i and j sites, then $(S_i^z)^2 = 1/4$ and the interactions corresponds to a J_z - J_z ferro or antiferro coupling.

The implementation of the interaction in `Predefined_Int_Jz` defines two operators:

```

Op_up%P(1) = I
Op_up%P(2) = J
Op_up%O(1,1) = cmplx(1.d0, 0.d0, kind(0.D0))
Op_up%O(2,2) = cmplx(-Jz/Abs(Jz), 0.d0, kind(0.D0))
Op_up%alpha = cmplx(0.d0, 0.d0, kind(0.D0))
Op_up%g = Sqrt(Cmplx(DTAU*Jz/8.d0, 0.d0, kind(0.D0)))
Op_up%type = 2

Op_do%P(1) = I
Op_do%P(2) = J
Op_do%O(1,1) = cmplx(1.d0, 0.d0, kind(0.d0))
Op_do%O(2,2) = cmplx(-Jz/Abs(Jz), 0.d0, kind(0.d0))
Op_do%alpha = cmplx(0.d0, 0.d0, kind(0.d0))
Op_do%g = -Sqrt(Cmplx(DTAU*Jz/8.d0, 0.d0, kind(0.d0)))
Op_do%type = 2

```

8.4 Predefined observables

@Jefferson. Could you please start this.

8.5 Predefined trial wave functions

When using the projective algorithm (see Sec. 3), trial wave functions must be specified. The ALF package provides a set of predefined trial wave functions $|\Psi_{T,L/R}\rangle = \text{WF_L/R}$, returned by the call:

```

Call Predefined_TrialWaveFunction(Lattice_type, Ndim, List, Invlist, Latt, Latt_unit, N_part,
                                   N_FL, WF_L, WF_R)

```

Twisted boundary conditions (Phi_X_vec=0.01) are implemented for some lattices so as to generate a non-degenerate trial wave function. Here the marker "_vec" indicates the variable may assume different values depending on the flavor (e.g., spin up and down). Currently predefined trial wave functions are flavor independent.

The predefined trial wave functions correspond to the solution of the non-interacting tight binding Hamiltonian on each of the predefined lattices. These solutions are the ground states of the predefined hopping matrices (Sec. 8.2) with default parameters, for each lattice, as follows.

8.5.1 Square

Parameter values for the predefined trial wave function on the square lattice:

```

Checkerboard = .false.
Symm         = .false.
Bulk         = .false.
N_Phi_vec    = 0
Phi_X_vec    = 0.01d0
Phi_Y_vec    = 0.d0
Ham_T_vec    = 1.d0
Ham_Chem_vec = 0.d0
Dtau         = 1.d0

```

8.5.2 Honeycomb

[JSEP: I'm not sure how to best describe the definition of the trial wave function for the honeycomb, since it doesn't use the Predefined Hopping module.

Also, do we want to mention the Kekule_Trial option?]

Parameter values for the predefined trial wave function on the Honeycomb lattice:

```

Checkerboard = .false.
Symm         = .false.
Bulk         = .false.
N_Phi_vec    = 0

```

```

Phi_X_vec    = 0.d0
Phi_Y_vec    = 0.d0
Ham_T_vec    = 1.d0
Ham_Tperp_vec = 0.d0
Ham_Chem_vec = 0.d0
Dtau         = 1.d0

```

8.5.3 N-leg ladder

Parameter values for the predefined trial wave function on the N-leg ladder lattice:

```

Checkerboard = .false.
Symm         = .false.
Bulk         = .false.
N_Phi_vec    = 0
Phi_X_vec    = 0.01d0
Phi_Y_vec    = 0.d0
Ham_T_vec    = 1.d0
Ham_Tperp_vec = 1.d0
Ham_Chem_vec = 0.d0
Dtau         = 1.d0

```

8.5.4 Bilayer square

Parameter values for the predefined trial wave function on the bilayer square lattice:

```

Checkerboard = .false.
Symm         = .false.
Bulk         = .false.
N_Phi_vec    = 0
Phi_X_vec    = 0.d0
Phi_Y_vec    = 0.d0
Ham_T_vec    = 1.d0
Ham_T2_vec   = 0.d0
Ham_Tperp_vec = 1.d0
Ham_Chem_vec = 0.d0
Dtau         = 1.d0

```

8.5.5 Bilayer honeycomb

Parameter values for the predefined trial wave function on the bilayer honeycomb lattice:

```

Checkerboard = .false.
Symm         = .false.
Bulk         = .false.
N_Phi_vec    = 0
Phi_X_vec    = 0.d0
Phi_Y_vec    = 0.d0
Ham_T_vec    = 1.d0
Ham_T2_vec   = 0.d0
Ham_Tperp_vec = 1.d0
Ham_Chem_vec = 0.d0
Dtau         = 1.d0

```

9 Model Classes

The ALF library comes with five model classes. a) SU(N) Hubbard models, (b) O(2N) t-V models, (c) Kondo models, (d) Models with long ranged coulomb and (e) Generic Z_2 lattice gauges theories couples to Z_2 matter and fermions. Below we will detail the functioning of these classes.

9.1 SU(N) Hubbard models `Hamiltonian_Hubbard_mod.F90`

The parameter space for this model class reads:

```
&VAR_Hubbard      !! Variables for the Hubbard class
Mz                = .T.      ! If true , sets the M_z-Hubbard model: Nf=2, N_SUN has to be even
.
.
.      ! HS field couples to the z-component of magnetization
ham_T            = 1.d0      ! Hopping parameter
ham_chem         = 0.d0      ! Chemical potential
ham_U            = 4.d0      ! Hubbard interaction
ham_T2          = 1.d0      ! For bilayer systems
ham_U2          = 4.d0      ! For bilayer systems
ham_Tperp       = 1.d0      ! For bilayer systems
/
```

In the above `ham_T` and `ham_T2` correspond to the hopping in the first and second layers respectively and `ham_Tperp` is to the interlayer hopping. The Hubbard U term has an orbital index, `ham_U` for the first and `ham_U2` for the second layers. Finally `ham_chem` corresponds to the chemical potential. If the flag `Mz` is set to `.False.`, then the code will simulate the following SU(N) symmetry Hubbard model.

$$\hat{H} = \sum_{(\mathbf{i}, \boldsymbol{\delta}), (\mathbf{j}, \boldsymbol{\delta}')} \sum_{\sigma=1}^N T_{(\mathbf{i}, \boldsymbol{\delta}), (\mathbf{j}, \boldsymbol{\delta}')} c_{(\mathbf{i}, \boldsymbol{\delta}), \sigma}^\dagger e^{\frac{2\pi i}{\Phi_0} \int_{\mathbf{i}+\boldsymbol{\delta}}^{\mathbf{j}+\boldsymbol{\delta}'} \mathbf{A}(\mathbf{l}) d\mathbf{l}} c_{(\mathbf{j}, \boldsymbol{\delta}'), \sigma} + \sum_{\mathbf{i}} \sum_{\boldsymbol{\delta}} \frac{U_{\boldsymbol{\delta}}}{N} \left(\sum_{\sigma=1}^N \left[\hat{c}_{(\mathbf{i}, \boldsymbol{\delta}), \sigma}^\dagger \hat{c}_{(\mathbf{i}, \boldsymbol{\delta}), \sigma} - 1/2 \right] \right)^2 - \mu \sum_{(\mathbf{i}, \boldsymbol{\delta})} \sum_{\sigma=1}^N \hat{c}_{(\mathbf{i}, \boldsymbol{\delta}), \sigma}^\dagger \hat{c}_{(\mathbf{i}, \boldsymbol{\delta}), \sigma} \quad (155)$$

The generic hopping is taken from Eq. 130 with appropriate boundary conditions given by Eq. 131. \mathbf{i} runs over the unit cells, $\boldsymbol{\delta}$ over the orbitals in each unit cell and σ from $1 \cdots N$ and encodes the SU(N) symmetry. Note that N corresponds to `N_SUN` in the code. The flavor index is set to unity such that it does not appear in the Hamiltonian. μ corresponds to the chemical potential and is relevant only for the finite temperature code.

If the variable `Mz` is set to `.True.`, then the code will require `N_SUN` to be even and will simulate the following Hamiltonian.

$$\hat{H} = \sum_{(\mathbf{i}, \boldsymbol{\delta}), (\mathbf{j}, \boldsymbol{\delta}')} \sum_{\sigma=1}^{N/2} \sum_{s=1,2} T_{(\mathbf{i}, \boldsymbol{\delta}), (\mathbf{j}, \boldsymbol{\delta}')} c_{(\mathbf{i}, \boldsymbol{\delta}), \sigma, s}^\dagger e^{\frac{2\pi i}{\Phi_0} \int_{\mathbf{i}+\boldsymbol{\delta}}^{\mathbf{j}+\boldsymbol{\delta}'} \mathbf{A}(\mathbf{l}) d\mathbf{l}} c_{(\mathbf{j}, \boldsymbol{\delta}'), \sigma, s} - \sum_{\mathbf{i}} \sum_{\boldsymbol{\delta}} \frac{U_{\boldsymbol{\delta}}}{N} \left(\sum_{\sigma=1}^{N/2} \left[\hat{c}_{(\mathbf{i}, \boldsymbol{\delta}), \sigma, 2}^\dagger \hat{c}_{(\mathbf{i}, \boldsymbol{\delta}), \sigma, 2} - \hat{c}_{(\mathbf{i}, \boldsymbol{\delta}), \sigma, 1}^\dagger \hat{c}_{(\mathbf{i}, \boldsymbol{\delta}), \sigma, 1} \right] \right)^2 - \mu \sum_{(\mathbf{i}, \boldsymbol{\delta})} \sum_{\sigma=1}^{N/2} \sum_{s=1,2} \hat{c}_{(\mathbf{i}, \boldsymbol{\delta}), \sigma, s}^\dagger \hat{c}_{(\mathbf{i}, \boldsymbol{\delta}), \sigma, s} \quad (156)$$

In this case, the flavor index `N_FL` takes the value 2. Clearly at $N = 2$, both modes correspond to the Hubbard model. For N even and $N > 2$ the models differ. In particular in the latter Hamiltonian the U(N) symmetry is broken down to $U(N/2) \otimes U(N/2)$.

Since this model class works for all predefined lattices (see Fig. 5) it includes the SU(N) periodic Anderson model on the square and Honeycomb lattices. Finally, we note that the executable for this class is given by `Hubbard.out`

If we do a good job in the previous sections we actually do not need much more explanation for this. We could also provide Jupyter notebooks to start a set of Hubbard hamiltonians. e.g.

- `Pam_square.ipynb` SU(N) Square lattice PAM
- `Pam_honeycomb.ipynb` SU(N) Honeycomb lattice PAM
- `Bilayer_Hubbard.ipynb` SU(N) Hubbard model on bilayers.
- `N_leg_ladder_Hubbard.ipynb` SU(N) n-leg-ladder Hubbard

• ...

Would be nice to discuss this point.

9.2 $O(2N)$ t-V models `tV_mod.F90`

This would include the $SU(N)$ $t - V$ models on various lattices. The defining property of this set of Hamiltonians would be the enlarged $O(2N)$ symmetry. Again this module should support our standard bipartite lattices.

9.3 $SU(N)$ Kondo lattice models `Kondo_mod.F90`

9.4 Models with long range Coulomb interactions `LRC_mod.F90`

This is the long range Coulomb. See above. Again we should include the standard lattices.

9.5 Z_2 lattice gauge theories coupled to fermion and Z_2 matter `Z2_mod.F90`

I suggest to work on the Hamiltonian of Ref. 13.1.5 since this is the most general model I can think of. Would be nice to add a Hubbard- U term. It is actually not so easy to generalize this model to arbitrary lattices, so that for the moment, I would concentrate only on the square lattice.

10 Maximum Entropy

If we want to compare the data we obtain from Monte Carlo simulations with experiments, we must extract spectral information from the imaginary-time output. This can be achieved through the maximum entropy method (MaxEnt), which generically computes the image $A(\omega)$ for a given data set $g(\tau)$ and kernel $K(\tau, \omega)$:

$$g(\tau) = \int_{\omega_{\text{start}}}^{\omega_{\text{end}}} d\omega K(\tau, \omega) A(\omega). \quad (157)$$

The ALF package includes a standard implementation of the stochastic MaxEnt, as formulated in the article of K. Beach [80], in the module `Libraries/Modules/maxent_stoch_mod.F90`. Its wrapper is contained in `Analysis/Max_SAC.F90` and the Green function is read from the output of the `cov_tau.F90` analysis program.

10.1 General setup

The stochastic MaxEnt is essentially a parallel-tempering Monte Carlo simulation. For a discrete set of τ_i points, $i \in 1 \dots n$, the goodness-of-fit functional, which we take as the energy reads

$$\chi^2(A) = \sum_{i,j=1}^n \left[g(\tau_i) - \overline{g(\tau_i)} \right] C^{-1}(\tau_i, \tau_j) \left[g(\tau_j) - \overline{g(\tau_j)} \right], \quad (158)$$

with $\overline{g(\tau_i)} = \int d\omega K(\tau_i, \omega) A(\omega)$ and C the covariance matrix. The set of inverse temperatures considered in the parallel tempering is given by $\alpha_m = \alpha_{st} R^m$, for $m = 1 \dots N_\alpha$ and a constant R . The phase space corresponds to all possible spectral functions satisfying a given sum rule and the required positivity. Finally, the partition function reads $Z = \int \mathcal{D}A e^{-\alpha \chi^2(A)}$ [80].

In the code, the spectral function is parametrized by a set of N_γ Dirac δ functions:

$$A(\omega) = \sum_{i=1}^{N_\gamma} a_i \delta(\omega - \omega_i). \quad (159)$$

In order to produce a histogram of $A(\omega)$ we divide the frequency range in `Ndis` intervals.

Besides the parameters included in the namelist `VAR_Max_Stoch` set in the file `parameters` (see Sec. 5.4), also the variable `N_cov`, from the namelist `VAR_errors`, is required to run the maxent code. Recalling: `N_cov = 1` (`N_cov = 0`) sets that the covariance will (will not) be taken into account.

Output files

The code produces the following output files:

- The files **Aom_n** correspond to the average spectral function at inverse temperature α_n . This corresponds to $\langle A_n(\omega) \rangle = \frac{1}{Z} \int \mathcal{D}A(\omega) e^{-\alpha_n \chi^2(A)} A(\omega)$. The file contains three columns: ω , $\langle A_n(\omega) \rangle$, and $\Delta \langle A_n(\omega) \rangle$.
- The files **Aom_ps_n** contain the average image over the inverse temperatures α_n to α_{N_γ} see Ref. [80] for more details. Its first three columns have the same meaning as for the files **Aom_n**.
- The file **Green** contains the Green function, obtained from the spectral function through

$$G(\omega) = -\frac{1}{\pi} \int d\Omega \frac{A(\Omega)}{\omega - \Omega + i\delta}, \quad (160)$$

where $\delta = \Delta\omega = (\omega_{\text{end}} - \omega_{\text{start}})/N_{\text{dis}}$ and the image corresponds to that of the file **Aom_ps_m** with $m = N_\alpha - 10$. The first column of the **Green** file is a place holder for post-processing. The last three columns correspond to ω , $\text{Re } G(\omega)$, $-\text{Im } G(\omega)/\pi$.

- One of the most important output files is **energies**, which lists α_n , $\langle \chi^2 \rangle$, $\Delta \langle \chi^2 \rangle$.
- **best_fit** gives the values of a_i and ω_i (recall that $A(\omega) = \sum_{i=1}^{N_\gamma} a_i \delta(\omega - \omega_i)$) corresponding to the last configuration of the lowest temperature run.
- The file **data_out** facilitates crosschecking. It lists τ , $g(\tau)$, $\Delta g(\tau)$, and $\int d\omega K(\tau, \omega) A(\omega)$, where the image corresponds to the best fit (i.e. the lowest temperature). This data should give an indication of how good the fit actually is. Note that **data_out** contains only the data points that have passed the tolerance test.
- Two dump files are also generated, **dump_conf** and **dump_Aom**. Since the MaxEnt is a Monte Carlo code, it is possible to improve the data by continuing a previous simulation. The data in the dump files allow you to do so. These files are only generated if the variable **checkpoint** is set to **.true..**

The essential question is: Which image should one use? There is no final answer to this question in the context of the stochastic MaxEnt. The only rule of thumb is to consider temperatures for which the χ^2 is comparable to the number of data points.

10.2 Single-particle quantities

For the single-particle Green function,

$$\langle \hat{c}_k(\tau) \hat{c}_k^\dagger(0) \rangle = \int d\omega K_p(\tau, \omega) A_p(k, \omega), \quad (161)$$

with

$$K_p(\tau, \omega) = \frac{1}{\pi} \frac{e^{-\tau\omega}}{1 + e^{-\beta\omega}} \quad (162)$$

and, in the Lehmann representation,

$$A_p(k, \omega) = \frac{\pi}{Z} \sum_{n,m} e^{-\beta E_n} (1 + e^{-\beta\omega}) |\langle n | c_n | m \rangle|^2 \delta(E_m - E_n - \omega). \quad (163)$$

Here $(\hat{H} - \mu\hat{N})|n\rangle = E_n|n\rangle$. Note that $A_p(k, \omega) = -\text{Im } G^{\text{ret}}(k, \omega)$, with

$$G^{\text{ret}}(k, \omega) = -i \int dt \Theta(t) e^{i\omega t} \langle \{ \hat{c}_k(t), \hat{c}_k^\dagger(0) \} \rangle. \quad (164)$$

Finally the sum rule reads

$$\int d\omega A_p(k, \omega) = \pi \langle \{ \hat{c}_k, \hat{c}_k^\dagger \} \rangle = \pi. \quad (165)$$

Using the `Max_Sac.F90` with `Channel="P"` will load the above kernel in the MaxEnt library. Note that in this case the back transformation is set to unity. Note that for each configuration of fields we have $\langle\langle\hat{c}_k(\tau=0)\hat{c}_k^\dagger(0)\rangle\rangle_C + \langle\langle\hat{c}_k(\tau=\beta)\hat{c}_k^\dagger(0)\rangle\rangle_C = \langle\langle\{\hat{c}_k, \hat{c}_k^\dagger\}\rangle\rangle_C = 1$, hence, if both the $\tau=0$ and $\tau=\beta$ data points are included, the covariance matrix will have a zero eigenvalue and the χ^2 measure is not defined. Therefore, for the particle channel the program omits the $\tau=\beta$ data point. There are special particle-hole symmetric cases where the $\tau=0$ data point shows no fluctuations – in such cases the code omits the $\tau=0$ data point as well.

10.3 Particle-hole quantities

Imaginary-time formulation

For particle-hole quantities such as spin-spin or charge-charge correlations, the kernel reads

$$\langle\hat{S}(q, \tau)\hat{S}(-q, 0)\rangle = \frac{1}{\pi} \int d\omega \frac{e^{-\tau\omega}}{1 - e^{-\beta\omega}} \chi''(q, \omega). \quad (166)$$

This follows directly from the Lehmann representation

$$\chi''(q, \omega) = \frac{\pi}{Z} \sum_{n,m} e^{-\beta E_n} |\langle n|\hat{S}(q)|m\rangle|^2 \delta(\omega + E_n - E_m) (1 - e^{-\beta\omega}). \quad (167)$$

Since the linear response to a Hermitian perturbation is real, $\chi''(q, \omega) = -\chi''(-q, -\omega)$ and hence $\langle\hat{S}(q, \tau)\hat{S}(-q, 0)\rangle$ is a symmetric function around $\beta = \tau/2$ for systems with inversion symmetry – the ones we consider here. The analysis file `cov_tau_ph.F90` produced at compilation time uses this to define an improved estimator.

The stochastic MaxEnt requires a sum rule, and hence the kernel and image have to be adequately redefined. Let us consider $\coth(\beta\omega/2)\chi''(q, \omega)$. For this quantity, we have the sum rule, since

$$\int d\omega \coth(\beta\omega/2)\chi''(q, \omega) = 2\pi\langle\hat{S}(q, \tau=0)\hat{S}(-q, 0)\rangle, \quad (168)$$

which is just the first point in the data. Therefore,

$$\langle\hat{S}(q, \tau)\hat{S}(-q, 0)\rangle = \int d\omega \underbrace{\frac{1}{\pi} \frac{e^{-\tau\omega}}{1 - e^{-\beta\omega}} \tanh(\beta\omega/2)}_{K_{pp}(\tau, \omega)} \underbrace{\coth(\beta\omega/2)\chi''(q, \omega)}_{A(\omega)} \quad (169)$$

and one computes $A(\omega)$. Note that since χ'' is an odd function of ω one restricts the integration range positive values of ω . Hence:

$$\langle\hat{S}(q, \tau)\hat{S}(-q, 0)\rangle = \int_0^\infty d\omega \underbrace{(K(\tau, \omega) + K(\tau, -\omega))}_{K_{ph}(\tau, \omega)} A(\omega). \quad (170)$$

In the code, ω_{start} is set to zero by default and the kernel K_{ph} is defined in the routine `XKER_ph`.

In general, one would like to produce the dynamical structure factor that gives the susceptibility according to

$$S(q, \omega) = \chi''(q, \omega) / (1 - e^{-\beta\omega}). \quad (171)$$

In the code the routine `BACK_TRANS_ph` transforms the image A to the desired quantity:

$$S(q, \omega) = \frac{A(\omega)}{1 + e^{-\beta\omega}}. \quad (172)$$

Matsubara-frequency formulation

The ALF library uses imaginary time. It is however possible to formulate the MaxEnt in Matsubara frequencies. Consider:

$$\chi(q, i\Omega_m) = \int_0^\beta d\tau e^{i\Omega_m\tau} \langle\hat{S}(q, \tau)\hat{S}(-q, 0)\rangle = \frac{1}{\pi} \int d\omega \frac{\chi''(q, \omega)}{\omega - i\Omega_m}. \quad (173)$$

Using the fact that $\chi''(q, \omega) = -\chi''(-q, -\omega) = -\chi''(q, -\omega)$ one obtains

$$\begin{aligned}\chi(q, i\Omega_m) &= \frac{1}{\pi} \int_0^\infty d\omega \left(\frac{1}{\omega - i\Omega_m} - \frac{1}{-\omega - i\Omega_m} \right) \chi''(q, \omega) \\ &= \frac{2}{\pi} \int_0^\infty d\omega \frac{\omega^2}{\omega^2 + \Omega_m^2} \frac{\chi''(q, \omega)}{\omega} \\ &\equiv \int_0^\infty d\omega K(\omega, i\Omega_m) A(q, \omega),\end{aligned}\tag{174}$$

with

$$K(\omega, i\Omega_m) = \frac{\omega^2}{\omega^2 + \Omega_m^2} \quad \text{and} \quad A(q, \omega) = \frac{2}{\pi} \frac{\chi''(q, \omega)}{\omega}.\tag{175}$$

The above definitions produce an image that satisfies the sum rule:

$$\int_0^\infty d\omega A(q, \omega) = \frac{1}{\pi} \int_{-\infty}^\infty d\omega \frac{\chi''(q, \omega)}{\omega} \equiv \chi(q, i\Omega_m = 0).\tag{176}$$

10.4 Particle-Particle quantities

Similarly to the particle-hole channel, the particle-particle channel is also a bosonic correlation function. Here, however, we do not assume that the imaginary time data is symmetric around the $\tau = \beta/2$ point. We use the kernel K_{pp} defined in Eq. (169) and consider the whole frequency range. The back transformation yields

$$\frac{\chi''(\omega)}{\omega} = \frac{\tanh(\beta\omega/2)}{\omega} A(\omega).\tag{177}$$

10.5 Zero-temperature, projective code

In the zero temperature limit, the spectral function associated to an operator \hat{O} reads:

$$A_o(\omega) = \pi \sum_n |\langle n | \hat{O} | 0 \rangle|^2 \delta(E_n - E_0 - \omega),\tag{178}$$

such that

$$\langle 0 | \hat{O}^\dagger(\tau) \hat{O}(0) | 0 \rangle = \int d\omega K_0(\tau, \omega) A_o(\omega),\tag{179}$$

with

$$K_0(\tau, \omega) = \frac{1}{\pi} e^{-\tau\omega}.\tag{180}$$

The zeroth moment of the spectral function reads

$$\int d\omega A_o(\omega) = \pi \langle 0 | \hat{O}^\dagger(0) \hat{O}(0) | 0 \rangle,\tag{181}$$

and hence corresponds to the first data point.

In the zero-temperature limit one does not distinguish between particle, particle-hole, or particle-particle channels. Using the `Max_Sac.F90` with `Channel="T0"` loads the above kernel in the `MaxEnt` library. In this case the back transformation is set to unity. The code will also cut-off the tail of the imaginary time correlation function if the relative error is greater than the variable `Tolerance`.

10.6 Performance, memory requirements and parallelization

Could this subsection be brought to Sec. 6.3 (Using the Code / performance & parameter optimization).

As mentioned in the introduction, the auxiliary field QMC algorithm scales linearly in inverse temperature β and cubic in the volume N_{dim} . Using fast updates, a single spin flip requires $(N_{\text{dim}})^2$ operations to update the Green function upon acceptance. As there are $L_{\text{Trotter}} \times N_{\text{dim}}$ spins to be visited, the total computational cost for one sweep is of the order of $\beta(N_{\text{dim}})^3$. This operation dominates the performance, see Fig. 7. A profiling analysis of our code shows that 80-90% of the CPU time is spend in ZGEMM calls of the BLAS library provided in the MKL package by Intel. Consequently, the single-core performance is next to optimal.

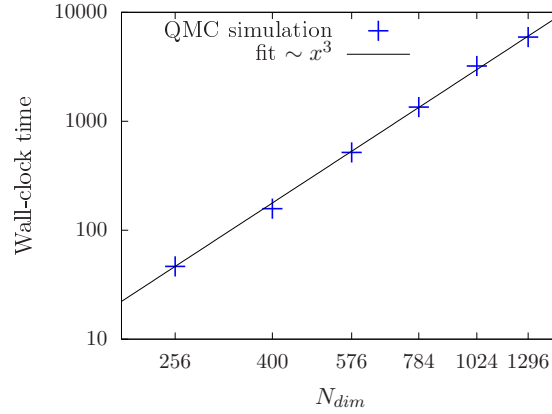


Figure 7: Volume scaling behavior of the auxiliary field QMC code of the ALF project on SuperMUC (phase 2/Haswell nodes) at the LRZ in Munich. The number of sites N_{dim} corresponds to the system volume. The plot confirms that the leading scaling order is due to matrix multiplications such that the runtime is dominated by calls to ZGEMM.

For the implementation which scales linearly in β , one has to store $L_{\text{Trotter}}/\text{NWrap}$ intermediate propagation matrices of dimension $N \times N$. For large lattices and/or low temperatures this dominates the total memory requirements that can exceed 2 GB memory for a sequential version.

At the heart of Monte Carlo schemes lies a random walk through the given configuration space. This is easily parallelized via MPI by associating one random walker to each MPI task. For each task, we start from a random configuration and have to invest the autocorrelation time T_{auto} to produce an equilibrated configuration. Additionally we can also profit from an OpenMP parallelized version of the BLAS/LAPACK library for an additional speedup, which also effects equilibration overhead $N_{\text{MPI}} \times T_{\text{auto}}/N_{\text{OMP}}$, where N_{MPI} is the number of cores and N_{OMP} the number of OpenMP threads. For a given number of independent measurements N_{meas} , we therefore need a wall-clock time given by

$$T = \frac{T_{\text{auto}}}{N_{\text{OMP}}} \left(1 + \frac{N_{\text{meas}}}{N_{\text{MPI}}} \right). \quad (182)$$

As we typically have $N_{\text{meas}}/N_{\text{MPI}} \gg 1$, the speedup is expected to be almost perfect, in accordance with the performance test results for the auxiliary field QMC code on SuperMUC (see Fig. 8 (left)).

For many problem sizes, 2 GB memory per MPI task (random walker) suffices such that we typically start as many MPI tasks as there are physical cores per node. Due to the large amount of CPU time spent in MKL routines, we do not profit from the hyper-threading option. For large systems, the memory requirement increases and this is tackled by increasing the amount of OpenMP threads to decrease the stress on the memory system and to simultaneously reduce the equilibration overhead (see Fig. 8 (right)). For the displayed speedup, it was crucial to pin the MPI tasks as well as the OpenMP threads in a pattern which keeps the threads as compact as possible to profit from a shared cache. This also explains the drop in efficiency from 14 to 28 threads where the OpenMP threads are spread over both sockets.

We store the field configurations of the random walker as checkpoints, such that a long simulation can be easily split into several short simulations. This procedure allows us to take advantage of chained jobs using the dependency chains provided by the batch system.

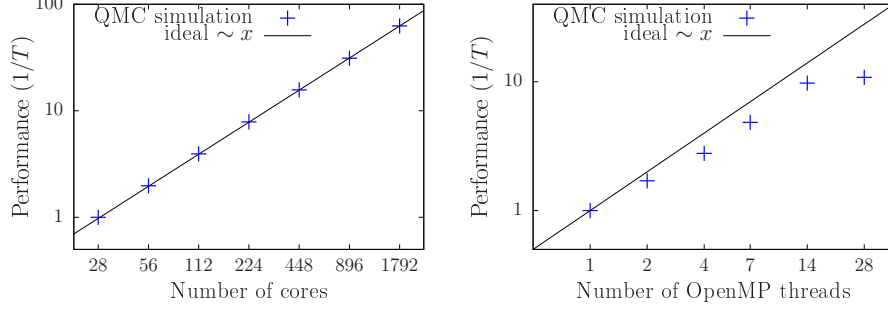


Figure 8: MPI (left) and OpenMP (right) scaling behavior of the auxiliary field QMC code of the ALF project on SuperMUC (phase 2/Haswell nodes) at the LRZ in Munich. The MPI performance data was normalized to 28 cores and was obtained using a problem size of $N_{\text{dim}} = 400$. This is a medium to small system size that is the least favorable in terms of MPI synchronization effects. The OpenMP performance data was obtained using a problem size of $N_{\text{dim}} = 1296$. Employing 2 and 4 OpenMP threads introduces some synchronization/management overhead such that the per-core performance is slightly reduced, compared to the single thread efficiency. Further increasing the amount of threads to 7 and 14 keeps the efficiency constant. The drop in performance of the 28 thread configuration is due to the architecture as the threads are now spread over both sockets of the node. To obtain the above results, it was crucial to pin the processes in a fashion that keeps the OpenMP threads as compact as possible.

11 Conclusions and Future Directions

In its present form, the auxiliary field QMC code of the ALF project allows to simulate a large class of non-trivial models, both efficiently and at minimal programming cost. There are many possible extensions which deserve to be considered in future releases. The model Hamiltonians we have presented so far are imaginary-time independent. This however can be easily generalized to imaginary-time dependent model Hamiltonians thus allowing, for example, to access entanglement properties of interacting fermionic systems [31, 90, 32, 33]. Generalizations to include global moves are equally desirable. This is a prerequisite to play with recent ideas of self-learning algorithms [91] so as to possibly avoid the issue of critical slowing down. At present, the QMC code of this package is restricted to discrete HS fields such that implementations of the long-range Coulomb repulsion – as introduced in [26, 92, 93] – are not yet included. Extensions to continuous HS fields are certainly possible, but require an efficient upgrading scheme. Finally, an implementation of the ground state projective QMC method is equally desirable.

OLD STUFF

12 Examples

TO BE DELETED, with parts being reused in sections Predefined Structures and Model classes.

12.1 The $SU(2)$ -Hubbard model on a square lattice coupled to a transverse Ising field

The model we consider here is very similar to the above, but has an additional coupling to a transverse field:

$$\mathcal{H} = \sum_{\sigma=1}^2 \sum_{x,y} c_{x\sigma}^\dagger T_{x,y} c_{y\sigma} + \frac{U}{2} \sum_x \left[\sum_{\sigma=1}^2 (c_{x\sigma}^\dagger c_{x\sigma} - 1/2) \right]^2 + \xi \sum_{\sigma, \langle x,y \rangle} \hat{Z}_{\langle x,y \rangle} (c_{x\sigma}^\dagger c_{y\sigma} + h.c.) - h \sum_{\langle x,y \rangle} \hat{X}_{\langle x,y \rangle} - J \sum_{\langle \langle x,y \rangle \rangle \langle \langle x',y' \rangle \rangle} \hat{Z}_{\langle x,y \rangle} \hat{Z}_{\langle x',y' \rangle} \quad (183)$$

We can make contact with the general form of the Hamiltonian by setting: $N_{\text{fl}} = 1$, $N_{\text{col}} \equiv N_{\text{SUN}} = 2$, $M_T = 1$, $T_{xy}^{(ks)} = T_{x,y}$, $M_V = N_{\text{unit-cell}} \equiv N_{\text{dim}}$, $U_k = -\frac{U}{2}$, $V_{xy}^{(ks)} = \delta_{x,y} \delta_{x,k}$, $\alpha_{ks} = -\frac{1}{2}$ and $M_I =$

$2N_{\text{unit-cell}}$. The last two terms of the above Hamiltonian describe a transverse Ising field model on the bonds of the square lattice. This type of Hamiltonian has recently been extensively discussed [20, 83, 17]. Here we adopt the notation of Ref. [17]. Note that $\langle\langle x, y \rangle \langle x', y' \rangle\rangle$ denotes nearest neighbor bonds. The modifications required to generalize the Hubbard model code to the above model are two-fold.

First, one has to specify the function `Real(Kind=8)functionS0(n,nt)`, and second, modify the interaction `Call Ham_V`.

A sample run for this model can be found in `Examples/Hubbard_SU2_Ising_Square/`.

12.1.1 The Ising term.

Since the Ising field lives on bonds we have to provide a data structure defining this quantity. A bond has an anchor site as well as an orientation. The routine `Setup_Ising_action` initializes the arrays `L_bond` and `L_bond_inv` that contain this information.

```
nc = 0
Do n_orientation = 1, N_coord
Do I = 1, Latt%N
  nc = nc + 1
  L_bond(I, n_orientation) = nc
  L_bond_inv(nc, 1) = I
  L_bond_inv(nc, 2) = n_orientation
enddo
enddo
```

The two legs of the bond are given by the anchor I and $I + \mathbf{a}_{n_{\text{orientation}}}$

12.1.2 The interaction term: Call Ham_V

The dimension of `Op_V` is now $(M_I + M_V) \times N_{\text{fl}} = ((N_{\text{coord}} + 1)N_{\text{dim}}) \times 1$ since each site has $N_{\text{coord}} = 2$ bonds for the square lattice.

```
do i = 1, N_coord*Ndim
  call Op_make(Op_V(i, 1), 2)
enddo
do i = N_coord*Ndim+1, (N_coord+1)*Ndim
  call Op_make(Op_V(i, 1), 1)
enddo
```

The first $N_{\text{coord}} \times N_{\text{dim}}$ operators run through the $2N$ bonds of the square lattice and are given by:

```
Do nc = 1, Ndim*N_coord
  I1 = L_bond_inv(nc, 1)
  if ( L_bond_inv(nc, 2) == 1 ) I2 = Latt%nnlist(I1, 1, 0)
  if ( L_bond_inv(nc, 2) == 2 ) I2 = Latt%nnlist(I1, 0, 1)
  Op_V(nc, 1)%P(1) = I1
  Op_V(nc, 1)%P(2) = I2
  Op_V(nc, 1)%O(1, 2) = cmplx(1.d0, 0.d0, kind(0.D0))
  Op_V(nc, 1)%O(2, 1) = cmplx(1.d0, 0.d0, kind(0.D0))
  Op_V(nc, 1)%g = cmplx(-dtau*Ham_xi, 0.D0, kind(0.D0))
  Op_V(nc, 1)%alpha = cmplx(0.d0, 0.d0, kind(0.D0))
  Op_V(nc, 1)%type = 1
Enddo
```

Here, `ham_xi` defines the coupling strength between the Ising and fermion degree of freedom. As for the Hubbard case, the last N_{dim} operators read:

```
nc = N_coord*Ndim
Do i = 1, Ndim
  nc = nc + 1
  Op_V(nc, 1)%P(1) = i
  Op_V(nc, 1)%O(1, 1) = cmplx(1.d0, 0.d0, kind(0.D0))
```

```

Op_V(nc,1)%g      = sqrt(cmplx(-dtau*ham_U/(DBLE(N_SUN)), 0.D0, kind(0.D0)))
Op_V(nc,1)%alpha   = cmplx(-0.5d0,0.d0, kind(0.D0))
Op_V(nc,1)%type    = 2
Enddo

```

12.1.3 The function Real (Kind=8) function S0(n,nt)

As mentioned above, a configuration now includes both HS spins and Ising spins and is given by

$$C = \{s_{i,\tau}, l_{j,\tau}, \text{ with } i = 1, \dots, M_I; j = 1, \dots, M_V; \tau = 1, \dots, L_{\text{Trotter}}\}. \quad (184)$$

This configuration is stored in the integer array `nsigma(M_V + M_I, Ltrot)`. With the above ordering of Hubbard and Ising interaction terms, and a for a given imaginary time, the first $2 * \text{Ndim}$ fields correspond to the Ising interaction and the next Ndim ones to the Hubbard interaction. The first argument of the function `S0`, namely `n`, corresponds to the index of the operator string `Op_V(n,1)`. If `Op_V(n,1)%type = 2` then `S0(n,nt)` returns 1. Note that `type=2` refers to spins that stem from a HS transformation. If however `Op_V(n,1)%type = 1` then function `S0` returns

$$\frac{e^{-S_{0,I}(s_{1,\tau}, \dots, -s_{n,\tau}, \dots, s_{M_I,\tau})}}{e^{-S_{0,I}(s_{1,\tau}, \dots, s_{n,\tau}, \dots, s_{M_I,\tau})}} \quad (185)$$

That is, if $n \leq 2 * \text{Ndim}$, `S0(n,nt)` returns the ratio of the new weight to the old weight of the Ising Hamiltonian upon flipping a single Ising spin $s_{n,\tau}$. Otherwise, `S0(n,nt)` returns unity.

13 Miscellaneous

13.1 Other models

The aim of this section is to briefly mention a small selection of other models that can be studied using the QMC code of the ALF project.

13.1.1 Kondo lattice model

Simulating the Kondo lattice with the QMC code of the ALF project requires rewriting of the model along the lines of Refs. [18, 19, 84]. Adopting the notation of these articles, the Hamiltonian that one will simulate reads:

$$\hat{\mathcal{H}} = \underbrace{-t \sum_{\langle i,j \rangle, \sigma} \left(\hat{c}_{i,\sigma}^\dagger \hat{c}_{j,\sigma} + \text{H.c.} \right)}_{\equiv \hat{\mathcal{H}}_t} - \frac{J}{4} \sum_i \left(\sum_\sigma \hat{c}_{i,\sigma}^\dagger \hat{f}_{i,\sigma} + \hat{f}_{i,\sigma}^\dagger \hat{c}_{i,\sigma} \right)^2 + \underbrace{\frac{U}{2} \sum_i \left(\hat{n}_i^f - 1 \right)^2}_{\equiv \hat{\mathcal{H}}_U}. \quad (186)$$

This form is included in the general Hamiltonian (2) such that the above Hamiltonian can be implemented in our program package. The relation to the Kondo lattice model follows from expanding the square of the hybridization to obtain:

$$\hat{\mathcal{H}} = \hat{\mathcal{H}}_t + J \sum_i \left(\hat{S}_i^c \cdot \hat{S}_i^f + \hat{\eta}_i^{z,c} \cdot \hat{\eta}_i^{z,f} - \hat{\eta}_i^{x,c} \cdot \hat{\eta}_i^{x,f} - \hat{\eta}_i^{y,c} \cdot \hat{\eta}_i^{y,f} \right) + \hat{\mathcal{H}}_U. \quad (187)$$

where the η -operators relate to the spin-operators via a particle-hole transformation in one spin sector:

$$\hat{\eta}_i^\alpha = \hat{P}^{-1} \hat{S}_i^\alpha \hat{P} \text{ with } \hat{P}^{-1} \hat{c}_{i,\uparrow} \hat{P} = (-1)^{i_x+i_y} \hat{c}_{i,\uparrow}^\dagger \text{ and } \hat{P}^{-1} \hat{c}_{i,\downarrow} \hat{P} = \hat{c}_{i,\downarrow} \quad (188)$$

Since the $\hat{\eta}^f$ - and \hat{S}^f -operators do not alter the parity $[(-1)^{\hat{n}_i^f}]$ of the f -sites,

$$[\hat{\mathcal{H}}, \hat{\mathcal{H}}_U] = 0. \quad (189)$$

Thereby, and for positive values of U , doubly occupied or empty f -sites – corresponding to even parity sites – are suppressed by a Boltzmann factor $e^{-\beta U/2}$ in comparison to odd parity sites. Choosing βU

adequately essentially allows to restrict the Hilbert space to odd parity f -sites. In this Hilbert space $\hat{\eta}^{x,f} = \hat{\eta}^{y,f} = \hat{\eta}^{z,f} = 0$ such that the Hamiltonian (186) reduces to the Kondo lattice model.

An implementation of the Kondo Lattice model on the Honeycomb lattice with additional z-z frustration considered in Ref. [85],

$$\hat{H}_{\text{Spin}} = J^z \sum_{\langle i,j \rangle} \hat{S}_i^z \hat{S}_j^z, \quad \hat{H}_{\text{Fermion}} = -t \sum_{\langle i,j \rangle, \sigma} \hat{c}_{i\sigma}^\dagger \hat{c}_{j\sigma}, \quad \hat{H}_{\text{Kondo}} = J^K \sum_i \frac{1}{2} \hat{c}_i^\dagger \boldsymbol{\sigma} \hat{c}_i \cdot \hat{\mathbf{S}}_i, \quad (190)$$

can be found in the `Hamiltonian_Kondo_Honey_mod.F90`

13.1.2 $SU(N)$ Hubbard-Heisenberg models

$SU(2N)$ Hubbard-Heisenberg [24, 25] models can be written as:

$$\hat{\mathcal{H}} = \underbrace{-t \sum_{\langle i,j \rangle} (\hat{c}_i^\dagger \hat{c}_j + \text{H.c.})}_{\equiv \hat{\mathcal{H}}_t} - \underbrace{\frac{J}{2N} \sum_{\langle i,j \rangle} (\hat{D}_{i,j}^\dagger \hat{D}_{i,j} + \hat{D}_{i,j} \hat{D}_{i,j}^\dagger)}_{\equiv \hat{\mathcal{H}}_J} + \underbrace{\frac{U}{N} \sum_i \left(\hat{c}_i^\dagger \hat{c}_i - \frac{N}{2} \right)^2}_{\equiv \hat{\mathcal{H}}_U}. \quad (191)$$

Here, $\hat{c}_i^\dagger = (\hat{c}_{i,1}^\dagger, \hat{c}_{i,2}^\dagger, \dots, \hat{c}_{i,N}^\dagger)$ is an N -flavored spinor, and $\hat{D}_{i,j} = \hat{c}_i^\dagger \hat{c}_j$. To use the QMC code of the ALF project to simulate this model, one will rewrite the J -term as a sum of perfect squares,

$$\hat{\mathcal{H}}_J = -\frac{J}{4N} \sum_{\langle i,j \rangle} \left(\hat{D}_{i,j}^\dagger + \hat{D}_{i,j} \right)^2 - \left(\hat{D}_{i,j}^\dagger - \hat{D}_{i,j} \right)^2, \quad (192)$$

so to manifestly bring it into the form of the general Hamiltonian(2). It is amusing to note that setting the hopping $t = 0$, charge fluctuations will be suppressed by the Boltzmann factor $e^{-\beta U/N(\hat{c}_i^\dagger \hat{c}_i - \frac{N}{2})^2}$ since in this case $[\hat{\mathcal{H}}_J, \hat{\mathcal{H}}_U] = 0$. This provides a route to use the auxiliary field QMC algorithm to simulate – free of the sign problem – $SU(2N)$ Heisenberg models in the self-adjoint antisymmetric representation⁹ For odd values of N recent progress in our understanding of the origins of the sign problem [37] allows us to simulate a set of non-trivial Hamiltonians [86, 17], without encountering the sign problem.

13.1.3 Hubbard model in the canonical ensemble

To simulate the Hubbard model in the canonical ensemble one can add the constraint:

$$\hat{\mathcal{H}} = \hat{\mathcal{H}}_{tU} + \underbrace{\lambda \left(\hat{N} - N \right)^2}_{\equiv \hat{H}_\lambda}. \quad (193)$$

In the limit $\lambda \rightarrow \infty$, the uniform charge fluctuations,

$$S(\mathbf{q} = 0) = \sum_{\mathbf{r}} [\langle \hat{n}_{\mathbf{r}} \hat{n}_{\mathbf{0}} \rangle - \langle \hat{n}_{\mathbf{r}} \rangle \langle \hat{n}_{\mathbf{0}} \rangle] \quad (194)$$

are suppressed and the grand-canonical simulation maps onto a canonical one. To implement this in the QMC code of the ALF project, we have adopted the following strategy. Since $(\hat{N} - N)^2$ effectively corresponds to a long-range interaction one may face the issue that the acceptance rate of a single HS flip becomes very small on large lattices. To circumvent this problem we have used the following decomposition:

$$e^{-\beta \hat{H}} = \prod_{\tau=1}^{L_{\text{Trotter}}} \left[e^{-\Delta\tau \hat{H}_t} e^{-\Delta\tau \hat{H}_U} \underbrace{e^{-\frac{\Delta\tau}{n_\lambda} \hat{H}_\lambda} \dots e^{-\frac{\Delta\tau}{n_\lambda} \hat{H}_\lambda}}_{n_\lambda\text{-times}} \right]. \quad (195)$$

Thereby, we need n_λ fields per time slice to impose the constraint. Since for each field the coupling constant is suppressed by a factor n_λ , we can monitor the acceptance. An implementation of this program can be found in `Prog/Hamiltonian_Hub_Canonical_mod.F90` and a test run in the directory `Examples/Hubbard_Mz_Square_Can`.

⁹This corresponds to a Young tableau with single column and $N/2$ rows.

13.1.4 Z_2 slave spin formulation of the Hubbard model

In this subsection, we demonstrate that the code can be used to simulate the attractive Hubbard model in the Z_2 -slave spin formulation [87]:

$$\hat{H} = -t \sum_{\langle i,j \rangle, \sigma} \hat{c}_{i,\sigma}^\dagger \hat{c}_{j,\sigma} - U \sum_i (\hat{n}_{i,\uparrow} - 1/2) (\hat{n}_{i,\downarrow} - 1/2). \quad (196)$$

In the Z_2 slave spin representation, the physical fermion, $\hat{c}_{i,\sigma}$, is fractionalized into an Ising spin carrying Z_2 charge and a fermion, $\hat{f}_{i,\sigma}$, carrying Z_2 and global $U(1)$ charge:

$$\hat{c}_{i,\sigma}^\dagger = \hat{\tau}_i^z \hat{f}_{i,\sigma}^\dagger. \quad (197)$$

To ensure that we remain in the correct Hilbert space, the constraint:

$$\hat{\tau}_i^x - (-1) \sum_\sigma \hat{f}_{i,\sigma}^\dagger \hat{f}_{i,\sigma} = 0 \quad (198)$$

has to be imposed locally. Since $(\tau_i^x)^2 = 1$ it is equivalent to

$$\hat{Q}_i = \tau_i^x (-1) \sum_\sigma \hat{f}_{i,\sigma}^\dagger \hat{f}_{i,\sigma} = 1. \quad (199)$$

In the Z_2 slave spin representation the Hubbard model now reads:

$$\hat{H}_{Z_2} = -t \sum_{\langle i,j \rangle, \sigma} \hat{\tau}_i^z \hat{\tau}_j^z \hat{f}_{i,\sigma}^\dagger \hat{f}_{j,\sigma} - \frac{U}{4} \sum_i \hat{\tau}_i^x \quad (200)$$

and one will readily see that the constraint will commute with Hamiltonian:

$$[\hat{H}_{Z_2}, \hat{Q}_i] = 0. \quad (201)$$

One can foresee that the constraint will be dynamically imposed and that at $T = 0$ on a finite lattice both models should give the same results.

To implement this Hamiltonian in the ALF, it is convenient to carry out the variable substitution

$$\hat{Z}_{\langle i,j \rangle} = \hat{\tau}_i^z \hat{\tau}_j^z \quad (202)$$

such that

$$\hat{\tau}_i^x = \hat{X}_{i,i+a_x} \hat{X}_{i,i-a_x} \hat{X}_{i,i+a_y} \hat{X}_{i,i-a_y}. \quad (203)$$

Since there are twice as many bond variables as site variables, a constraint has to be imposed on the $\hat{Z}_{\langle i,j \rangle}$ variables. In fact, it is easy to see that the flux per plaquette has to take a unit value:

$$\hat{Z}_{i,i+a_x} \hat{Z}_{i+a_x,i+a_x+a_y} \hat{Z}_{i+a_x+a_y,i+a_y} \hat{Z}_{i+a_y,i} = 1 \quad \forall \quad i. \quad (204)$$

Within this formulation the model takes the form:

$$\hat{H}_{Z_2} = -t \sum_{\langle i,j \rangle, \sigma} \hat{Z}_{\langle i,j \rangle} \hat{f}_{i,\sigma}^\dagger \hat{f}_{j,\sigma} - \frac{U}{4} \sum_i \hat{X}_{i,i+a_x} \hat{X}_{i,i-a_x} \hat{X}_{i,i+a_y} \hat{X}_{i,i-a_y}. \quad (205)$$

The fermion part has formally the same form as in the Hubbard model coupled to a dynamical Ising field discussed in Sec. 12.1. There are however two important differences.

- The moves have to respect the constraint of Eq. 204. Thereby single spin flip terms are prohibited and the minimal move one can carry out on a given time slice is the following. We randomly choose a site i and propose a move where: $Z_{i,i+a_x} \rightarrow -Z_{i,i+a_x}$, $Z_{i,i-a_x} \rightarrow -Z_{i,i-a_x}$, $Z_{i,i+a_y} \rightarrow -Z_{i,i+a_y}$ and $Z_{i,i-a_y} \rightarrow -Z_{i,i-a_y}$. One can carry out such moves by using the global move in real space option presented in Secs. 2.2.3 and 5.4.1.
- The map from $\{\tau_i^z\}$ to $\{Z_{\langle i,j \rangle}\}$ is unique. The reverse however is valid only up to a global sign. To pin down this sign (and thereby the relative signs between different time slices) we store per time slice the $Z_{\langle i,j \rangle}$ fields as well as the value of the Ising field at a reference site $\tau_{i=1}^z$. Within the ALF, this can be done by adding a dummy operator in the `Op_V` list which will carry this degree of freedom. With this extra degree of freedom we can switch between the two representations, without losing any information. To compute the Ising part of the action it is certainly more transparent to work with the $\{\tau_i^z\}$ variables. For the fermion determinant, the $\{Z_{\langle i,j \rangle}\}$ are more convenient.

We have carried out some test simulations at half-filling and at low temperatures. The simulation can be found in directory `Examples/Z2_Slave` and the Hamiltonian in `Hamiltonian_Z2_slave_spins_mod.F90`. The simulations are carried out at half-filling such that particle-hole symmetry leads to

$$\langle \hat{Q}_i \rangle_{H_{Z_2}} = 0. \quad (206)$$

However the simulations suggest that

$$\frac{1}{N} \sum_{i,j} \langle \hat{Q}_i \hat{Q}_j \rangle_{H_{Z_2}} = N \quad (207)$$

at low temperatures where N corresponds to size of the lattice. Note that this measurement is very noisy, and suffers from very long autocorrelation times. Thereby, the constraint is dynamically imposed and simulations of the attractive Hubbard model with `Hamiltonian_Examples_mod.F90` should yield identical results. To test this, we have computed equal-time Green functions:

$$\langle \hat{\tau}_i^z \hat{f}_{i,\sigma}^\dagger \hat{\tau}_j^z \hat{f}_{j,\sigma} \rangle_{H_{Z_2}} = \langle \hat{c}_{i,\sigma}^\dagger \hat{c}_{j,\sigma} \rangle_H \quad (208)$$

as obtained from the `Hamiltonian_Examples_mod.F90` and `Hamiltonian_Z2_slave_spins_mod.F90` codes. A test run for the 8×8 lattice at $U/t = 4$ and $\beta t = 40$ gives:

k	$\langle n_k \rangle_H$	$\langle n_k \rangle_{H_{Z_2}}$
(0, 0)	$1.93348548 \pm 0.00011322$	$1.93336807 \pm 0.00080473$
$(\pi/4, \pi/4)$	$1.90120688 \pm 0.00014854$	$1.90107164 \pm 0.00097029$
$(\pi/2, \pi/2)$	$0.99942957 \pm 0.00091377$	$1.00000000 \pm 0.00000000$
$(3\pi/4, 3\pi/4)$	$0.09905425 \pm 0.00015940$	$0.09892836 \pm 0.00097029$
(π, π)	$0.06651452 \pm 0.00011321$	$0.06663193 \pm 0.00080473$

Here a Trotter time step of $\Delta\tau t = 0.05$ was used so as to minimize the systematic error which should be different between the two codes.

This code was used in Ref. [88].

13.1.5 Z_2 gauge theory coupled to Z_2 matter.

The Hamiltonian we will consider here reads

$$\begin{aligned} \hat{H} = & -t_{Z_2} \sum_{\langle i,j \rangle, \sigma} \hat{Z}_{\langle i,j \rangle} \left(\hat{\Psi}_{i,\sigma}^\dagger \hat{\Psi}_{j,\sigma} + h.c. \right) - \mu \sum_{i,\sigma} \hat{\Psi}_{i,\sigma}^\dagger \hat{\Psi}_{i,\sigma} - g \sum_{\langle i,j \rangle} \hat{X}_{\langle i,j \rangle} + K \sum_{\square} \prod_{\langle i,j \rangle \in \partial \square} \hat{Z}_{\langle i,j \rangle} \\ & + J \sum_{\langle i,j \rangle} \hat{\tau}_i^z \hat{Z}_{\langle i,j \rangle} \hat{\tau}_j^z - h \sum_i \hat{\tau}_i^x - t \sum_{\langle i,j \rangle, \sigma} \hat{\tau}_i^z \hat{\tau}_j^z \left(\hat{\Psi}_{i,\sigma}^\dagger \hat{\Psi}_{j,\sigma} + h.c. \right) \end{aligned} \quad (209)$$

Here the $\hat{\Psi}_{i,\sigma}^\dagger$ creates an orthogonal fermion with Z_2 and electric charges. The implementation of this Hamiltonian can be found in the file `Hamiltonian_Z2_Matter_mod.F90`. For this Hamiltonian, the the Z_2 local conservation law reads:

$$\hat{Q}_i = (-1)^{\sum_{\sigma} \hat{\Psi}_{i,\sigma}^\dagger \hat{\Psi}_{i,\sigma}} \hat{\tau}_i^x \hat{X}_{i,i+a_x} \hat{X}_{i,i-a_x} \hat{X}_{i,i+a_y} \hat{X}_i. \quad (210)$$

The Hamiltonian was investigated in Ref. [89]. Here is a todo list.

- Include an attractive U -term. This breaks the $O(4)$ symmetry down to $SU(2) \times SU(2)$ and selects the $\hat{Q}_i = 1$ sector. Note that a repulsive U should also be included and should produce equivalent results under particle-hole symmetry.
- Include dynamics, so as to study the dynamics of the OSM to FL^* phase. Note that the FL^* phase will ultimately be unstable to the AFM^* phase, but the energy scale is expected to be extremely small at small U .
- Include a projective version, with different left and right wave functions. The right imposes translation invariance and the left the constraint. That is, we choose the right trial wave function to be the ground state of

$$\hat{H}_T^R = -t \sum_{\langle i,j \rangle, \sigma} \left(\hat{\Psi}_{i,\sigma}^\dagger \hat{\Psi}_{j,\sigma} + h.c. \right) - h \sum_i \left(\hat{X}_{i,i+a_x} + \hat{X}_{i,i+a_y} + \tau_i^x \right) \quad (211)$$

and the left one to be the ground state of

$$\hat{H}_T^L = -U \sum_{i,\sigma} e^{i\mathbf{Q} \cdot \mathbf{i}} \hat{\Psi}_{i,\sigma}^\dagger \hat{\Psi}_{i,\sigma} - h \sum_i \left(\hat{X}_{i,i+a_x} + \hat{X}_{i,i+a_y} + \tau_i^x \right) \quad (212)$$

with $\mathbf{Q} = (\pi, \pi)$.

13.1.6 Generalized t-V model

The example code `Hamiltonian_Examples_mod.F90` contains an implementation of the $SU(N)$ t-V model, given by:

$$\hat{H}_{tV} = -t \sum_{\langle i,j \rangle} \sum_{\sigma=1}^N \left(\hat{c}_{i,\sigma}^\dagger \hat{c}_{j,\sigma} + h.c. \right) - \frac{V}{N} \sum_{\langle i,j \rangle} \left(\sum_{\sigma=1}^N \left(\hat{c}_{i,\sigma}^\dagger \hat{c}_{j,\sigma} + h.c. \right) \right)^2. \quad (213)$$

This model possesses a higher $O(2N)$ symmetry and shows no sign problem for all values of N . The model is implemented on the π -flux and square lattices. Tests are included in the test suite git `Testsuite_General_QMCT_code`.

13.1.7 Long range Coulomb

The model we consider here reads:

$$\hat{H} = -t \sum_{i,j,\sigma=1}^N \hat{c}_{i,\sigma}^\dagger T_{i,j} \hat{c}_{j,\sigma} + \frac{1}{N} \sum_{i,j} \left(\hat{n}_i - \frac{N}{2} \right) V_{i,j} \left(\hat{n}_j - \frac{N}{2} \right), \quad \text{with } \hat{n}_i = \sum_{\sigma=1}^N \hat{c}_{i,\sigma}^\dagger \hat{c}_{i,\sigma}. \quad (214)$$

The interaction is specified in the following way:

$$V_{i,j} = U \begin{cases} 1 & \text{if } i - j = 0 \\ \frac{\alpha}{|i-j|^{d_{\min}}} & \text{otherwise} \end{cases} \quad (215)$$

Here d_{\min} is the minimal distance between two orbitals. The code uses the following HS decomposition:

$$e^{-\Delta\tau\hat{H}_V} = \int \prod_{\mathbf{i}} d\phi_{\mathbf{i}} e^{-\frac{N\Delta\tau}{4}\phi_{\mathbf{i}}V_{\mathbf{i},\mathbf{j}}^{-1}\phi_{\mathbf{j}} - \sum_{\mathbf{i}} i\Delta\tau\phi_{\mathbf{i}}(n_{\mathbf{i}} - \frac{N}{2})} \quad (216)$$

The implementation follows Ref. [26] but now supports various lattice geometries. The definition of the Coulomb repulsion is as follows. A general lattice site \mathbf{I}, \mathbf{n} where $\mathbf{I}: 1 \dots \text{Latt\%N}$ is the unit cell and $\mathbf{n} = 1 \dots \text{Latt_unit\%NORB}$ the orbital is given by:

```
X_p(:) = Latt%list(I,1)*latt%a1_p(:) + Latt%list(I,2)*latt%a2_p(:)
        + Latt_unit%0rb_pos_p(no_j,:)
```

or in more compact notation $\mathbf{i} + \delta_{\mathbf{i}}$. By definition $\text{Latt_unit\%0rb_pos_p}(1, :) = 0$. The Coulomb repulsion between points $\mathbf{i} + \delta_{\mathbf{i}}$ and $\mathbf{j} + \delta_{\mathbf{j}}$ reads:

$$V(\mathbf{i} + \delta_{\mathbf{i}}, \mathbf{j} + \delta_{\mathbf{j}}) = \frac{U d_{\min} \alpha}{|\mathbf{i} - \mathbf{j} + \delta_{\mathbf{i}} - \delta_{\mathbf{j}}|} \quad (217)$$

Here we use periodic boundary conditions such that $\overline{\mathbf{i} - \mathbf{j}}$ is an element of the real space lattice. Note that this is encoded in the array `Latt%imj(I, J)`.

Acknowledgments

To be updated

Future: - Improved overall usability - Improved I.O., HDF5 - Improved post-processing - Implementation with classes - Trotter options - Time-dependent Hamiltonians

We are very grateful to S. Beyl, M. Hohenadler, F. Parisen Toldin, M. Raczkowski, T. Sato, J. Schwab, Z. Wang, and M. Weber for constant support during the development of this project. **MB: I think we should acknowledge also RRZE Erlangen: We equally thank G. Hager, M. Wittmann, and G. Wellein for useful discussions and support.** FFA would also like to thank T. Lang and Z. Y. Meng for developments of the auxiliary field code as well as T. Grover. MB thanks the Bavarian Competence Network for Technical and Scientific High Performance Computing (KONWIHR) for financial support. FG and JH thank the SFB-1170 for financial support under projects Z03 and C01. FFA thanks the DFG-funded FOR1807 and FOR1346 for partial financial support. Part of the optimization of the code was carried out during the Porting and Tuning Workshop 2016 offered by the Forschungszentrum Jülich. Calculations to extensively test this package were carried out both on SuperMUC at the Leibniz Supercomputing Centre and on JURECA [94] at the Jülich Supercomputing Centre. We thank both institutions for generous allocation of computing time.

References

- [1] R. Blankenbecler, D. J. Scalapino, and R. L. Sugar, Phys. Rev. D **24**, 2278 (1981).
- [2] S. White, D. Scalapino, R. Sugar, E. Loh, J. Gubernatis, and R. Scalettar, Phys. Rev. B **40**, 506 (1989).
- [3] G. Sugiyama and S. Koonin, Annals of Physics **168**, 1 (1986).
- [4] S. Sorella, S. Baroni, R. Car, and M. Parrinello, EPL (Europhysics Letters) **8**, 663 (1989).
- [5] S. Duane, A. D. Kennedy, B. J. Pendleton, and D. Roweth, Phys. Lett. **B195**, 216 (1987).
- [6] F. Assaad and H. Evertz, in *Computational Many-Particle Physics*, Vol. 739 of *Lecture Notes in Physics*, edited by H. Fehske, R. Schneider, and A. Weiße (Springer, Berlin Heidelberg, 2008), pp. 277–356.
- [7] D. J. Scalapino, in *Handbook of High-Temperature Superconductivity: Theory and Experiment*, edited by J. R. Schrieffer and J. S. Brooks (Springer New York, New York, NY, 2007), pp. 495–526.

- [8] J. P. F. LeBlanc, A. E. Antipov, F. Becca, I. W. Bulik, G. K.-L. Chan, C.-M. Chung, Y. Deng, M. Ferrero, T. M. Henderson, C. A. Jiménez-Hoyos, E. Kozik, X.-W. Liu, A. J. Millis, N. V. Prokof'ev, M. Qin, G. E. Scuseria, H. Shi, B. V. Svistunov, L. F. Tocchio, I. S. Tupitsyn, S. R. White, S. Zhang, B.-X. Zheng, Z. Zhu, and E. Gull, *Phys. Rev. X* **5**, 041041 (2015).
- [9] M. Hohenadler, T. C. Lang, and F. F. Assaad, *Phys. Rev. Lett.* **106**, 100403 (2011).
- [10] D. Zheng, G.-M. Zhang, and C. Wu, *Phys. Rev. B* **84**, 205121 (2011).
- [11] F. F. Assaad and I. F. Herbut, *Phys. Rev. X* **3**, 031010 (2013).
- [12] F. Parisen Toldin, M. Hohenadler, F. F. Assaad, and I. F. Herbut, *Phys. Rev. B* **91**, 165108 (2015).
- [13] Y. Otsuka, S. Yunoki, and S. Sorella, *Phys. Rev. X* **6**, 011029 (2016).
- [14] S. Chandrasekharan and A. Li, *Phys. Rev. D* **88**, 021701 (2013).
- [15] V. Ayyar and S. Chandrasekharan, *Phys. Rev. D* **91**, 065035 (2015).
- [16] Z.-X. Li, Y.-F. Jiang, S.-K. Jian, and H. Yao, *ArXiv:1512.07908* (2015).
- [17] F. F. Assaad and T. Grover, *Phys. Rev. X* **6**, 041049 (2016).
- [18] F. F. Assaad, *Phys. Rev. Lett.* **83**, 796 (1999).
- [19] S. Capponi and F. F. Assaad, *Phys. Rev. B* **63**, 155114 (2001).
- [20] Y. Schattner, S. Lederer, S. A. Kivelson, and E. Berg, *Phys. Rev. X* **6**, 031028 (2016).
- [21] X. Y. Xu, K. Sun, Y. Schattner, E. Berg, and Z. Y. Meng, *Phys. Rev. X* **7**, 031058 (2017).
- [22] E. Berg, M. A. Metlitski, and S. Sachdev, *Science* **338**, 1606 (2012).
- [23] H.-K. Tang, X. Yang, J. Sun, and H.-Q. Lin, *Europhys. Lett.* **107**, 40003 (2014).
- [24] F. F. Assaad, *Phys. Rev. B* **71**, 075103 (2005).
- [25] T. C. Lang, Z. Y. Meng, A. Muramatsu, S. Wessel, and F. F. Assaad, *Phys. Rev. Lett.* **111**, 066401 (2013).
- [26] M. Hohenadler, F. Parisen Toldin, I. F. Herbut, and F. F. Assaad, *Phys. Rev. B* **90**, 085146 (2014).
- [27] H.-K. Tang, E. Laksono, J. N. B. Rodrigues, P. Sengupta, F. F. Assaad, and S. Adam, *Phys. Rev. Lett.* **115**, 186602 (2015).
- [28] M. Rigol, A. Muramatsu, G. G. Batrouni, and R. T. Scalettar, *Phys. Rev. Lett.* **91**, 130403 (2003).
- [29] D. Lee, *Progress in Particle and Nuclear Physics* **63**, 117 (2009).
- [30] T. Grover, *Phys. Rev. Lett.* **111**, 130402 (2013).
- [31] P. Broecker and S. Trebst, *Journal of Statistical Mechanics: Theory and Experiment* **2014**, P08015 (2014).
- [32] F. F. Assaad, T. C. Lang, and F. Parisen Toldin, *Phys. Rev. B* **89**, 125121 (2014).
- [33] F. F. Assaad, *Phys. Rev. B* **91**, 125146 (2015).
- [34] C. Wu and S.-C. Zhang, *Phys. Rev. B* **71**, 155115 (2005).
- [35] E. F. Huffman and S. Chandrasekharan, *Phys. Rev. B* **89**, 111101 (2014).
- [36] Z.-X. Li, Y.-F. Jiang, and H. Yao, *Phys. Rev. B* **91**, 241117 (2015).
- [37] Z. C. Wei, C. Wu, Y. Li, S. Zhang, and T. Xiang, *Phys. Rev. Lett.* **116**, 250601 (2016).
- [38] J. Hubbard, *Phys. Rev. Lett.* **3**, 77 (1959).
- [39] M. Troyer and U.-J. Wiese, *Phys. Rev. Lett.* **94**, 170201 (2005).

- [40] S. Duane and J. B. Kogut, Phys. Rev. Lett. **55**, 2774 (1985).
- [41] J. Hirsch, Phys. Rev. B **28**, 4059 (1983).
- [42] A. D. Sokal, Monte Carlo Methods in Statistical Mechanics: Foundations and New Algorithms, 1989, lecture notes from Cours de Troisième Cycle de la Physique en Suisse Romande. Updated in 1996 for the Cargèse Summer School on “Functional Integration: Basics and Applications”.
- [43] H. G. Evertz, G. Lana, and M. Marcu, Phys. Rev. Lett. **70**, 875 (1993).
- [44] A. W. Sandvik, Phys. Rev. B **59**, R14157 (1999).
- [45] O. Syljuåsen and A. Sandvik, Phys. Rev. E **66**, 046701 (2002).
- [46] J. E. Hirsch and R. M. Fye, Phys. Rev. Lett. **56**, 2521 (1986).
- [47] E. Gull, A. J. Millis, A. I. Lichtenstein, A. N. Rubtsov, M. Troyer, and P. Werner, Rev. Mod. Phys. **83**, 349 (2011).
- [48] F. F. Assaad, in *DMFT at 25: Infinite Dimensions: Lecture Notes of the Autumn School on Correlated Electrons*, edited by E. Pavarini, E. Koch, D. Vollhardt, and A. Lichtenstein (Verlag des Forschungszentrum Jülich, Jülich, 2014), Vol. 4, Chap. 7. Continuous-time QMC Solvers for Electronic Systems in Fermionic and Bosonic Baths, iSBN 978-3-89336-953-9.
- [49] F. F. Assaad and T. C. Lang, Phys. Rev. B **76**, 035116 (2007).
- [50] R. T. Scalettar, D. J. Scalapino, and R. L. Sugar, Phys. Rev. B **34**, 7911 (1986).
- [51] S. Dür, Z. Fodor, J. Frison, C. Hoelbling, R. Hoffmann, S. D. Katz, S. Krieg, T. Kurth, L. Lellouch, T. Lippert, K. K. Szabo, and G. Vulvert, Science **322**, 1224 (2008).
- [52] F. F. Assaad, in *Lecture notes of the Winter School on Quantum Simulations of Complex Many-Body Systems: From Theory to Algorithms.*, edited by J. Grotendorst, D. Marx, and A. Muramatsu. (Publication Series of the John von Neumann Institute for Computing, Jülich, 2002), Vol. 10, pp. 99–155.
- [53] Y. Motome and M. Imada, Journal of the Physical Society of Japan **66**, 1872 (1997).
- [54] F. F. Assaad, M. Imada, and D. J. Scalapino, Phys. Rev. B **56**, 15001 (1997).
- [55] R. M. Fye, Phys. Rev. B **33**, 6271 (1986).
- [56] M. Iazzi and M. Troyer, Phys. Rev. B **91**, 241118 (2015).
- [57] S. M. A. Rombouts, K. Heyde, and N. Jachowicz, Phys. Rev. Lett. **82**, 4155 (1999).
- [58] E. Gull, P. Werner, O. Parcollet, and M. Troyer, EPL (Europhysics Letters) **82**, 57003 (2008).
- [59] S. Rombouts, K. Heyde, and N. Jachowicz, Physics Letters A **242**, 271 (1998).
- [60] D. Rost, E. V. Gorelik, F. Assaad, and N. Blümer, Phys. Rev. B **86**, 155109 (2012).
- [61] D. Rost, F. Assaad, and N. Blümer, Phys. Rev. E **87**, 053305 (2013).
- [62] N. Blümer, ArXiv e-prints (2008).
- [63] K. Hukushima and K. Nemoto, Journal of the Physical Society of Japan **65**, 1604 (1996).
- [64] C. J. Geyer, in *Computing Science and Statistics: Proceedings of the 23rd Symposium on the Interface* (American Statistical Association, New York, 1991), pp. 156–163.
- [65] C. W. Gardiner, *Handbook of Stochastic Methods* (Springer, ADDRESS, 1985).
- [66] S. Beyl, Doctoral thesis, Universität Würzburg, 2020.
- [67] Z. Wang, M. P. Zaletel, R. S. K. Mong, and F. F. Assaad, arXiv:2003.08368 .
- [68] Z. Bai, C. Lee, R.-C. Li, and S. Xu, Linear Algebra and its Applications **435**, 659 (2011).

- [69] A. van der Sluis, *Numerische Mathematik* **14**, 14 (1969).
- [70] J. W. Negele and H. Orland, *Quantum Many body systems, Frontiers in physics* (Addison-Wesley, Redwood City, Calif. u.a., 1988).
- [71] W. Krauth, *Statistical Mechanics: Algorithms and Computations* (Oxford University Press, ADRESS, 2006).
- [72] C. J. Geyer, *Statistical Science* **7**, 473 (1992).
- [73] R. M. Neal, (1993).
- [74] M. Bercx, J. S. Hofmann, F. F. Assaad, and T. C. Lang, *Phys. Rev. B* **95**, 035108 (2017).
- [75] B. Efron and C. Stein, *Ann. Statist.* **9**, 586 (1981).
- [76] S. Chakravarty, B. I. Halperin, and D. R. Nelson, *Phys. Rev. Lett.* **60**, 1057 (1988).
- [77] M. B. Thompson, *ArXiv e-prints* (2010).
- [78] M. Feldbacher and F. F. Assaad, *Phys. Rev. B* **63**, 073105 (2001).
- [79] D. Ixert, F. F. Assaad, and K. P. Schmidt, *Phys. Rev. B* **90**, 195133 (2014).
- [80] K. S. D. Beach, *eprint arXiv:cond-mat/0403055* (2004).
- [81] I. Milat, F. Assaad, and M. Sigrist, *Eur. Phys. J. B* **38**, 571 (2004), <http://xxx.lanl.gov/cond-mat/0312450>.
- [82] M. Bercx, T. C. Lang, and F. F. Assaad, *Phys. Rev. B* **80**, 045412 (2009).
- [83] X. Y. Xu, K. S. D. Beach, K. Sun, F. F. Assaad, and Z. Y. Meng, *ArXiv:1602.07150* (2016).
- [84] K. S. D. Beach, P. A. Lee, and P. Monthoux, *Phys. Rev. Lett.* **92**, 026401 (2004).
- [85] T. Sato, F. F. Assaad, and T. Grover, *Phys. Rev. Lett.* **120**, 107201 (2018).
- [86] Z.-X. Li, Y.-F. Jiang, and H. Yao, *New Journal of Physics* **17**, 085003 (2015).
- [87] A. Rüegg, S. D. Huber, and M. Sigrist, *Phys. Rev. B* **81**, 155118 (2010).
- [88] M. Hohenadler and F. F. Assaad, *Phys. Rev. B* **100**, 125133 (2019).
- [89] S. Gazit, F. F. Assaad, and S. Sachdev, *arXiv:1906.11250 arXiv:1906.11250* (2019).
- [90] F. F. Assaad, *Nat Phys* **10**, 905 (2014).
- [91] X. Y. Xu, Y. Qi, J. Liu, L. Fu, and Z. Y. Meng, *arXiv:1612.03804* (2016).
- [92] M. V. Ulybyshev, P. V. Buividovich, M. I. Katsnelson, and M. I. Polikarpov, *Phys. Rev. Lett.* **111**, 056801 (2013).
- [93] R. Brower, C. Rebbi, and D. Schaich, *PoS(Lattice 2011)056* (arXiv:1204.5424) .
- [94] Jülich Supercomputing Centre, *Journal of large-scale research facilities* **2**, A62 (2016).

License

The ALF code is provided as an open source software such that it is available to all and we hope that it will be useful. If you benefit from this code we ask that you acknowledge the ALF collaboration as mentioned on our homepage alf.physik.uni-wuerzburg.de. The git repository at alf.physik.uni-wuerzburg.de gives us the tools to create a small but vibrant community around the code and provides a suitable entry point for future contributors and future developments. The homepage is also the place where the original source files can be found. With the coming public release it was necessary to add copyright headers to our source files. The Creative Commons licenses are a good way to share our documentation and it is also well accepted by publishers. Therefore this documentation is licensed to you under a CC-BY-SA license. This means you can share it and redistribute it as long as you cite the original source and license your changes under the same license. The details are in the file `license.CCBySA` that you should have received with this documentation. The source code itself is licensed under a GPL license to keep the source as well as any future work in the community. To express our desire for a proper attribution we decided to make this a visible part of the license. To that end we have exercised the rights of section 7 of GPL version 3 and have amended the license terms with an additional paragraph that expresses our wish that if an author has benefitted from this code that he/she should consider giving back a citation as specified on alf.physik.uni-wuerzburg.de. This is not something that is meant to restrict your freedom of use, but something that we strongly expect to be good scientific conduct. The original GPL license can be found in the file `license.GPL` and the additional terms can be found in `license.additional`. In favour to our users, the ALF code contains part of the lapack implementation version 3.6.1 from <http://www.netlib.org/lapack>. Lapack is licensed under the modified BSD license whose full text can be found in `license.BSD`.

With that being said, we hope that the ALF code will prove to you to be a suitable and high-performance tool that enables you to perform quantum Monte Carlo studies of solid state models of unprecedented complexity.

The ALF project's contributors.

COPYRIGHT

Copyright © 2016, 2017, The *ALF* Project.

The ALF Project Documentation is licensed under a Creative Commons Attribution-ShareAlike 4.0 International License. You are free to share and benefit from this documentation as long as this license is preserved and proper attribution to the authors is given. For details see the ALF project homepage alf.physik.uni-wuerzburg.de and the file `license.CCBySA`.